Report No. NW/SSD/RR/45/80

Central Electricity Generating Board
North Western Region
Scientific Services Department

THE INFLUENCE OF CRACK GROWTH CONDITIONS AND COMPRESSIVE STRESS ON THE ULTRASONIC DETECTION AND SIZING OF FATIGUE CRACKS.

by

A.B. Wooldridge and G. Steel

Date: April 1980

THE INFLUENCE OF CRACK GROWTH CONDITIONS AND COMPRESSIVE STRESS ON THE ULTRASONIC DETECTION AND SIZING OF FATIGUE CRACKS

BY

A.B. WOOLDRIDGE, AND G. STEEL*

* Miss G. Steel was seconded to the NDT Applications Centre from NEI Parsons Limited

Date:- April 1980

CEGB UNCLASSIFIED

REPORT NW/SSD/RR/ 45/80

SUMMARY SHEET

TITLE THE INFLUENCE OF CRACK GROWTH CONDITIONS AND COMPRESSIVE STRESS ON THE ULTRASONIC DETECTION AND SIZING OF FATIGUE CRACKS

BY A.B. WOOLDRIDGE, G. STEEL

TO Controller of Research

APPROVED M.J. Whittle Section Head, NDT Applications Centre

DATE: April 1980
JOB NO. ZE 301
'SPIC' CAT. NO.
TECH. HEAD
PAGES 26
FIGURES 30

SUMMARY

A series of fatigue cracks in mild steel parent metal and weld metal grown under constant stress intensity conditions have been examined ultrasonically for compressive stresses up to 150 MN m^{-2}. Various angles of shear waves and the Delta technique were employed to study the corner echoes. Reductions in reflectivity at zero load and under stress have been shown to correlate with the crack growth conditions and with the roughness of the crack faces. We also measured the ultrasonic echoes from the crack tips which are small even at zero load and become undetectable for small compressive stresses. The detectability with shear waves of cracks containing liquid has been measured and compared with theoretical predictions derived from a thin parallel-sided gap model.

CONCLUSIONS

1. The growth conditions of fatigue cracks have a significant effect on their ultrasonic response, both at zero load and when under compressive stress. The cyclic change in stress intensity factor during crack growth correlates well with the roughness of the fatigue crack surfaces and this is believed to cause the changes in ultrasonic response.

2. Both increasing crack roughness and increasing compressive stresses reduce the specular reflection from cracks but the roughest cracks show the least variation with stress.

3. Crack tip echoes are small; typically they are 50 dB down on a back wall echo at the same range when using a compression wave probe at grazing incidence, and they are practically impossible to identify reliably if the cracks are in compression or if the material contains other defects such as inclusions.

4. The errors in sizing cracks in clean material by detecting the tip echoes are typically $\pm$ 1 mm if averaged for several probes. Individual readings, however, may be in error by several millimetres.

5. The presence of liquid in a crack causes a marginal increase in reflection for shear wave beams incident at 20° to the crack normal. Modest decreases in reflection occur for beams incident at 45°, while considerable decreases are likely at 30° incidence.

CIRCULATION LIST

(F = FULL REPORT, S = SUMMARY)

HEADQUARTERS

F&S Reports Library, H.Q.

RESEARCH DIVISION

F Director General, Research Division
F Mr. R.B. Hill
F Dr. P. Melville
S Divisional Secretary

G.D.C.D.

S Director General
S Deputy Director General
F Mr. H. Cochrane
F Mr. M. Gemmill
F Mr. G.D. Branch
F Mr. W. Kemmish
F Mr. P. Bolt

ENGINEERING SERVICES

F G.R.O. Shaw, NNDTU, Leeds

NORTH WESTERN REGION

F Director General
F Controller of Scientific Services
F Research Manager (2)
F Section Head, NDT Applications Centre
F Section Head, Fracture Mechanics
F Section Head, Automation and Control
F Manager, Metallurgy and NDT Services
F Mr. K. James
F Mr. H.L. Carson (via Section Head - NDT Developments)
F Mr. A.B. Wooldridge (3)
F Dr. J.M. Coffey
F Dr. J.R. Tomlinson
F Mr. J.A. Deane
F&S Library

N.E. REGION

S Controller of Scientific Services
F Dr. M. Jagger, S.S.D.
F Dr. A. Lichnowski, SSD
F Mr. J. Kenny, Engineering Department
F&S Library

MIDLANDS REGION

S Controller of Scientific Services
F Mr. R.H. Robins, SSD
F Mr. B.L. Freeman
F Mr. I. Graham, Engineering Department
F&S Library

F Mr. D. H. Turner, Bankside House
F Mr. G. Alderman, Engineering Dept., Littlebrook
F&S Library

M.E.L.

S Director
S Dr. L.A. Mitchell
S Dr. B.A. Tozer
F Mr. M.J. Little
S Research Planning Officer
F&S Library

B.N.L.

S Director
S Research Planning Officer
F Mr. N. Haines
F&S Library
F Mr. D.B. Langston
F Mr. A.F. George

C.E.R.L.

S Director
S Research Planning Officer
S Dr. J. Baylis
F Dr. T. Lindley
F&S Library

S.S.E.B.

F&S Library (4)
F Mr. F. Darroch (East Kilbride)
F Dr. Platt (East Kilbride)
F Dr. R. Shipp (East Kilbride)

EXCHANGE AGREEMENTS AND CONTRACTS

F N.I.E.S. Mr. W.J. Adair
F E.S.B.I. Mr. W.F. Lang
F EPRI (2)) Via Research
F T.V.A.) Programme Co-ordinator
F Ontario Hydro)
F Canadian Welding Institute, Via Research Manager, N.W. Region
F Mr. R.W. Urie, SECV.

NON-C.E.G.B.

F Mr. D. Gibb, NEI Power Engineering
F Dr. J.M. Farley, Babcock & Wilcox, Renfrew
S Dr. P. Greenfield, GEC Turbo Generators, Whetstone
F Miss. G. Steel, NEI Power Engineering

CIRCULATION LIST (CONT'D)

S.W. REGION

S Controller of Scientific Services
F Mr. P. Johnson
F&S Library

S.E. REGION

S Controller of Scientific Services
S Director of Engineering

NON-C.E.G.B.

S Mr. I.P. Bell, RNPDL, Risley
F Mr. B.S. Gray " "
F Mr. R. Sharpe, AERE, Harwell
F Mr. T. Jessop, Welding Institute
Abington, Cambridge
F Mr. V. Whittaker, Aston University
S Mr. B. Watkins, RNPDL, Risley
F Mr. R.A. Murgatroyd, RNPDL, Risley
F Dr. V.M. Baborovsky, TI Research Labs
Hinxton Hall, Cambridge
F Mr. H. Smallman, Nuclear
Installations Inspectorate

CONTENTS

LIST OF FIGURES

LIST OF FIGURES (CONT'D)

FIGURES

1. INTRODUCTION

The ability of ultrasonic techniques to detect cracks may be reduced if compressive stress forces the crack faces together. High cycle fatigue cracks whose surfaces are very smooth are likely to be particularly sensitive to such compression. A previous report (Wooldridge 1979) investigated the changes in reflection and transmission of ultrasound at machine ground surfaces which were under compressive loading. Measurements of transmission and diffuse backscattering were also made on a fatigue crack grown at constant load. In each case it was found that whereas the transmission approaches unity at high load, the specular reflection may still be detected readily. This report concentrates on the corner echoes and crack tip echoes from surface-breaking fatigue cracks grown at constant stress intensity factor. In this way we have established a strong correlation between the roughness of the surfaces and the ultrasonic response at both zero load and under stress.

The reflection of ultrasound from cracks depends on many factors. Those relating to the crack itself include its size and shape, the morphology of the crack surfaces, the nature of the material between the crack faces and the net stress acting on these faces. Important parameters of the ultrasonic probe include the ultrasonic frequency and the angle of incidence and size of the beam at the crack.

The experiments described in this report were designed primarily to study the effects of compressive stress, but in order to obtain results of general applicability it was necessary to incorporate studies of several of the important factors listed above. Particular attention was paid to the crack growth conditions since these affect not only the size and shape of the crack, but also the morphology of the surface and the residual stresses acting on the crack (Elber 1970, 1971). Faced with these inter-related experimental variables, a wide range of measurements were necessary in order to distinguish the various effects. In this way we have obtained quantitative estimates of these effects which will be useful to those designing ultrasonic inspections. We believe that it also increases our understanding of the interaction of ultrasound with real defects.

Most of the fatigue cracks were grown by three-point bending of bright finished mild steel (EN3B) bars as described in Section 2. In addition, cracks were grown in similar specimens containing high quality manual metal-arc welds, both in the as-welded condition and after stress relief. The amplitude of the cyclic loading applied during crack growth was continuously adjusted as the crack extended to maintain a constant change in stress intensity factor at the crack tip. The aim was to produce a crack of uniform roughness throughout its length and the results of destructive examination indicate that this had been achieved. It was also hoped that residual crack closure stresses (Elber 1971) would be evenly distributed over the length of the crack. During constant-load crack growth, such stresses are concentrated near the crack tip.

When crack growth had been completed, the starter notches were machined away to obtain surface-breaking fatigue cracks. All machining operations were done dry, and care was taken to prevent subsequent entry of liquid into the cracks. Sections 3 to 6 of the report describe the measurements carried out on these dry cracks. The ultrasonic measurements obtained with no external stress on the cracks are described in Section 3, while the next section outlines the changes in echo amplitude which occurred when the

cracks were compressed. Although echoes from the crack tips are weak, they have been measured under zero load and under compressive and tensile loads as described in Section 5. The next section describes the effects of weld metal on the crack response and the changes caused by stress relief of the welds. Since surface-breaking defects often contain water or oil, Section 7 describes a number of measurements which were repeated after liquid had soaked into the cracks.

In Section 8 our understanding of the interaction of angled beams with cracks is summarised and the significance of these results to inspection problems is discussed. The appendices describe two theoretical models for thin planar cracks. The first concerns resonant interference effects which may be significant for liquid filled cracks while the second considers the increase in real area of contact which occurs when a crack is loaded.

2. THE FATIGUE CRACKS

2.1 Production of the Fatigue Cracks

Of all the cracks which occur in metals, fatigue cracks are probably the easiest to reproduce under controlled conditions in the laboratory. Although it is difficult to predict initiation times for fatigue cracks, the mechanisms of subsequent crack growth have been extensively studied, (e.g. Schijve 1979) and are comparatively well understood. Consequently when planning the experiments we were able to choose a design of test block and specify the crack growth conditions so that the shape, orientation and roughness of the resultant cracks could be controlled and reproducible. Figure 1(a) shows the dimensions of the initial specimens which were cyclically loaded in three-point bend so that fatigue cracks grew from the V-grooves. Cylindrical side grooves parallel to the direction of growth were used to restrain the cracks to the vertical plane and also to reduce the tendency of the cracks to grow with a convex leading edge.

It is well known that the changes in the cyclic stresses applied to the crack tip influence the nature of the crack surfaces, and in particular, sudden changes in load amplitude can create beachmarks (Stewart 1978). Constant-load fatiguing is often used to grow cracks in the laboratory and often occurs in service, but this leads to a continuous gradation in surface roughness as the crack propagates. A correlation between the roughness and the stress intensity factor during fatigue crack growth has been noted by Wooldridge (1979) and Manning (1979). Consequently we decided to reduce the cyclic load amplitude continuously during crack growth so as to maintain constant the change in stress intensity factor, ΔK, at the crack tip. The frequency of cycling was not thought likely to influence the morphology significantly; a rate of 8 Hz was generally used. To monitor the crack depth a microscope was focussed on the edge of the block and the fatigue cycle rate reduced to 1 Hz during each measurement. These readings of crack depth were used to predict the stress intensity factor at the crack tip and the fatigue load amplitude was decreased in small increments so that ΔK remained constant within $\pm$ 2%. Three values of ΔK were chosen in the range 20-60 MN $m^{-3/2}$ and details of the crack growth conditions are listed in Figure 2(a).

In the case of block J, a beachmark was deliberately introduced by increasing ΔK from 20.7 MN $m^{-3/2}$ to 37.2 MN $m^{-3/2}$ for ten cycles. Following this overload, crack growth was continued with a constant ΔK of 20.7 MN $m^{-3/2}$. The ratio of minimum to maximum stress (R factor) was between 0.03 and 0.32.

The equation of Paris for fatigue crack growth is:-

$$\frac{da}{dn} = C (\Delta K)^n$$ where da/dn is the growth rate per cycle, and C, n are constants.

A logarithmic transformation of this equation gives a straight line of slope n. This prediction has been tested in Figure 2(b) which plots the number of cycles per mm of crack growth versus ΔK for cracks grown in this programme, and shows that the Paris expression is a good approximation over a wide range of growth rates.

Six of the cracks were grown in EN3B mild steel, whose metallurgical properties are listed in Figure 3(a), but three were in blocks of the same dimensions containing a mild steel manual metal-arc weld. After the crack growth, the V-shaped starter notches were machined away and the top and bottom surfaces ground flat and parallel to facilitate ultrasonic examination of the resultant surface-breaking cracks. As shown in Figure 1(b), the blocks were also reduced to a length of 200 mm to enable them to be compressed in the Denison hydraulic machine. In some cases, crack growth was continued after the machining, the final cracks being approximately 5, 10 or 15 mm deep.

The weld specimens showed a higher growth rate than equivalent cracks in mild steel. This is discussed more fully in Section 6.

2.2 Destructive Examination

When all the ultrasonic measurements had been completed, some of the blocks were split open to reveal the fatigue cracks. A typical crack surface, that of crack F, is shown in Figure 3(b). The surface is macroscopically very flat, lies in a plane perpendicular to the testing surfaces and the crack is slightly deeper at the edges than at the centre. Fatigue cracks would normally be deepest at the centre, but the side grooves at the edges of the block have slightly over-compensated resulting in a concave profile. However, over the central region used for ultrasonic measurements, the crack tips were all straight within 0.5 mm. The crack tip profiles of all the cracks examined were very similar although the surface roughness varied considerably.

There are various ways of describing the statistical properties of rough surfaces; frequently the Roughness Average, Ra, is used to describe the variations normal to the surface as described in BS 1134 while the correlation length is used for variations in the plane of the surface. However since both these parameters depend on the sampling length, George (1979) has suggested the use of the power spectral density function which contains more information and is independent of sampling length, l_o, for all wavelengths shorter than l_o. Studies of the topography of fatigue cracks in a variety of materials by Manning (1979) have shown that the spectral density, P(W), may be described approximately by:-

$$P(W) = \frac{A}{W^2} \qquad \text{equation 1}$$

where W = angular spatial frequency

A = constant

for $W_{max} > W > W_{min}$. W_{min} represents a long wavelength cut-off which depends on the geometry and the macroscopic stress conditions in the fatigue crack specimen. The short wavelength cut-off W_{max} is determined by the diameter of the stylus used to measure the surface topography. Measurements on the cracks used for our work yielded similar power spectra as indicated in Figure 4(b) for block F.

If the power spectrum satisfies equation 1 we can show that the measured root mean square roughness, R_{rms}, satisfies the following relationship:-

$$(R_{rms})^2 = \frac{A}{\sqrt{2\pi}} \left[\frac{1}{W_{min}} - \frac{1}{W_{max}} \right]$$

$$\approx \frac{A}{\sqrt{2\pi}} \cdot \frac{1}{W_{min}} \qquad \text{when } W_{max} >> W_{min}$$

The relationship between R_{rms} and R_a values depends on the statistics of the surface but if we assume that the roughness is random and the distribution of the surface heights is Gaussian then:-

$$R_a = \sqrt{2/\pi}\ R_{rms}$$

and hence $(R_a)^2 \approx \frac{A}{\pi} \sqrt{\frac{2}{\pi}} \cdot \frac{1}{W_{min}}$

Consequently we believe that in spite of the limited information contained in the R_a value, it is a good indication of the surface condition of the fatigue cracks for all spatial frequencies between W_{min} and W_{max}.

Measurement of the roughness (Ra value) was carried out using a Surtronic 2 profile meter taking scans parallel to the crack tip at various depths. The stylus radius was 2.5μm and the cut-off length 2.5 mm. As intended, for all the cracks grown at constant K the roughness did not vary with depth. Figure 2(a) includes the measured mean Ra values for those blocks which have been examined. There is a steady increase in the mean Ra value with increasing ΔK for the cracks in parent metal as shown in Figure 4(a). The straight line OP has been fitted to the results obtained so far. Although we produced no cracks with stress intensities less than 20 MN $m^{-3/2}$, Manning (1979) has measured low ΔK cracks with Ra values down to about 5 μm and his measurements for such cracks agree reasonably well with the line OP. Figure 4(a) shows that the weld specimen G which had not been stress relieved is anomalously rough; its roughness being equivalent to that of a crack in parent metal grown at a ΔK of 50 MN $m^{-3/2}$. Most of the ultrasonic results are plotted as a function of ΔK during crack growth, but Figure 4(a) may be used to relate these to the Ra value of the cracks.

It is instructive to consider the various mechanisms which are associated with the topography of these fatigue cracks. The W^{-2} dependence of the power spectra is similar to that of grit-blasted surfaces which suggests that the processes determining the macroscopic roughness ($\gtrsim$1μm) are essentially random. On the other hand, the microscopic roughness ($\lesssim$1μm) as observed under the scanning electron microscope shows a pronounced linear striation structure, each striation being associated with a particular fatigue cycle. From the measured crack growth rates, the striation spacing is expected to vary from about 0.05 μm for $\Delta K = 20$ to 1.3μm for $\Delta K = 62$. These values are in reasonable agreement with those predicted by the equation of Paris if we use the commonly accepted values of the constants C and n so that the growth rate per fatigue cycle is given by:-

$$\frac{da}{dn} = 10^{-11} (\Delta K)^3 \qquad \text{S.I. units}$$

The individual striations, whose spacing is directly related to ΔK, are too small to be measured with the profilometer. The reasons for the ΔK dependence of the macroscopic roughness are not well understood, but we may speculate that it is associated with the size of the reversed plastic zone around the crack tip. In this region irreversible deformation processes are most severe; in particular the movement of dislocations leads to work hardening while at higher stress intensities the coalescence of microvoids associated with dislocations or inclusions may cause microcracks. The radius of the reversed plane strain plastic zone r_p is given by:-

$$r_p = \frac{(\Delta K)^2}{6\pi (2\sigma_y)^2} \qquad \text{where } \sigma_y \text{ is the yield stress (Knott 1973)}$$

If $\sigma y = 370$ MN m^{-2}, r_p varies from 39 μm for $\Delta K = 20$ to .37 mm for $\Delta K = 62$ and these dimensions are similar in scale to the roughness revealed by the surface power spectra. At the higher stress intensities, monotonic failure modes such as microvoid coalescence and cleavage fracture may also occur. This is likely to be particularly important in the case of our specimens of EN3B since hardness testing indicated that they had a high yield stress and hence a relatively low fracture toughness.

The roughness of cracks which have grown by monotonic modes is likely to be controlled by the maximum stress intensity, K_{max}, rather than ΔK. However since our cracks were grown with low R-values, K_{max} is similar to ΔK and it is difficult to distinguish between these two cases. Whether crack growth is dominated by striation formation or monotonic failure modes, the random nature of the macroscopic roughness presumably arises from the random orientation of both the grains and the distribution of microvoids in the material.

3. ULTRASONIC REFLECTIONS FROM THE CRACK CORNERS WITH NO APPLIED LOAD

Fatigue growth involves plastic deformation of the material ahead of the propagating crack tip which can result in a residual compressive stress on the crack faces (Elber 1970, 1971). These crack closure stresses may affect the ultrasonic response. Since these intrinsic stresses may be modified by externally applied tensile or compressive loads, all the

cracks were tested ultrasonically both before and after the main experiments on the effects of external load were carried out. This comparison revealed that no significant changes greater than ± 1 dB had occurred.

Measurements of the corner echoes were made using 45°, 60° and 70° shear wave angle probes in pulse-echo. In addition a 60° shear wave and a normal compression probe were used together in a Delta-Scan arrangement. Certain measurements were also made using a surface-wave probe on the crack-breaking surface. Figure 5(a) lists the important probe parameters while 5(b) shows the various arrangements on the blocks. A Baugh and Weedon PA1020 flaw detector, whose proportional output had been calibrated, was used for all the readings. The potential drop arrangement shown in Figure 5(b) was only used while the blocks were under compression.

Before considering the relative amplitudes of the corner echoes of the various cracks, it is instructive to study the variations in echo amplitude obtained by scanning various probes over the blocks. Figure 6 shows the amplitudes of the corner echoes for block F (15 mm crack) using 45°, 60° and 70° probes as their beams are scanned over the crack. The 45° probe gives a strong echo only when the beam intersects the corner between the crack and the surface. The 70° probe gives a very broad response. This is partly because of the increased beamwidth and partly because at this angle of incidence the crack face gives a diffusely scattered echo. The pulse echo response of the 60° probe is different from either 45° or 70° probes in that the maximum echo is not obtained when the beam axis intersects the corner. Rather a strong conversion to compression waves occurs at the vertical crack, these travel downwards and are reflected at the bottom surface. As they travel upwards, some are re-converted to shear waves at the crack according to the Reciprocity Theorem and return along their original path back to the probe. The true corner echo for the 60° probe is considerably smaller and gives rise to the tail of the echodynamic trace. For subsequent tests, the 60° probe was positioned to maximise the height of the "corner" echo. The variety of mode conversions which can occur with angled beams of shear waves is demonstrated by the Schlieren visualisation system of Baborovsky et al (1975). In particular, much of the energy converted to compression waves reaches the upper surface where it may readily be detected using a compression wave probe; this is the basis of the Delta-Scan arrangement.

The corner echoes obtained using the 45° probe are plotted in Figure 7(a) against the ΔK values for each crack. As a calibration, the echo from a smooth 90° corner at the same range is also shown. The readings for cracks of high ΔK were very sensitive to the position and squint of the probe and this is reflected in the error bars. There is a steady decrease in echo amplitude with increasing ΔK, but little or no dependence on crack length. The ΔK dependence is believed to be caused by the increase in roughness (see Figure 4) and by the tendency for tiny cracks to propagate away from the plane of maximum stress as ΔK increases (Wooldridge 1979). Figure 7(a) shows clearly that the response of crack G grown in weld metal is about 10 dB less than one would predict from the ΔK value. This effect also occurred with 60° and 70° probes and is believed to be caused by the increased roughness of the weld crack and by residual compressive stresses in the weld. This is discussed more fully in Section 6.

Figures 7(b) and 7(c) for 60° and 70° probes respectively show the same roughness dependence as in the case of the 45° probe, and although the scatter in the results is larger, there is no obvious dependence on crack length. In

particular, the 5 mm crack for which ΔK was 37 MN m^{-2} produced an unusually large echo. These readings were repeated after the blocks had been compressed a number of times as described in Section 4. This produced no change in the 45° readings and only small changes in the 60° and 70° readings Since the compression cycles are expected to have relieved any crack closure stresses, it appears that these stresses do not have a significant effect on the corner response of cracks, at least for surface-breaking cracks exceeding 4 mm in depth. Certain measurements were also made by loading the blocks in three-point bend to apply a small tensile stress to the crack faces. The corner echo amplitudes did not change thus providing further support for the above conclusion.

Results for the Delta-Scan measurements are as shown in Figure 7(d). The signal amplitudes obtained are comparable with that of a 45° pulse-echo probe, but the dependence on ΔK is rather less pronounced. These measurements were taken after the compression cycles, but in view of the above discussion, this is not thought likely to affect their validity.

4. THE EFFECTS OF COMPRESSIVE STRESS ON THE ULTRASONIC CORNER REFLECTIONS

Compressive stresses were applied perpendicular to the crack faces by loading the blocks along their long axis using a Denison hydraulic machine. Once the probe was fixed in position and the corner echo maximised, the load was increased steadily. A chart recorder monitored the signal amplitude and the applied load simultaneously. The flaw detector monitor gate had a limited dynamic range so it was necessary to change the gain setting at 8 dB intervals using the previously calibrated attenuator.

The first time each crack was compressed, the echo response during the loading cycle was considerably higher than that during the unloading cycle. As a typical example, Figure 8(a) shows the 45° shear wave response for the first loading cycle of block I up to a compressive stress of 150 MN m^{-2} (10.0 tons in $^{-2}$) and back to zero. Subsequent loading and unloading responses were very similar to the first unloading cycle as seen in Figure 8(b). These results are consistent with localised plastic deformation of the crack surfaces occurring during the first compression. One expects elastic deformation to predominate for later cycles. Subsequent destructive examination of the cracks revealed a number of small areas where plastic deformation of the surfaces appeared to have occurred.

For each block, the corner response over one or more compressive cycles was recorded for 45°, 60° and 70° and for the Delta-scan arrangement. Measurements were also made on some blocks using surface wave probes. Whereas, many probe and crack combinations showed a monotonic decrease in signal with increasing stress, a significant number showed a small increase at low stresses as seen in Figures 8(a), (b) and 9(a). A similar effect has already been reported for diffuse back-scattering from the crack tip region (Wooldridge 1979). We believe that this is caused by complex variations in the reflection and mode conversion processes occurring at the crack as the faces mate together. These may be further complicated by a non-uniform stress distribution on the crack face. To aid the interpretation of the ultrasonic responses a d.c. potential drop system was set up as shown in Figure 5(b). A stabilised current of 60 amps was passed through the blocks and electrodes measured the potential difference developed across the crack. Recordings of ultrasonic

signals and potential drop (p.d) readings were taken simultaneously as the load varied. In all cases the potential drop decreases steadily even when there is a pronounced peak in the ultrasonic response, as shown in Figure 9(a) for the 70° probe. This implies that the initial rise in the ultrasonic signal with applied stress is not due to a slight opening of the crack faces, before they begin to be pressed together.

The 45° probe response (Figure 9(b)) did not decrease significantly until a mean stress of 70 MN m^{-2} was applied, and this is also the stress at which the surface wave echo begins to decrease rapidly. Both probes will be most sensitive to the stresses close to the open end of the crack, so it appears that the crack is not fully closed at low loads. The 60° probe and Delta-scan measurements are most sensitive to the stresses on the central part of the crack, as discussed in Section 3, and both decrease steadily for loads above 10 MN m^{-2} (Figure 9(c)). The 70° probe response is intermediate between that of the 45° and 60° probes and the echo amplitude is probably determined by the stress over a considerable area of the crack near the open end.

The rate at which the ultrasonic responses decrease for small applied loads depends on the crack length. All the probe responses for Block E, which has a 5 mm crack, decreased steadily with load, whereas 10 mm and 15 mm cracks (J and F) exhibited temporary increases at low load. However, for higher stresses there was little dependence on the length of crack. This suggests either that significant non-uniform stress distributions are set up on the deeper cracks for small loads, or that interference effects caused by mode conversions are more important for deep cracks.

The position and orientation of the blocks between the platens of the machine also had an effect. The top platen is forced down by two hydraulic pistons and if the block is not placed in the centre there is a tendency for the platen to tilt slightly resulting in a non-uniform stress on the block. Most tests were carried out with the blocks aligned centrally; but comparative tests showed that by placing a block slightly off-centre, with the crack facing towards the centre of the Denison, larger decreases in signal were obtained, particularly at low load. Figures 10(a), (b), and (c) show the effect of off-centre loading for block L, the crack in weld metal. It is significant that the mean slopes of all three curves are very similar (about 0.16 dB/MN m^{-2}). When the block was aligned centrally, the 60° pulse-echo and Delta-scan signals showed the biggest changes with stress while the 45° signal decreased least. We believe this is caused by a non-uniform stress distribution such that the stresses at the mouth of the crack are significantly less than those nearer the centre of the block

Let us consider now the effect of crack roughness on the ultrasonic response when the cracks are compressed. The results described in Appendix A indicate that significant transmission of shear waves can only occur across an air-filled crack if solid contact exists. The affect of increasing contact area on the ultrasonic response is discussed in Appendix B. More complete contact will be achieved with smooth cracks, and this explains why the low ΔK cracks show the largest variations when compressed. Figure 11(a) shows the maximum decreases in the corner echoes for 45° shear waves; these maximum decreases are achieved when the mean stress on the crack was increased from zero to 160 MN m^{-2}. This is plotted against ΔK for the various blocks. Figures 11(b), (c) and (d) show similar results for 60°, 70° and Delta-scan arrangements. There is a steady trend towards smaller changes as ΔK

increases. The one exception is the point at $\Delta K = 60.7$ in the Delta-scan arrangement. Another general point is that, as one might expect, there is no clear dependence on crack depth. The maximum changes recorded for stresses of 160 MN m^{-2} were -18 dB for a 45° probe (block J), -32 dB, for 60° (block F), -20 dB for 70° (blocks F and J) and -25 dB for Delta-scan (blocks F and E).

Typical residual stresses in heat treated steel welds are within $\pm$ 60 MN m^{-2}. The results for the weld crack, L, (Figures 10(a), (b) and (c)) show that with the block slightly off-centre there is a decrease of about 10 dB at 60 MN m^{-2} mean stress, and this is practically independent of the probe angle. Under central loading, however, the recorded changes in echo amplitude at these lower stresses show considerable variability, presumably because of the non-uniform stresses set-up as the cracks close. The maximum reductions in echo amplitude observed when the blocks were centrally loaded to a mean compressive stress of 60 MN m^{-2} are listed below. The largest changes always occurred for the blocks of lowest ΔK.

TABLE 1 MAXIMUM REDUCTIONS IN ECHO FOR UNIFORM STRESSES OF 60 MN m^{-2}

Probe	Block No.	dB decrease at 60 MN m^{-2} mean stress
45°	J	11.6
60°	F	21.6
70°	E	11.9
Δ-Scan	E	14.8

These may be regarded as an upper limit to the changes in ultrasonic response which may be caused by residual stresses in welds.

To enable comparisons to be made with early work on machine-ground surfaces, experiments were also carried out using compression and shear waves at normal incidence to the cracks, but discussion of these results has been included in Appendix B.

5. CRACK TIP ECHOES

5.1 Measurements Under Zero Load

Whereas amplitude techniques are used to size defects smaller than the beamwidth, sizing of larger cracks is often carried out by detecting signals from their opposite edges. To assess the applicability and accuracy of this sizing technique for fatigue cracks, measurements were made of the crack tip echoes for various angles of incidence. Several probes were used and their results compared. Scanning was carried out from both the crack-breaking surface and the opposite side; these are referred to as the "near" side and "far" side respectively. The blocks had all been subjected previously to compressive loading cycles so we were confident that any crack closure stresses set up in the material around the crack tip would have been substantially relieved by plastic deformation. Instead of the Baugh and Weedon PA1020 flaw detector a Krautkramer USM2 was used for these studies because of its higher output voltage and increased receiver sensitivity.

Figure 12 shows the crack tip echoes recorded with the compression probe at grazing incidence. A testing sensitivity of at least 50 dB above the back wall echo is necessary and there is no clear dependence on ΔK. The results for 45° shear waves incident from the near side are shown in Figure 13. For this angle the tip echoes are about 30 dB below the back wall echo and the effect of crack depth is more significant than the ΔK dependence.

To compensate for the decrease in probe sensitivity with depth, the echoes from 1.5 mm diameter side-drilled cylindrical holes at various depths were measured for each probe. Typical curves are shown in Figure 14. The crack tip echoes were then all related to the echo from a cylindrical hole at the same depth. Figures 15(a) and 15(b) compare the results obtained with the 45° and 70° 5 MHz probes when testing on the far and near surfaces respectively. In each case values below the dotted line correspond to the 45° probe. Similarly, Figures 16(a) and 16(b) compare the two 70° probes of 5 MHz and 10 MHz frequency.

Figure 15(a) and (b) show that smaller signals are obtained with the 45° probe than with the 70° probes. Also, for all the angle probes, smaller signals are obtained when scanning on the far surface than on the near surface. Coffey (1978) describes calculations by Wickham of the echoes to be expected from a planar, semi-infinite Griffith crack whose faces are just separated. Figure 17 compares the calculated amplitudes with those measured on the fatigue cracks. The theory predicts the experimental observation that with the probe on the far surface, echoes are smaller than when it is on the near surface. However, there is considerably less difference in the experimental values from the two faces than the theory predicts. This discrepancy probably occurs because the theory is for a perfectly smooth crack having no fine structure in the region of the crack tip. For example, when testing from the far surface, the 70° probes gave signals much bigger than those predicted and these increased signals may occur because micro-cracks on the fatigue crack surface cause extra scattering. In contrast to the crack corner echoes, the tip echoes show little dependence on the crack growth conditions. The scatter in signals from cracks of the same roughness but varying depth is as large as that from cracks of the same depth but different roughness. During fatigue growth a residual plastic zone is set up in the region of the crack tip (Knott 1973) and the size of this zone depends on ΔK. It has been suggested by Silk (1977) that crack tip echoes are determined by plastic deformation around the crack tip but our results indicate that the size of this plastic zone does not have a very significant effect on the crack tip echo.

5.2 The Effect of Stress

Following the investigations of the tip echoes under zero load, their responses under compressive and tensile loads were studied for angled shear waves. Axial loading was used for the compression tests whereas a three point bend arrangement was used to put the cracks in tension. On compression, the tip echoes decreased slowly but steadily up to a stress of about 40 MN m^{-2}, the maximum decrease being 3 dB. At higher stresses, the echoes were indistinguishable from the background noise. No change in amplitude occurred when the blocks were subjected to a tensile load.

5.3 The Effect of Liquid in the Cracks

All the results obtained so far were from clean, dry cracks. To evaluate the effect on the tip echoes of liquid in the cracks, some of the blocks were sprayed with a penetrating fluid, "Freeway", and left for several hours for penetration to occur, in some cases the cracks were put under a light tensile load to aid penetration. Only small changes of 1 to 2 dB occurred, which is within the experimental error. Consequently, although we cannot be certain that fluid had penetrated fully to the crack tip, it appears that the presence of liquid in a crack does not appreciably affect the amplitude of the crack tip echoes.

5.4 Sizing Accuracy

The accuracy of measuring the depths of cracks using various probes may be compared by reference to Figure 18. The ultrasonic measurements of crack depth are compared with those measured optically during the crack growth and with the direct measurements made after splitting open the cracks. Although the mean ultrasonic and the optical measurements are in reasonable agreement, there is considerable variation between the individual ultrasonic measurements. In particular, the sizing of the weld crack (Specimen G) was inaccurate when testing from the far surface, probably because the echo from a small defect in the weld was mistaken for the crack tip echo. From the results of Figure 18, and taking into account the relative ease with which the crack tip echoes may be identified, we conclude that for general use the 45° shear wave or the compression probe are to be preferred. The exception is that for cracks at short range the 70° 10 MHz probe gives the most reliable results. Because of its low sensitivity, however, this probe is not suitable for locating crack tips which are more than 10 mm below the testing surface.

5.5 Focussed Probes

Focussed probes offer the advantages of reduced beamwidths and increased power density in the focal region. To assess these potential benefits, some measurements were taken using focussed immersion probes. The blocks were supported in the jig above a water bath in such a way that no water could enter the cracks. By rotating the block, shear wave beams could be refracted at various angles in the steel. The separation of the 5 MHz 100 mm focal length probe from the block was adjusted so that the focal spot coincided with the position of the crack tip. To provide a comparison, the measurements were repeated with an unfocussed but otherwise identical probe. Figure 19 shows the crack tip echoes for compression waves "end-on" and for 45° shear waves, the appropriate reference echoes being the backwall and corner echoes respectively. At grazing incidence there is some advantage in using focussed probes, in particular the signal to grass ratio is improved by up to 10 dB. The results for 45° suggest that focussing is of little advantage, the only improvement being a slight increase in sensitivity.

6. WELD METAL

The growth rate of fatigue cracks in high quality mild steel welds is believed to be similar to that in the parent material (Maddox 1970). The presence of residual welding stresses or tiny slag inclusions, however, are likely to affect both the crack growth rates and the roughness of the crack surfaces. To investigate this three specimens were prepared containing

manual metal arc welds. The weld quality was checked using 10 MHz compression waves and 5 MHz angled shear waves; no defects greater than an equivalent flatbottomed hole size of 0.5 mm were detected.

Two specimens, K and L, were stress relieved by baking at 650°C for 4 hours and then cooling slowly. The third block, G, was left in the as-welded condition. When cracks were grown in these specimens at a ΔK of 20.7 MN $m^{-3/2}$, the growth rate was somewhat higher for block G than for K and L, and all three grew faster than the cracks in EN3B parent material. Figure 2(b) shows that the reciprocal crack growth rates for K and L were about 11,000 cycles/mm compared with about 20,000 cycles/mm for EN3B mild steel.

Figures 7(a - d) show that the zero load echoes from K and L are very similar to those obtained from cracks in mild steel. However, the echoes from block G are consistently smaller than those from K and L. Similarly, when an external compressive stress was applied, the decrease in signal for blocks K and L was close to that which occurred with cracks in parent material, whereas block G showed very small changes under load. These results suggest either that there is a residual compressive stress on crack G or that the surfaces are rougher than one would expect from its growth conditions.

After ultrasonic tests, block G was carefully stress-relived in an argon atmosphere and the zero load echoes re-measured. There was a relatively small increase of about 3 dB for 45° and 60° shear waves and a small decrease for 70° as shown in Figure 7. A similar control experiment performed with block E showed no detectable change in signal after stress relief. We conclude that any residual stress in block G had only a small effect on the corner echoes.

Finally block G was split open and measurement of the crack roughness gave an Ra value varying between 10 and 50 μm. The rms roughness was 35 μm which is slightly higher than that of the cracks grown at a K of 37 in mild steel. If the echoes from block G in Figures 7 (a - d) are re-plotted for an effective ΔK of about 40 to take account of the increased roughness, the disparity appears.

In conclusion, it appears that residual welding stresses in block G caused the subsequent fatigue crack to be rougher than cracks in stress-relieved welds or mild steel, and this in turn modified the ultrasonic response. Cracks grown in stress-relieved welds are not significantly different from those grown in parent material.

7. THE EFFECTS OF LIQUID IN THE CRACKS

There are many practical situations in which fatigue cracks are likely to be partly or totally filled with water or other liquid. In such a situation, if the crack separation is very much less than a wavelength, almost perfect transmission of compression waves may occur at normal incidence. As discussed in Appendix A, however, the behaviour of shear waves is very different and with angled shear waves, theory predicts results which are, at first sight, rather surprising. When the separation of the faces of a planar, liquid-filled crack becomes less than about a tenth of a wavelength, the reflection of shear waves decreases for angles of

incidence greater than the critical angle of 33° whereas there is an increase in reflection for angles less than the critical angle. A 45° probe gives an angle of incidence of 45° on a vertical crack so a decrease in reflectivity is expected with this probe when liquid is introduced. On the other hand 60° and 70° give incident angles of 30° and 20° respectively, so an increase is predicted in both these cases.

To investigate this experimentally, the cracks were put in tension by applying small loads in three-point bend and then sprayed with Freeway penetrating fluid. The acoustic impedance of this particular liquid was measured as $1.08 \pm 0.5 \times 10^6$ kg $m^{-2} s^{-1}$, but theory predicts that the reflection coefficients are sensitive to the impedance of the liquid and will be similar to those for water. Measurements of the corner echoes were made with the blocks under zero load and for compressive stresses up to 160 MN m^{-2}. The 45° probe results (Figure 20(a)) show an initial decrease at zero load of about 3 dB and the high stress values are reduced by rather more, particularly when the crack is smooth. The idealised model used in Appendix A predicts that the reflected signal at 45° incidence tends to zero for a very thin liquid gap, but the largest change observed was -9 dB. This should be compared with the variation caused by stress (up to 14 dB) or the effect of crack roughness on the zero load signal (about 10 dB).

The 70° probe results (Figure 20(c)) show only small changes at zero load but the high stress results are higher by up to 5 dB in the liquid-filled case. (This is consistent with the results of Appendix A which predict an increase of 3.3 dB for a thin wet gap compared with an air gap). The 60° probe (Figure 20(b)) gave larger variations. In particular, block D showed an initial decrease of 16 dB, but the value at maximum stress was 10 dB less than the air-filled case. Such a decrease is not consistent with the theory of Appendix A, but the discrepancy may be associated with the rapid variations in reflection coefficient with angle and the strong mode conversions which occur for angles of incidence close to 33°.

To summarise these results, it seems that introducing liquid into the cracks causes fairly small decreases in signal for 45° probes, either no change or a small increase for 70° probes and significant decreases in signal for 60° probes. The effect of introducing the liquid seems to be insensitive to the roughness of the crack faces.

8. DISCUSSION

8.1 Mechanisms Affecting the Echo Amplitudes

It is convenient at this point to summarise our understanding of the reflection of angled beams from cracks both at zero load and under compression, and to list some of the supporting evidence.

The zero load "corner echoes" comprise a direct shear wave corner echo which may be modified by interference with mode conversions occurring at the crack face or the bottom surface. The effect of these mode conversions is most pronounced for the 60° probes, less for 70° and least for 45° (Lumb et al 1978). They gave rise to a complicated variation of the echo amplitude with increasing defect depth which has been reported by several authors. These effects have been extensively studied by Baborovsky et al. (1975) and many of the observed effects in the far field may be predicted using their computer model. However, this semi-empirical model does not include the conversion of grazing incidence compression waves to shear waves and cannot fully represent the response of 60° probes.

The echoes may be further modified by the presence of multiple reflections set up in the gap between the crack faces. Appendix A describes our studies of energy partitioning at a parallel-sided fluid-filled gap which has been computed by summing the multiple reflections occurring at the interfaces. Complicated changes in the reflection coefficients are predicted which depend on the wave mode and angle of incidence, gap thickness and wavelength. Nevertheless, resonance effects are only likely to be significant for liquid-filled cracks. In the case of an air-filled gap, the separation at which appreciable resonance occurs is about a millionth of a wavelength, which is much smaller than the roughness of real surfaces.

When a crack is compressed, the dominant effect is a steady reduction in echo amplitude caused by the increase in actual area of solid contact between the crack faces. However, there are two processes in particular which may modify this response. Firstly, the direct shear wave echo is not necessarily reduced at the same rate as the various mode converted signals which interfere with it. Secondly, the stress distribution on the crack faces may be non-uniform, either because of local plastic deformation of the faces which occurred during crack growth or because the external loading is slightly mis-aligned. The experimental evidence suggests that for low stresses, the tip region is usually under more stress than the open end. This means that as far as the ultrasonic probe is concerned, the effective crack depth is progressively reduced as the stress increases. Consequently, the echoes show an oscillation similar to those observed for cracks or slots of varying depth.

Experimental evidence supporting these mechanisms is as follows:-

1. All the potential drop measurements indicated a steady decrease in signal as the stress increased from zero (e.g. Figure 9(a)). This indicates that at least part of the crack closes even for very low loads.

2. Changing the position of the blocks between the platens of the hydraulic press affected the load at which significant signal changes occurred. In particular if the crack was "pinched" by positioning the block off-centre with the crack towards the centre (Figure 10(c)), the signal decreased more rapidly for the same load.

3. The responses of liquid-filled cracks under compression are very similar to those of similar dry cracks under the same loading conditions. Peaks in the response occur for the same load. This suggests that resonance effects are of minor importance even for liquid-filled cracks and that they are not the main cause of those peaks in the response which also occur for dry cracks.

8.2 Applicability of the Results

The experiments described in the preceding sections have confirmed our original hypothesis that crack growth conditions have a very pronounced effect on the response of cracks. The value of growing cracks at constant ΔK has also been indicated. Although the ultrasonic measurements were made on surface-breaking cracks, the results should also be a guide to the sensitivity required of tandem and Delta-scan techniques for detecting planar embedded defects. The pulse-echo

measurements of crack tips are relevant to sizing any kind of fatigue crack, whether embedded or surface-breaking. Our results have indicated that the Ra value of cracks grown in EN3B mild steel increases steadily with ΔK, but more information about the roughness of fatigue cracks in other materials would be desirable. Manning (1979) has measured Ra values for constant load fatigue cracks in carbon-manganese pressure vessel steel, stainless steel and mild steel weld metal. Because of the continuous gradation in roughness along these cracks, an exact comparison with our results is not possible, but his results which are for ΔK values in the range 5-30 MN $m^{-3/2}$ are in reasonable agreement with our mean line OP in Figure 4(a).

8.3 The Effect of Residual Compressive Stress on Fracture Mechanics Predictions

The results described in this report have shown that the size of the ultrasonic echoes obtained from fatigue cracks depends strongly on the net compressive stress. Engineering components may have regions which although subject to tensile stress when operating, are in compression under shut-down conditions. Such regions may be subject to fatigue during operation but any cracking may be difficult to detect when off-load and this must be taken into account when specifying the inspection procedure.

Whereas it is normally possible to calculate stresses caused by changes in the operating conditions of plant, residual stresses, particularly in welds and castings, are usually variable and largely unknown. Although residual compressive stresses will lead to defects being undersized by ultrasonics, such stresses also reduce the likelihood of fatigue crack growth. In this part of the discussion we consider how this affects the validity of fracture mechanics predictions based on the apparent size of defects.

If the crack tip echoes are detected and used to size a large crack, compressive stresses may make this procedure very inaccurate, if not impossible. However, if the crack is viewed near normal incidence and is small enough for amplitude sizing techniques to be used, the situation is much more encouraging. The error in sizing the defect will cause the calculated stress intensity factor at the crack tip to be an underestimate. However, because of this residual stress, the peak tensile stress in service is less than that used to predict the crack growth rate which is normally based on zero residual stress. Consequently, the two effects oppose each other. In the one case which has been fully analysed using the apparent defect size and assuming zero residual stress, we derived a higher predicted growth rate than would be predicted using the true values for residual stress and defect size. Consequently, in this case the fracture mechanics predictions err on the safe side but we cannot necessarily assume that this will always be true.

8.4 The Importance of Stress Analysis to the Design of Inspections

We have seen that both increasing crack roughness and increasing compressive stress reduce the specular reflection from fatigue cracks. Decreases of up to 10 dB may be caused by crack roughness while large compressive stresses may cause decreases of up to 20 dB. Fortunately the two effects are not cumulative since the roughest cracks show little variation with stress. It is particularly important in the case of smooth, high-cycle fatigue cracks to detect the specularly

reflected signals by appropriate choice of the beam angle since the diffuse scattering is weak. In some cases it may be possible to compensate for the effects of misorientation and compressive stress by increasing the test sensitivity. However, this approach will be limited in practice by the number of insignificant inclusions which give ultrasonic echoes of similar amplitude. It then becomes extremely difficult to distinguish cracks from other permissible defects. If the most favourable beam angles and scanning directions are to be chosen for in-service inspections, stress analysis studies must be carried out in advance to predict the likely orientations of crack growth. Realistic estimates of crack growth rates (i.e. roughness) and compressive stresses are also desirable if the complexity and expense of inspections is to be kept within reasonable limits. Excessively pessimistic estimates of these variables may result in ultrasonic recording levels which are very expensive, if not impossible, to achieve in practice.

9. CONCLUSIONS

1. The growth conditions of fatigue cracks have a significant effect on their ultrasonic response, both at zero load and when under compressive stress. The stress intensity factor, K, during crack growth correlates well with the roughness of the fatigue crack surfaces and this is believed to cause the changes in ultrasonic response.

2. Both increasing crack roughness and increasing compressive stresses reduce the specular reflection from fatigue cracks. Decreases of up to 10 dB may be caused by crack roughness while large compressive stresses may cause decreases of up to 20 dB. However, the two effects are not cumulative as the roughest cracks show little variation with stress. To some extent it may be possible to compensate for these effects by increasing the test sensitivity, but this will be limited in practice by the number of insignificant inclusions which give ultrasonic echoes similar in amplitude to those from cracks.

3. If echo amplitude comparison techniques like DGS are used, then variations in compressive stress or crack roughness will lead to appreciable sizing errors. The reduced response may also result in defects being missed entirely if an echo amplitude threshold is used to define recordable defects.

4. Crack tip echoes are small; typically they are 50 dB down on a back wall echo at the same range when using a compression wave probe at grazing incidence, and they are practically impossible to identify if the cracks are in compression or if the material contains other defects such as inclusions.

5. The errors in sizing cracks in clean material by detecting the tip echoes are typically $\pm$ 1 mm if averaged for several probes. Individual readings, however, may be in error by several millimetres. When testing from the crack-breaking surface, the values of crack depth are usually slightly less than those recorded when testing from the opposite surface.

6. The presence of liquid in a crack causes a marginal increase in reflection for shear wave beams incident at 20° to the crack normal. Modest decreases in reflection occur for beams incident at 45°, while considerable decreases are likely at 30° incidence.

7. Although compressive residual stresses may lead to cracks being undersized, fracture mechanics predictions of growth rates may nevertheless be conservative because these stresses reduce the resultant stress intensity at the crack tip.

10. RECOMMENDATIONS

1. When designing inspections to detect high cycle fatigue cracks the orientations of the ultrasonic beams relative to the likely directions of crack growth should be such that the specularly reflected waves are detected. Realistic estimates of crack growth directions and compressive stresses during testing are necessary if reliable and cost-effective inspections are to be achieved.

2. Sizing using crack tip echoes should only be relied upon if the region of the crack tip is known to be unstressed or under tension.

3. The ultrasonic responses and surface profiles of fatigue cracks should be measured for a wide range of ΔK and R values so that the dependence of the crack roughness on the growth conditions can be firmly established. This should be repeated for several materials with different values of yield stress using both parent plate and weld metal.

11. REFERENCES

V.M. Baborovsky, E.A. Slater, D.M. Marsh, 1975
The response of ultrasound to defects.
Ultrasonics International 1975.

L.M. Brekhovskikh, 1960
Waves in layered media.
Academic Press N.Y. 1960.

Chang, F.H.S. Couchman, J.C. Yee, B.G.W. 1973.
The Effects of stress on the detection of fatigue cracks by ultrasonic techniques.
Proc. 9th Symp. on NDE. San Antonio, April 1973, 424-433.

Coffey, J.M. 1978.
Quantitative Assessment of the reliability of ultrasonics for detecting and measuring defects in thick-section welds.
Proc. Conf. on "Tolerance of Flaws in Pressurised Components",
Inst. Mech. Eng. 16-18 May 1978, London.

Elber, W. 1970.
Fatigue crack closure under cyclic tension.
Eng. Frac. Mech. Vol. 2 1970, 37-45.

Elber, W. 1971.
The Significance of Fatigue Crack Closure.
Damage Tolerance in Aircraft Structures ASTM STP 486, 1971, 230-242.

A.F. George, 1978.
A Guide to the Statistical analysis of surface profiles.
C.E.G.B. Report - RD/B/N3932.

J.A. Greenwood, 1967
The area of contact between rough surfaces and flats.
Trans. of the ASME. Jnl. of Lubric. Technol. January 1967.

N.F. Haines, 1980
The theory of sound transmission and reflection of contacting surfaces
C.E.G.B. Report RD/B/4744.

Kendall, K. Tabor, D. 1971
An Ultasonic Study of the area of contact between stationary and sliding surfaces.
Proc. Roy. Soc. Lond. A. 323. 321-340.

J.F. Knott, 1973.
Fundamentals of Fracture Mechanics.
Butterworths 1973.

R.F. Lumb, H. Bosselaar, V.M. Baborovsky, 1978.
Ultrasonic Inspection of seamless drill casing and line pipe.
Mat. Eval. Vol. 36. No. 10 1978.

S.J. Maddox, 1970.
Fracture Mechanics applied to fatigue in welded structures.
Conf. on Fatigue of welded structures - Cambridge 1970.

REFERENCES (CONT'D)

P.T. Manning, 1979.
The surface topography of some fatigue crack surfaces.
C.E.G.B. Report RD/B/N4570, 1979.

M.G. Silk, 1977.
The transfer of ultrasonic energy in the geometry of the diffraction technique for crack sizing.
Harwell Report No. AERE R8665.

J. Schijve, 1979.
Four lectures on fatigue crack growth.
Eng. Frac. Mech. Vol. 11 pp. 167-221 - 1979.

A.T. Stewart, 1978.
Fatigue cracking in the rotor of a 500 Megawatt alternator.
C.E.G.B. Research No. 8, 1978.

T. Tsukizoe, T. Hisakado 1968.
On the mechanism of contact between metal surfaces : Part 2 - The real area and the number of contact points.
Trans. of the ASME Jnl. of Lubric. Tech. Jan 1968.

A.B. Wooldridge, 1979.
The effects of compressive stress on the ultrasonic response of steel-steel interfaces and of fatigue cracks.
C.E.G.B. Report No. NW/SSD/RR/42/79.

B.G.W. Yee, J.C. Couchman and F.H. Chang, 1976.
Resonance effects on energy coefficients for ultrasonic interactions with thin gap discontinuities in titanium.
Materials Evaluation - November 1976.

12. ACKNOWLEDGEMENTS

The authors gratefully acknowledge the advice and guidance received from colleagues in both the Non-Destructive Testing and Fracture Mechanics Sections at N.W. Region S.S.D. Particular thanks are due to Dr. J.M. Coffey for his helpful suggestions and critical reading of the manuscript and to Mr. A. George of Berkeley Nuclear Laboratories who measured the power spectra of the fatigue cracks.

APPENDIX A

REFLECTION AND TRANSMISSION COEFFICIENTS FOR ULTRASONIC WAVES AT A FLUID-FILLED THIN GAP IN A SOLID MEDIUM

If the two surfaces of a fluid-filled crack are not actually touching, we may model them by two planar parallel interfaces separated by a fluid medium. As shown in Figure A1, when shear waves are incident on the first interface from the solid there will be, in general, reflected shear and compression waves and a transmitted compression wave in the fluid. Each time this compression wave is reflected in the gap it gives rise to shear and compression waves in the solid media. The reflection and transmission coefficients for a fluid gap may be derived by summing the infinite series for each type of wave. For example, the coefficient for incident shear waves reflected as shear waves is given by:-

$$R_s = r_{12} + \frac{t_{12}\ r_{23}\ t_{21}}{\{\exp(-i.2\pi p) - r_{23}\ r_{21}\}}$$

where the reflection and transmission coefficients depend on the angle of incidence and are, in general, complex. (Born and Wolf 1975).

r_{12} = Reflection coefficient for shear waves at boundary 1→2.

r_{23} = Reflection coefficient for compression waves at boundary 2→3.

t_{12} = Transmission coefficient for incident shear waves in medium 1 converted to compression waves in medium 2.

t_{21} = Transmission coefficient for compression waves in medium 2 converted to shear waves in medium 1.

and $p = \frac{2t \cos\beta}{\lambda}$ where t = gap thickness.

λ = wavelength of compression waves in fluid.

β = angle of refraction in fluid.

R_s has been evaluated using plane wave solutions for r_{12}, t_{12}, etc., which are derived directly from the elastic wave equation (Brekhovskikh 1960). Since R_s may be complex, the results have been plotted in terms of the reflected flux, FREF, where FREF = $(R_s)^2$. Figure A2 shows the reflected flux as a function of the incident shear wave angle for a water gap in steel whose thickness equals one wavelength. Similarily, Figure A3 shows the reflected flux for a gap of $\lambda/100$ while Figure A4 shows both the reflected and transmitted flux for a gap of vanishing thickness. As the gap thickness tends to zero, FREF falls to zero for incident angles close to 45^o, but for angles less than the critical angle of 33^o, FREF increases. If the gap contains air rather than a liquid, the gap separation would have to be extremely small before any change in FREF occurred. This is because of the very large impedance difference between a solid and air. Figure A5 shows FREF for gaps of $10^{-4}\lambda$ and $10^{-6}\lambda$ and it is only when the gap approaches $10^{-6}\lambda$, that a marked change occurs. Such a gap is extremely small, being of the order of a nanometer for 4 MHz waves in air. Consequently, since even surfaces which are optically flat will have a roughness several orders greater than this, any surfaces which are realised in practice will have their

high points in contact long before a mean separation of $10^{-6}\lambda$ is achieved. In the limit, for a fluid gap of vanishing thickness, the impedance of the fluid becomes irrelevant and the reflection and transmission coefficients shown in Figure A4 are the same as those of a steel to steel boundary with slip.

The reflection coefficients for incident compression waves reflected in the same mode are less complicated. Figure A6 shows the corresponding FREF for an infinitely thin fluid gap in steel. However, as mentioned above, such a thin gap is only achievable in practice for a liquid-filled gap and not for an air-filled one. For comparison, Figure A6 also shows the reflection coefficients for compression waves at a single steel-water or steel-vacuum interface corresponding to the case of an infinitely wide gap.

The results of Section 4 indicated that with 70° and 60° probes, the corner echoes often increased temporarily with loading. For a liquid-filled gap, this effect could be attributed to the increase in the reflection coefficients for 20° and 30° incidence angle which should occur as the crack closes before there is appreciable solid contact between the sides of the crack. However, if this were the case, the theory also predicts that in the case of an air-filled crack, solid contact would occur long before the reflection coefficient increased and this conflicts with the experimental results. Note that stringent precautions were taken to keep the cracks dry. Consequently we believe that the explanation for the increase in signal is mainly due to changes in the stresses on the crack face as described in Section 8.1 rather than to resonance effects occurring before the crack closes.

APPENDIX B

THE RELATIONSHIP BETWEEN THE ULTRASONIC PROPERTIES AND THE STIFFNESS OF CONTACTING ROUGH SURFACES

In this appendix we consider the mechanism by which sound is transmitted through a compressed crack and attempt to explain the observed variations in reflectivity with applied load. A theory is, as yet, only available for normal incidence and this is described in the first part, while the second part describes our attempt to extend the theory for the case of angled incidence.

B1. Normal Incidence

When nominally flat metal surfaces are in contact, the true area of contact is much less than the geometric area. The true area increases with the load applied and consequently we expect the ultrasonic reflection coefficient to decrease steadily with increasing load. However the rate of decrease with load is likely to depend on the roughness of the surfaces and the frequency, wave mode and angle of incidence. Most of the experiments described in this report involve angled beams of shear waves whereas the only theoretical results available at present are applicable to normal incidence compression waves. Consequently further experiments were carried out using compression waves incident normally on the fatigue cracks to enable a realistic comparison with theory to be made.

Kendall and Tabor (1971) have shown that in the case of compression waves at normal incidence, the reflection coefficient may be expressed in terms of an effective "stiffness" of the interface. Their deviation assumes that the ultrasonic wavelength is much greater than the spacing between the contacting asperities so that diffuse scattering may be ignored and the stress conditions caused by the ultrasonic waves will vary quasi-statically. The stiffness, S, of the interface between two contacting rough surfaces is defined as the ratio of incremental load to incremental displacement and this determines the change in separation of the surfaces caused by an incident acoustic wave. Kendall and Tabor show that the reflection coefficient, R, may be written thus:-

$$R = \frac{a/S}{\sqrt{1 + a^2/S^2}} \qquad B1$$

where $a = \frac{1}{2} A_o \omega Z = \frac{1}{2} A_o \frac{\omega E}{c}$

a	=	constant, units of stiffness
A_o	=	geometric area of contact
ω	=	ultrasonic angular frequency
Z	=	acoustic impedance
E	=	Young's modulus
c	=	compression wave velocity

The stiffness, S, depends on the number of contracting asperities, N, and the mean radius of the contacts, $\bar{r}$. Kendall and Tabor show that the stiffness of isolated elastic contacts is proportional to N and $\bar{r}$. In general, both elastic and plastic deformation occurs but after the first loading cycle the deformation will be predominantly elastic. Both N and $\bar{r}$ depend on the roughness of the surfaces and will vary with the applied stress. However it is empirically established that the real area of contact, a_c, between two surfaces is proportional to the applied stress.

we may write $$\frac{a_c}{A_o} = \frac{\sigma}{\sigma_p}$$

where σ_p, the flow stress, is approximately constant for a particular material. Greenwood (1967) showed that this proportionality is to be expected whatever the mode of deformation of the asperities if the distribution of surface heights is exponential. This conclusion is only slightly modified for a Gaussian distribution.

But $$a_c = N\pi\bar{r}^2$$

$$\therefore \frac{A_o\sigma}{\sigma_p} = N\pi\bar{r}^2$$

$$\therefore S \propto \frac{A_o\sigma}{\pi\sigma_p\bar{r}}$$

i.e. $$S = m\,.\,\frac{\sigma}{\bar{r}} \qquad m = \text{constant}$$

The variation of N and $\bar{r}$ with applied stress has been investigated by Tsukizoe and Hisakado (1968) and more recently by Haines (1980) using a particular model for the contacting rough surfaces. They predict that N will vary much more rapidly than $\bar{r}$ because as the compressive stress increases, more small points of contact are continuously created so that the mean radius remains nearly constant. A previous report (1979) describes experiments on machine-ground blocks using compression and shear waves at normal incidence. Haines has shown that these experimental results are in good agreement with those derived theoretically provided one assumes that the true rms roughness of the surfaces is considerably greater than that measured with the profilometer.

In view of the small changes predicted for $\bar{r}$, we expect the stiffness to vary approximately as

$$S = k\sigma^n$$

where the exponent, n, is close to unity and k is a constant. Substituting in equation B1,

$$R = \left\{1 + \frac{k^2\sigma^{2n}}{a^2}\right\}^{-\frac{1}{2}} \quad \ldots\ldots\ldots \text{B2}$$

Then $$\text{Log}\left\{\frac{1}{R^2} - 1\right\} = 2n \log \sigma + 2 \log \left(\frac{k}{a}\right)$$

Consequently using a logarithmic plot of $(\frac{1}{R_2} - 1)$ and the best fit value of n may be found. The experimental results for normal incidence compression waves using machine ground surfaces fitted a relationship of the form $S = k\sigma^{0.5}$ at low stresses although at higher stresses the exponent was closer to 0.7. The theoretical transmission and reflection curves for $S = k\sigma^{0.5}$ are shown in Figure B1. To test the theory for normal incidence compression waves on a fatigue crack, Block E was modified to allow an ultrasonic beam to strike the crack at normal incidence. A slot was milled in one end so that various ultrasonic probes could be inserted in the slot while the block was under compression. The slot was sufficiently far from the fatigue crack that it was not expected to modify the stress distribution on the crack significantly. Absolute values of the reflectivity could not be obtained because the crack only partially filled the beam, but we were primarily interested in the variation with load. Figure B2 shows the experimental results for log R obtained with 10 MHz compression waves together with the theoretical curve derived from equation B2. The value of b^2 has been chosen as 9 MN m^{-2} so that the theoretical and experimental curves match at the -3 dB point.

Although Kendall and Tabor's theory was derived for compression waves Haines has suggested that it may be modified to predict the behaviour of normal shear waves if we define the "shear stiffness" as:-

S_{shear} = increment in shear force/increment in shear displacement.

Then a relation of the same form as equation B2 may be obtained where Young's modulus and the compression wave velocity are replaced by the shear modulus and shear velocity respectively. Assuming that $S_{shear} = K_1 \sigma^{\frac{1}{2}}$, good agreement with experimental results for 2.25 MHz shear waves was obtained. This is shown in Figure B3 where, as before, the two curves have been matched at the -3 dB point giving $b^2 = 15.6$ MN m^{-2}.

B2. Angled Incidence

Most of the experiments described in this report were carried out using angled shear waves and we have as yet no plausible theoretical model to describe the observed behaviour. However we have found that a good fit to the experimental data may often be obtained using equation B2 with an appropriate value for the exponent n. For block L, n was found to lie in the range 1.4 to 2.1. As an example, Figure B4 shows the Δ-Scan reflection coefficient for block L and the semi-empirical curve with $n = 1.5$ and $b^{2/3} = 25$ MN m^{-2}).

The table below lists values of the exponents obtained with blocks E, L and F using various beam angles and methods of loading.

Block	Probe Angle	Frequency (MHz)		Loading	Value of Exponent n
E	45°	4.0	shear	axial	.55 ± .1
	0°	2.25	shear	axial	.48 ± .1
	45°	4.0	shear	3 point bend	.5 .9
	0°	5.0	comp-ression		.3 .5
L	45°	4.0	shear	axial	1.4 1.8
	Scan	4.0		axial	1.5
	45°	4.0	shear	3 point bend	2.1 ± .2
	0°	2.25	shear		1.7
	0°	10	comp-ression		.9 1.8
F	45°	4.0		axial	3.6
	60°	4.0		axial	1.6

Where two values of n are given, a pronounced change in slope was observed for intermediate stresses and the first value corresponds to low stress. There is clearly a wide variation in the value of n but the values for block E (5 mm deep) are consistently less than for L and F which were 12 and 15 mm deep respectively. We have no convincing explanation for the occurrence of high values of the exponent, but one possibility is that because of the similarity between the mating fatigue crack surfaces, the number of contact points increases more rapidly than for two random surfaces.

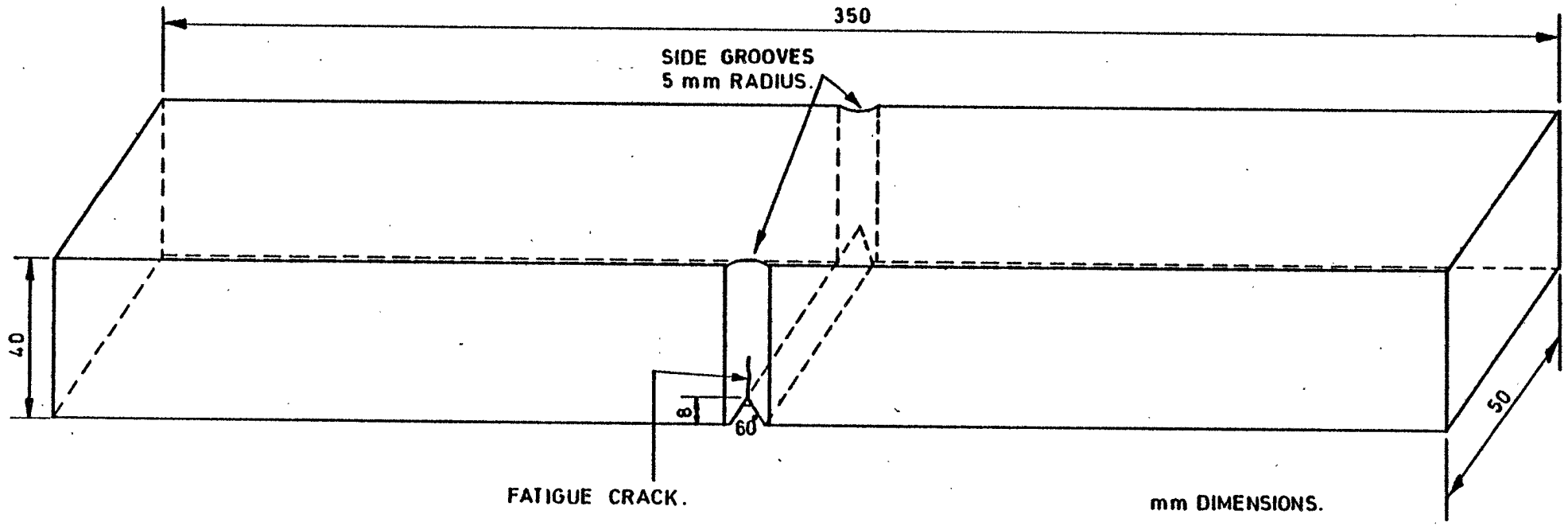

FIG.1(a). INITIAL FATIGUE CRACK SPECIMEN.

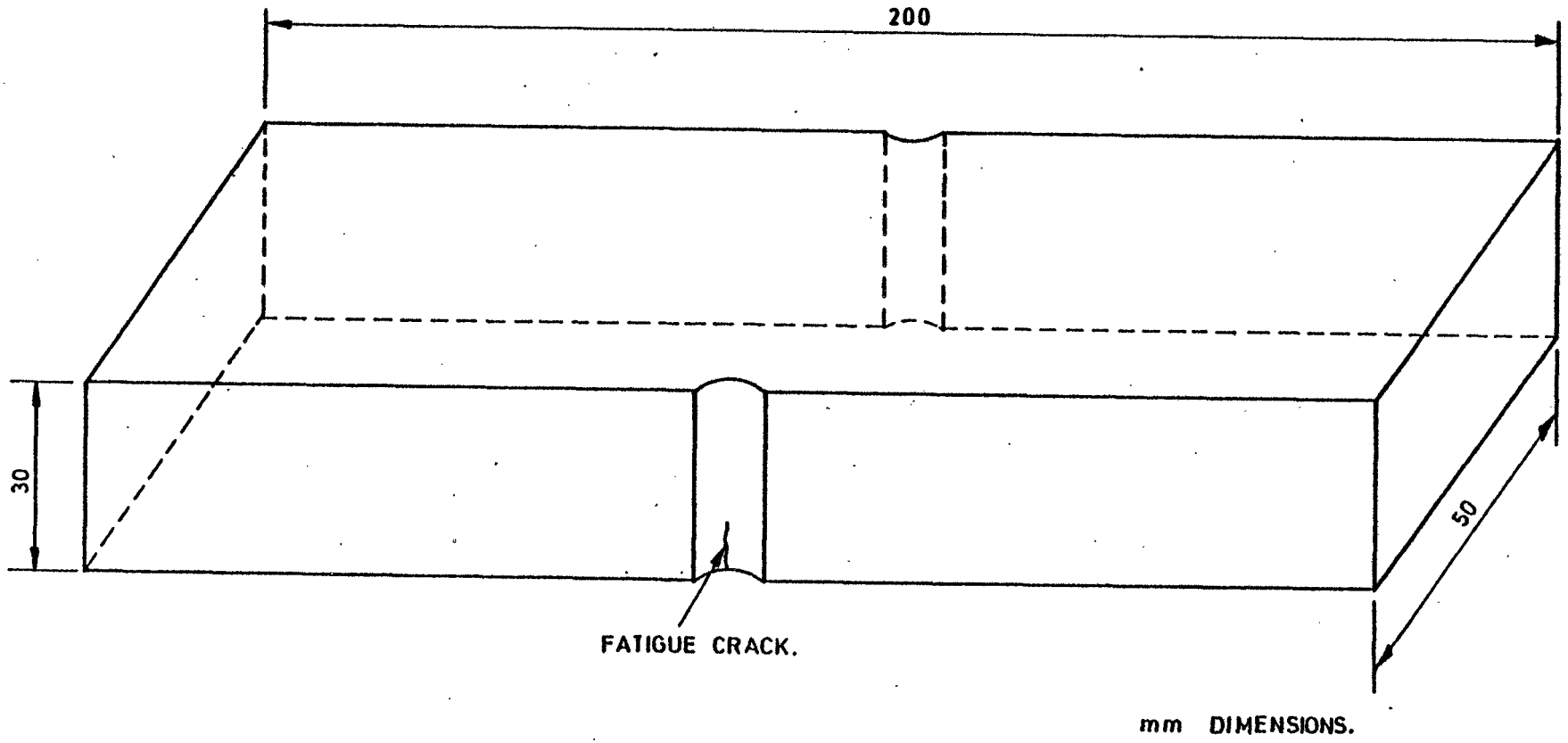

FIG. 1(b). FATIGUE CRACK SPECIMEN AFTER REMOVAL OF STARTER NOTCH.

BLOCK No.	NUMBER OF FATIGUE CYCLES	CHANGE IN CRACK DEPTH (mm)	NUMBER OF CYCLES (PER mm)	CALCULATED ΔK ($MNm^{-3/2}$)	R VALUE K MIN / K MAX.	Ra (μm)	rms ROUGHNESS (μm)
B	5,600	0 → 7·0	800	62·1	·03 → ·05		
D	24,600	0 → 7·5	3275	37·2	·05 → ·08	20	35
I	46,000	0 → 11·9	3870	37·2	·10 → ·19		
E	116,000	0 → 7·0	16,570	20·7	·16 → ·22		
F	112,000	0 → 7·0	16,000	20·7	·16 → ·22	10	18
	28,000	6·0 → 10·0	6,625	27·4	·18 → ·24	12	19
	42,200	10·0 → 15·0	8,608	24·6	·24 → ·32	10	
J	133,000	0 → 7·0	19,000	20·7	·16 → ·23		
				37·2 FOR 10 CYCLES			
	30,000	7·0 → 8·0	30,000	20·7	·14 → ·26		
	75,000	8·0 → 12·0	18,750	20·7	·29		
G (WELD)	55,000	0 → 5·6	9,820	20·7	·16 → ·21	10 → 50	39
K (WELD)	86,000	0 → 7·4	11,622	20·7	·16 → ·22		
L (WELD)	109,000	0 → 9·7	11,237	20·7	·16 → ·22		
	6,000	9·7 → 14·0	(SUDDEN JUMP)				

FIG. 2(a) CRACK GROWTH CONDITIONS FOR EACH SPECIMEN.

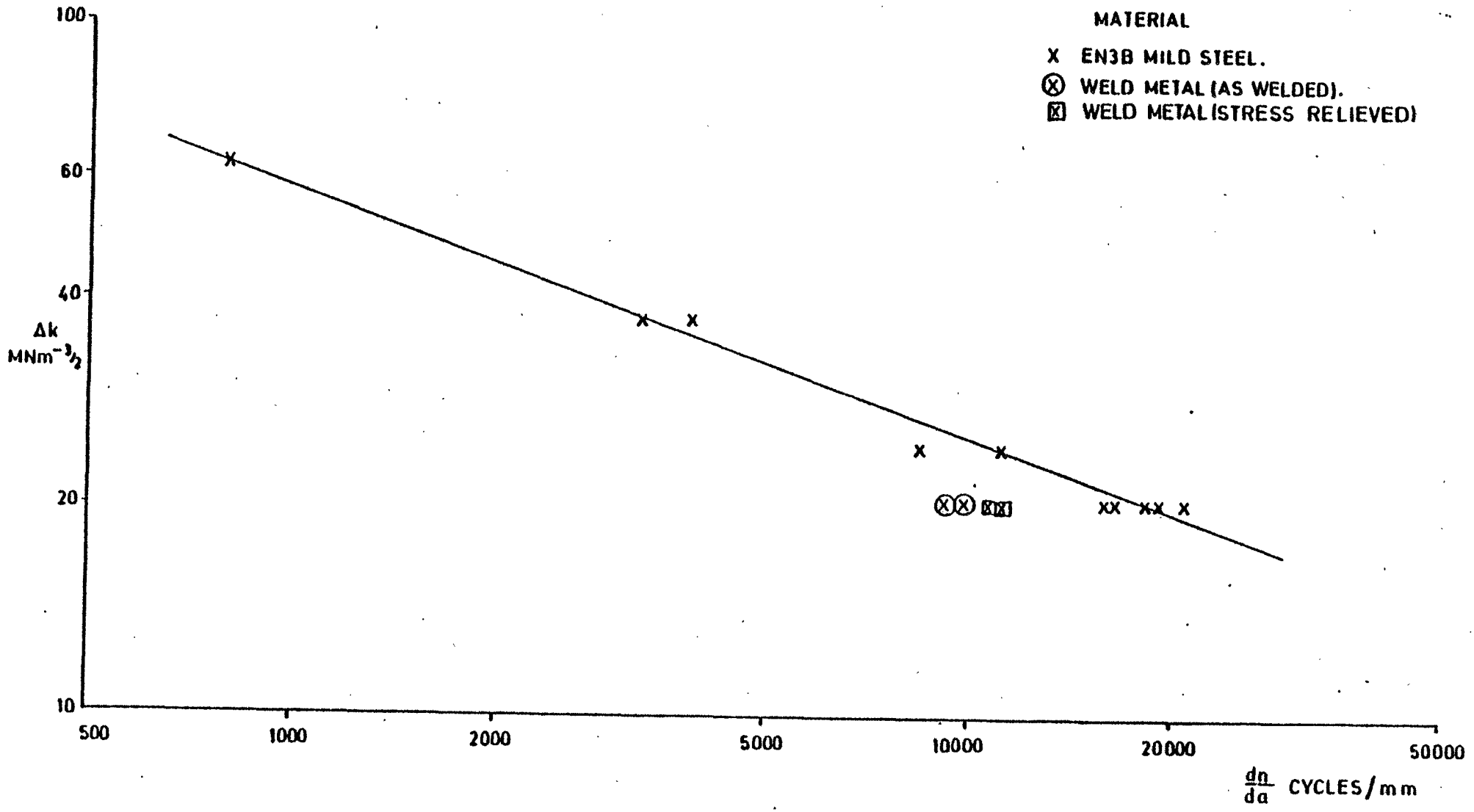

FIG. 2(b). STRESS INTENSITY FACTOR Δk VERSUS RECIPROCAL CRACK GROWTH RATE.

RC/SSR/A4/1562

MATERIAL : EN3B COLD ROLLED

CHEMICAL ANALYSIS (% BY WEIGHT).

C	S	P	Si	Mn	Ni	Cr	Mo	V
·16	·02	·02	·18	·73	·15	·14	<0·1	<0·1

VICKERS HARDNESS Hv 30 = 170

ULTIMATE TENSILE STRENGTH 570 MNm^{-2} (ESTIMATED)

YIELD STRESS 370 MNm^{-2} (ESTIMATED)

MICROSTRUCTURE: EQUI-AXED FERRITE GRAINS AND PEARLITE.
MEAN GRAIN DIAMETER 30 μm.

FIG. 3(a). METALLURGICAL PROPERTIES OF THE FATIGUE SPECIMENS.

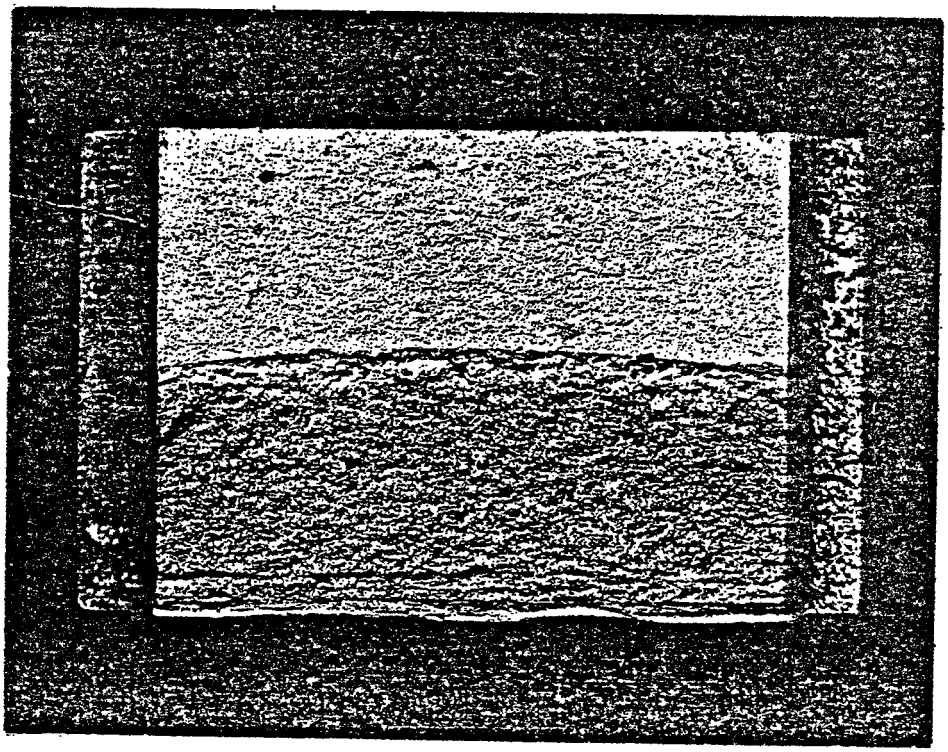

Berkeley (Keith Priddle)

TEST 1 — FC1
TEST 3 — FC2
A533B

K52 - 3
K50 4
K16 5
K51 6
K46 7
K48 8

FIG. 3(b) THE SURFACE OF FATIGUE CRACK F

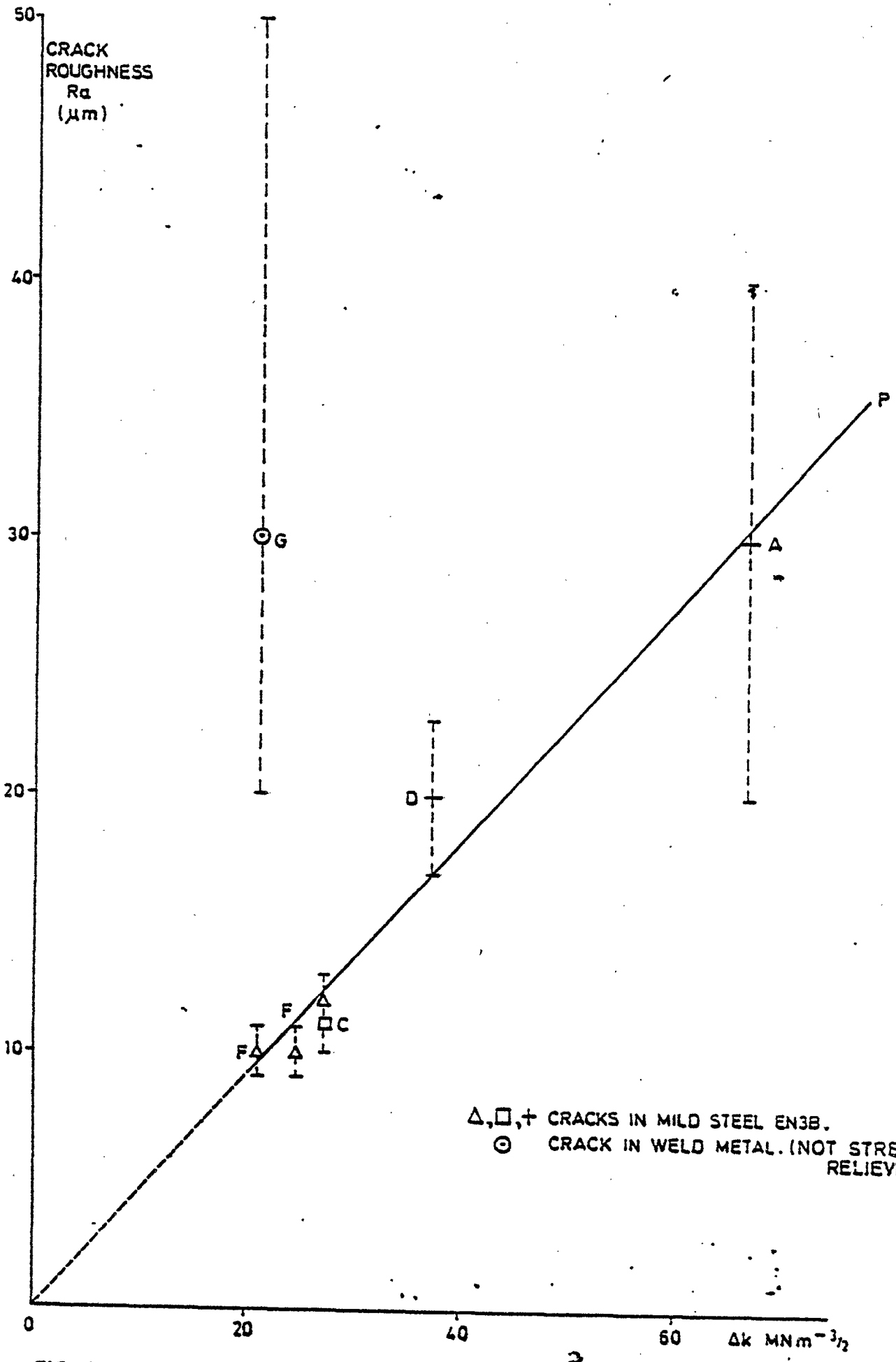

FIG. 4(a) STRESS INTENSITY FACTOR Δk VERSUS CRACK ROUGHNESS.

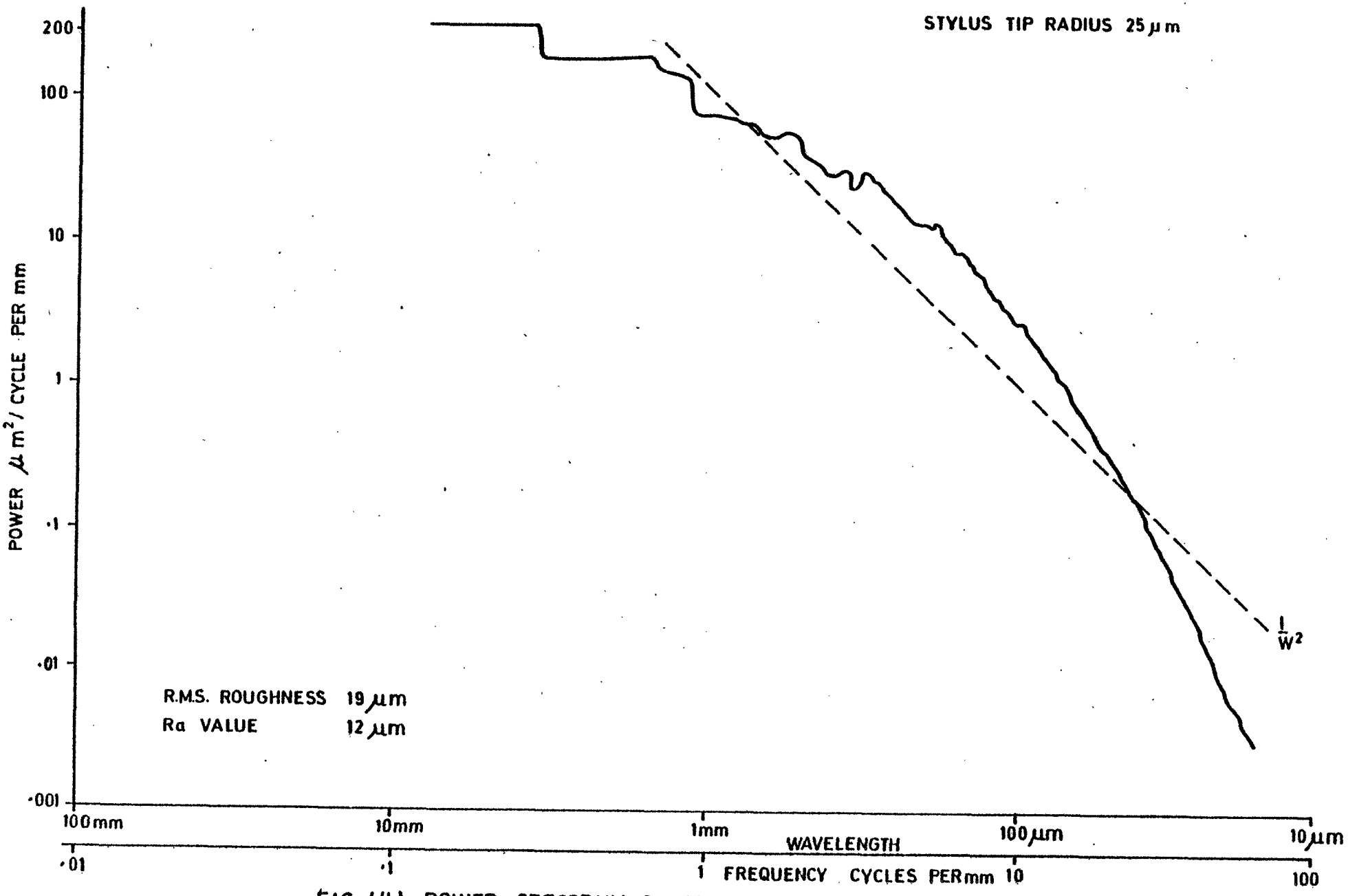

FIG. 4(b). POWER SPECTRUM OF FATIGUE CRACK SURFACE F.

RC/SSR/A4/1781

	PROBE ANGLE	MAKE	FREQUENCY (MHz)	CRYSTAL DIAMETER (mm)	ECHO FROM RADIUS AT 40mm RANGE .
CRACK CORNER ECHOES	45°	MATEVAL (B-SCAN)	4	10·0	44 db .
	60°	MATEVAL (B-SCAN)	4	10·0	44 db
	70°	SONATEST	5	10·0	48 db
	0°	PANAMETRICS V109	5	12·7	
CRACK TIP ECHOES	45°	PANAMETRICS	5	6·4	
	70°	PANAMETRICS	5	15·9 UNFOCUSSED	
	0°	PANAMETRICS	5	15·9 FOCAL LENGTH 100mm	
	0°	W·K·K·	10	6·4	
	70°	MATEVAL (B-SCAN)	4	10·0	

FIG 5(a) PARAMETERS OF ULTRASONIC PROBES USED FOR CORNER AND TIP ECHOES.

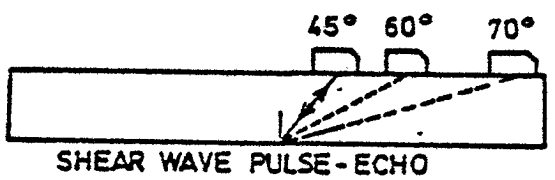

SHEAR WAVE PULSE-ECHO

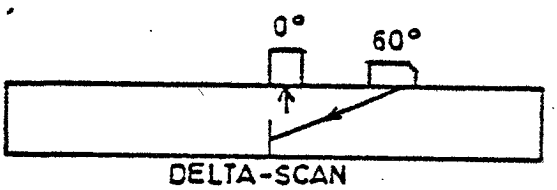

DELTA-SCAN

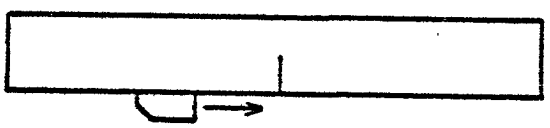
SURFACE WAVE PROBE

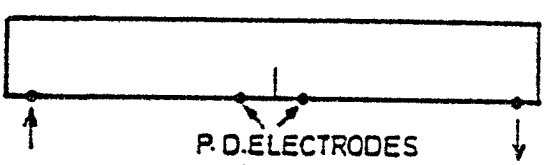

POTENTIAL DROP ARRANGEMENT.

FIG 5(b) ULTRASONIC PROBE ARRANGEMENTS

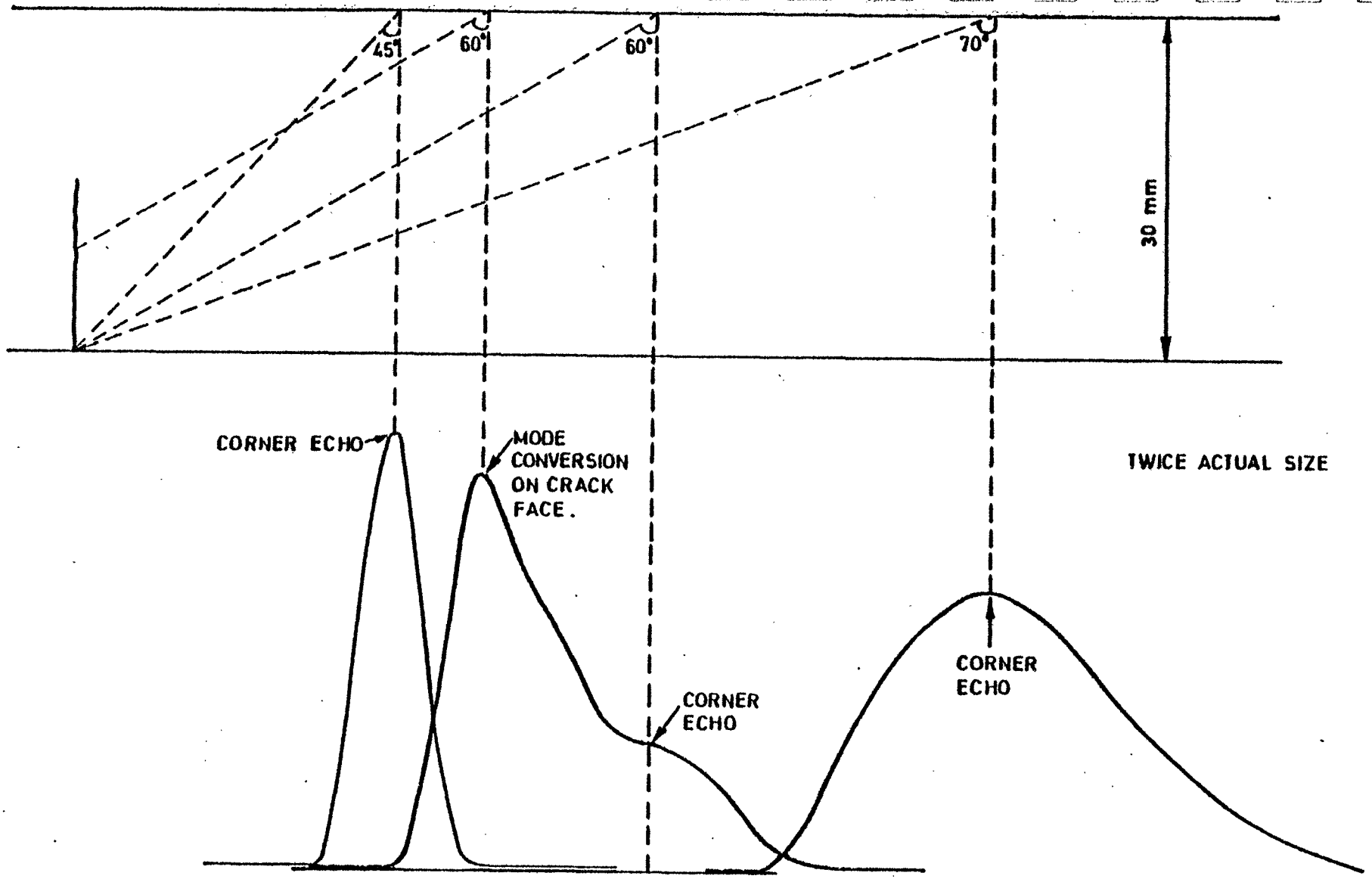

FIG. 6. CORNER ECHOES OBTAINED BY SCANNING CRACK F (15 mm DEEP).

RC/SSR/A4/156

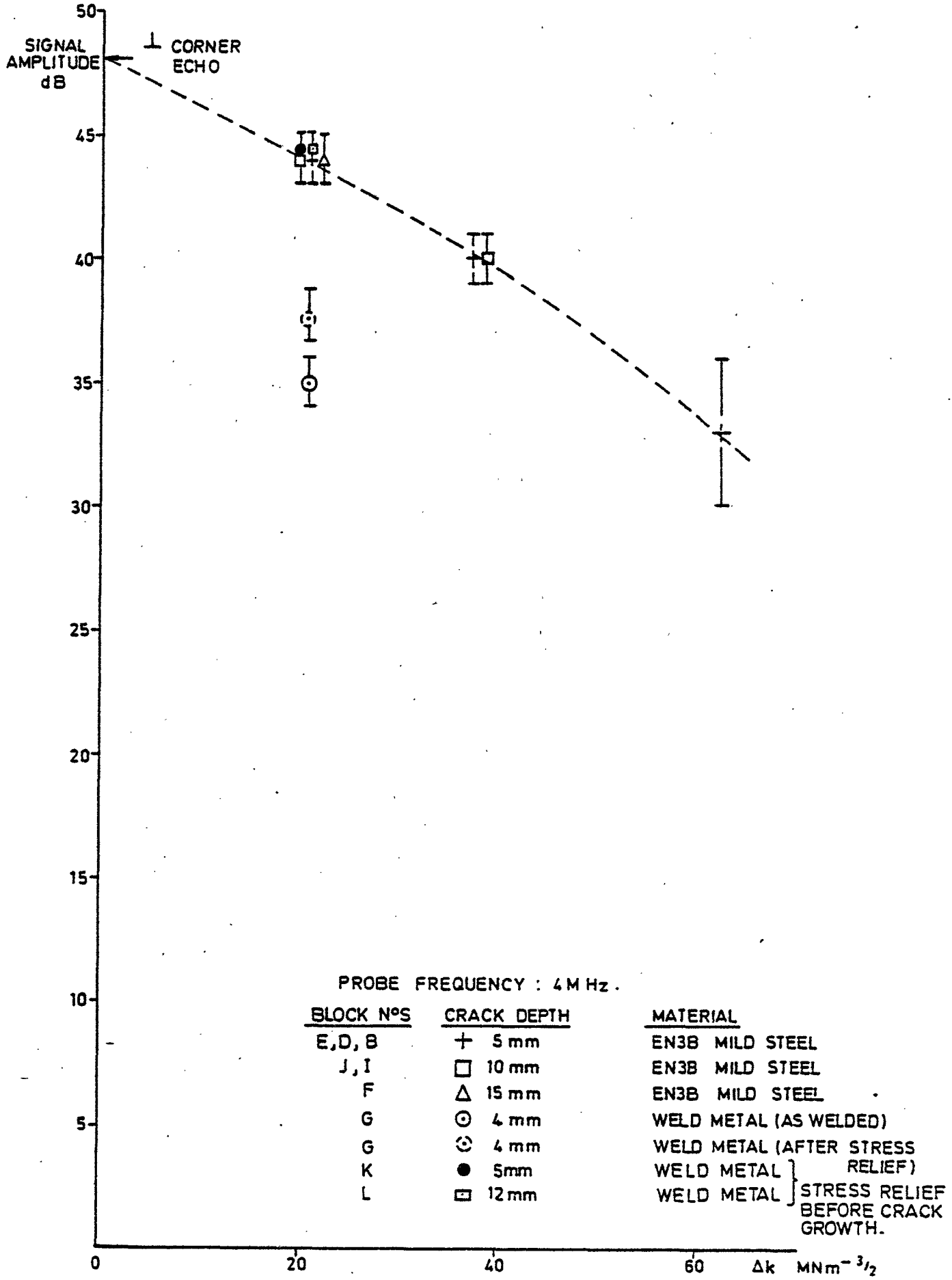

FIG.7(a). CORNER ECHOES AT ZERO LOAD VERSUS Δk: 45° PROBE.

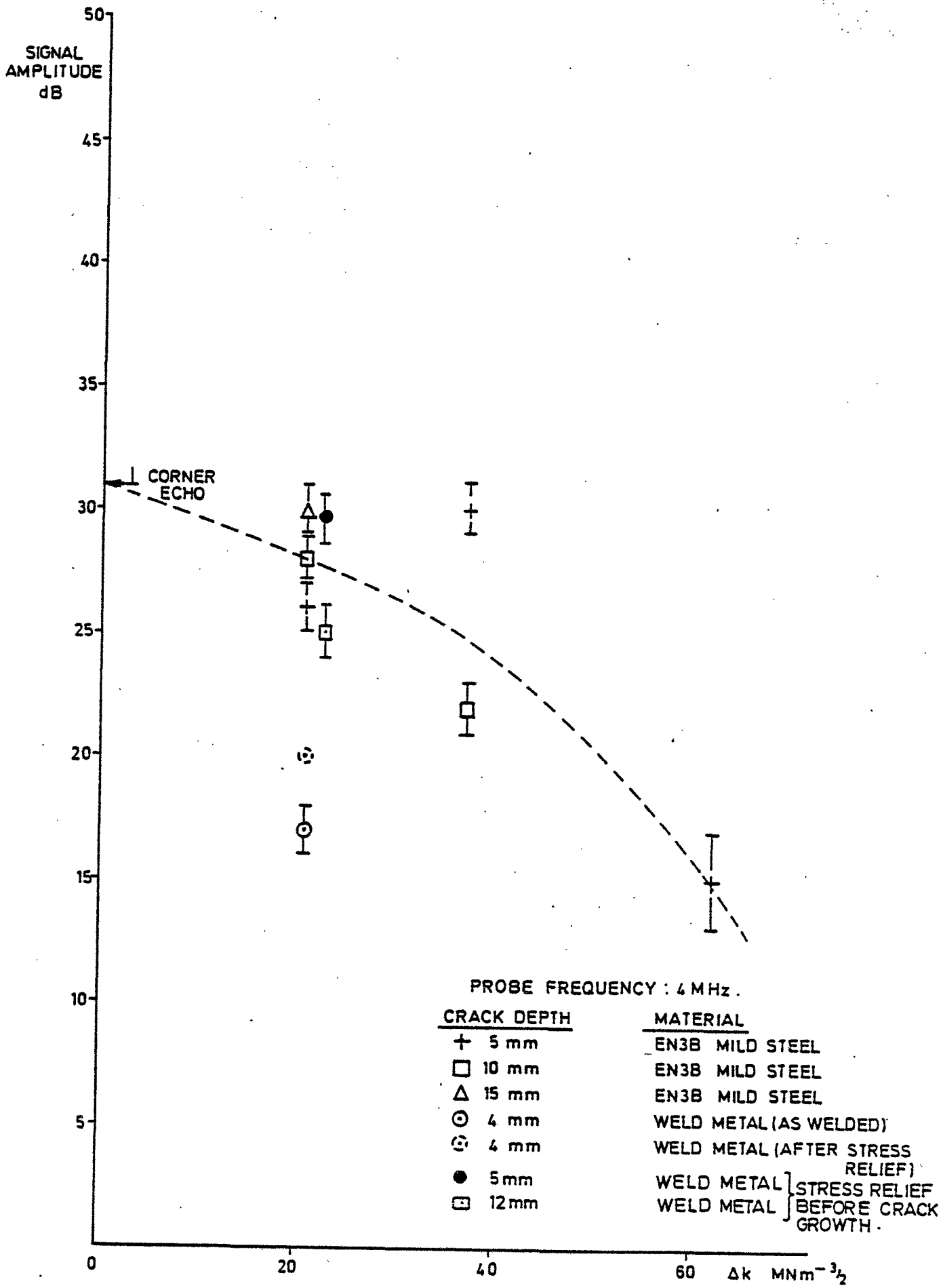

FIG. 7(b). CORNER ECHOES AT ZERO LOAD VERSUS Δk : 60° PROBE.

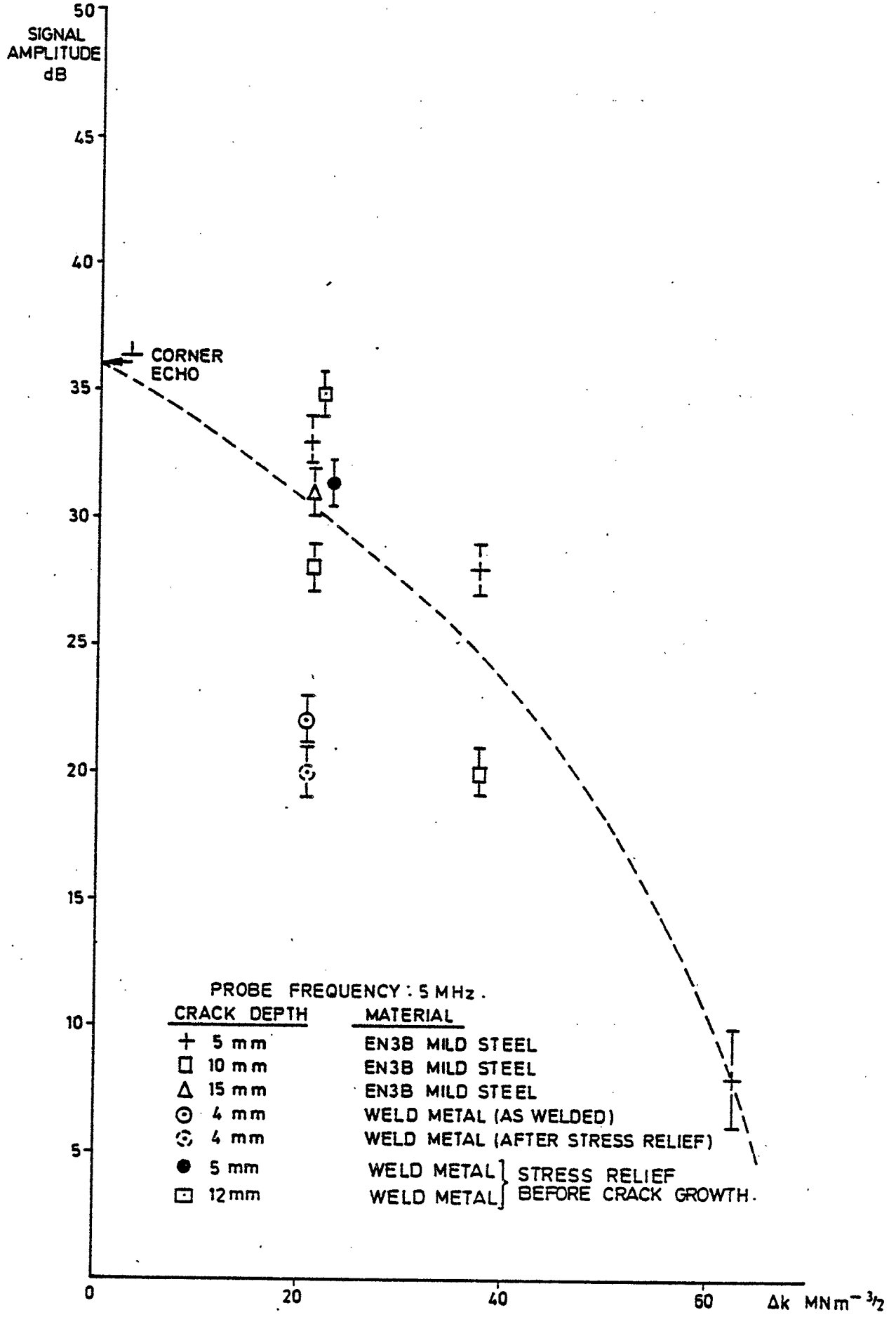

FIG. 7(c). CORNER ECHOES AT ZERO LOAD VERSUS Δk: 70° PROBE.

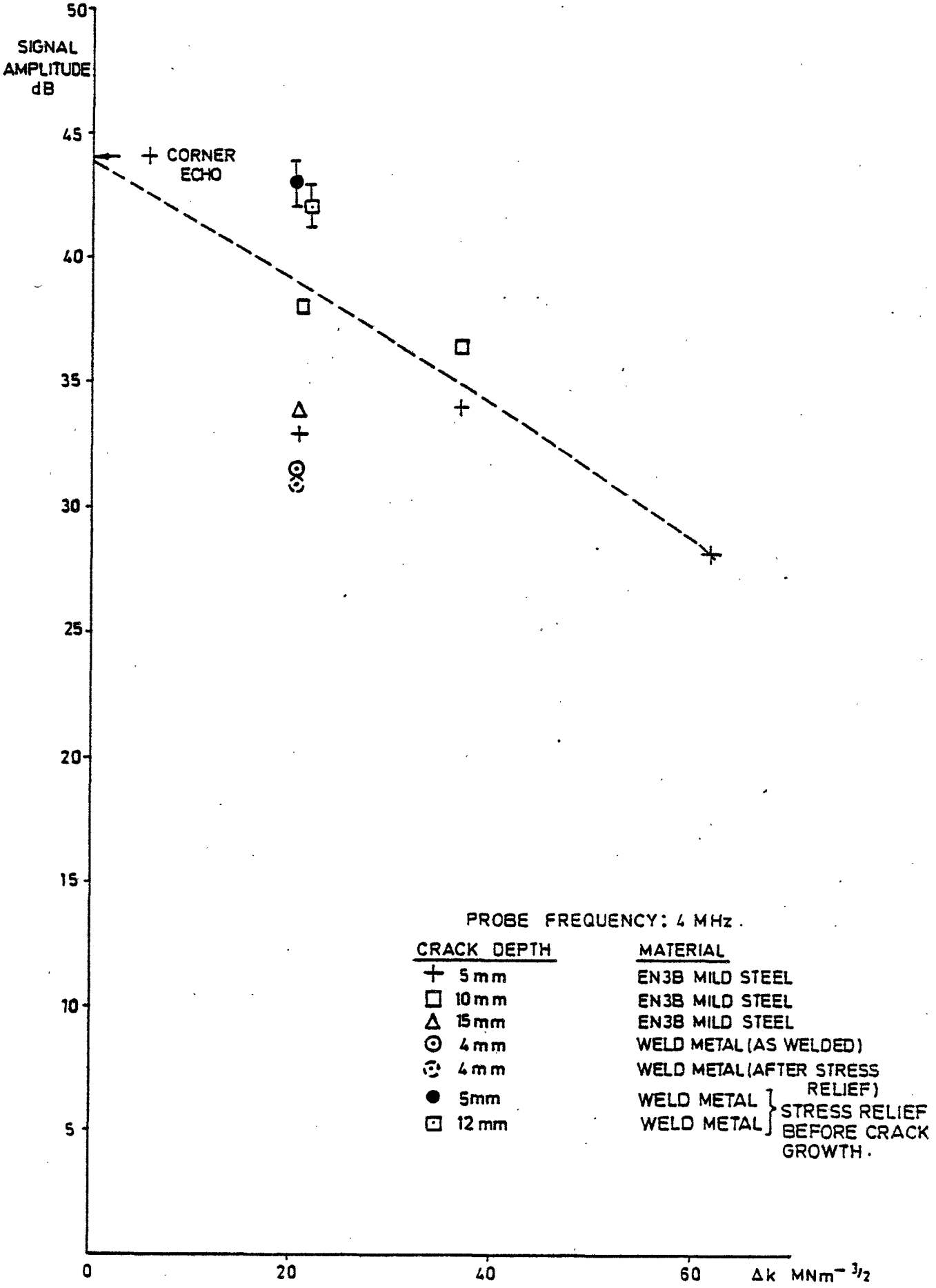

FIG. 7(d). CORNER ECHOES AT ZERO LOAD VERSUS Δk: DELTA - SCAN ARRANGEMENT.

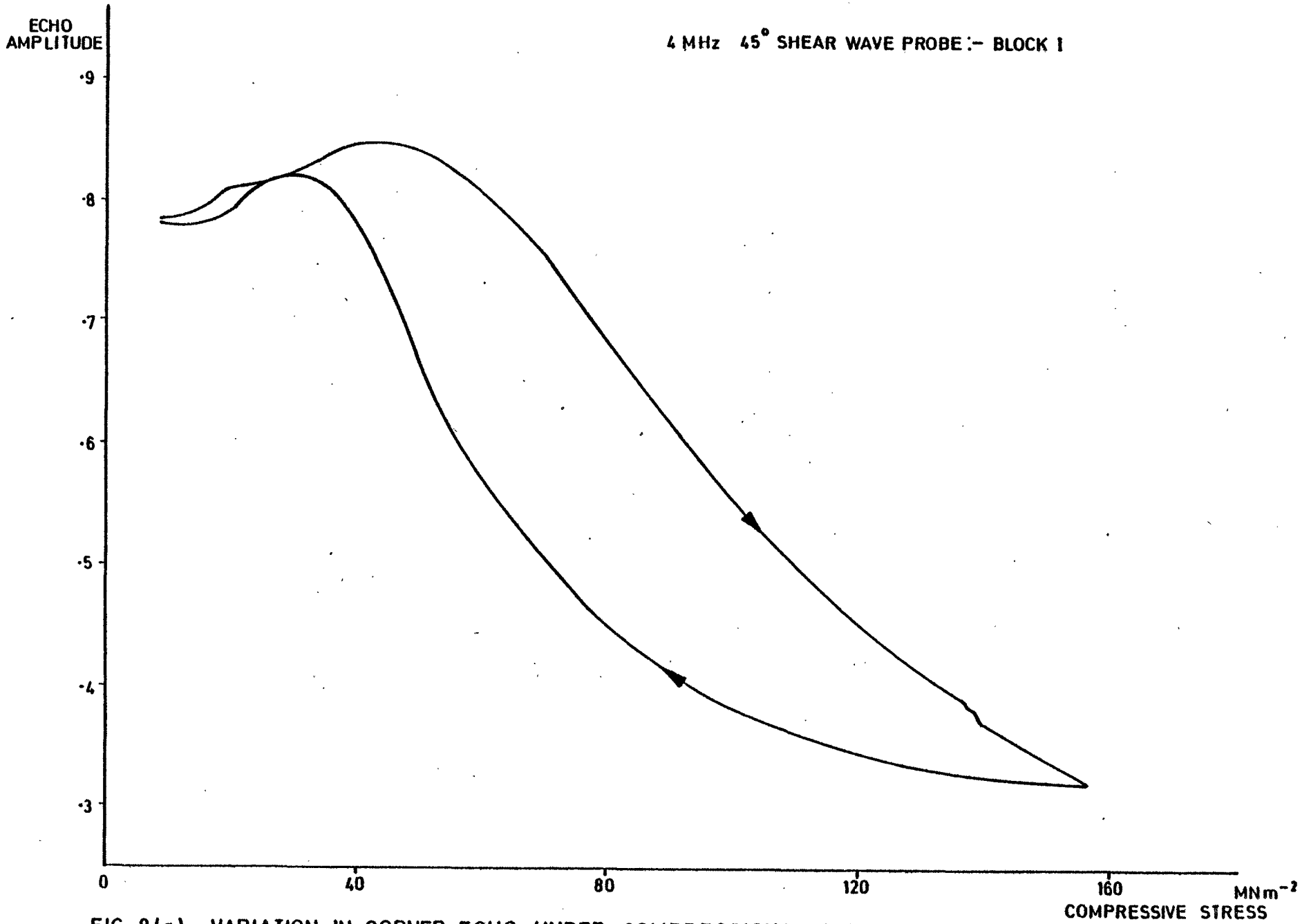

FIG. 8(a). VARIATION IN CORNER ECHO UNDER COMPRESSION: FIRST LOADING CYCLE.

RC/SSR/A4/1569

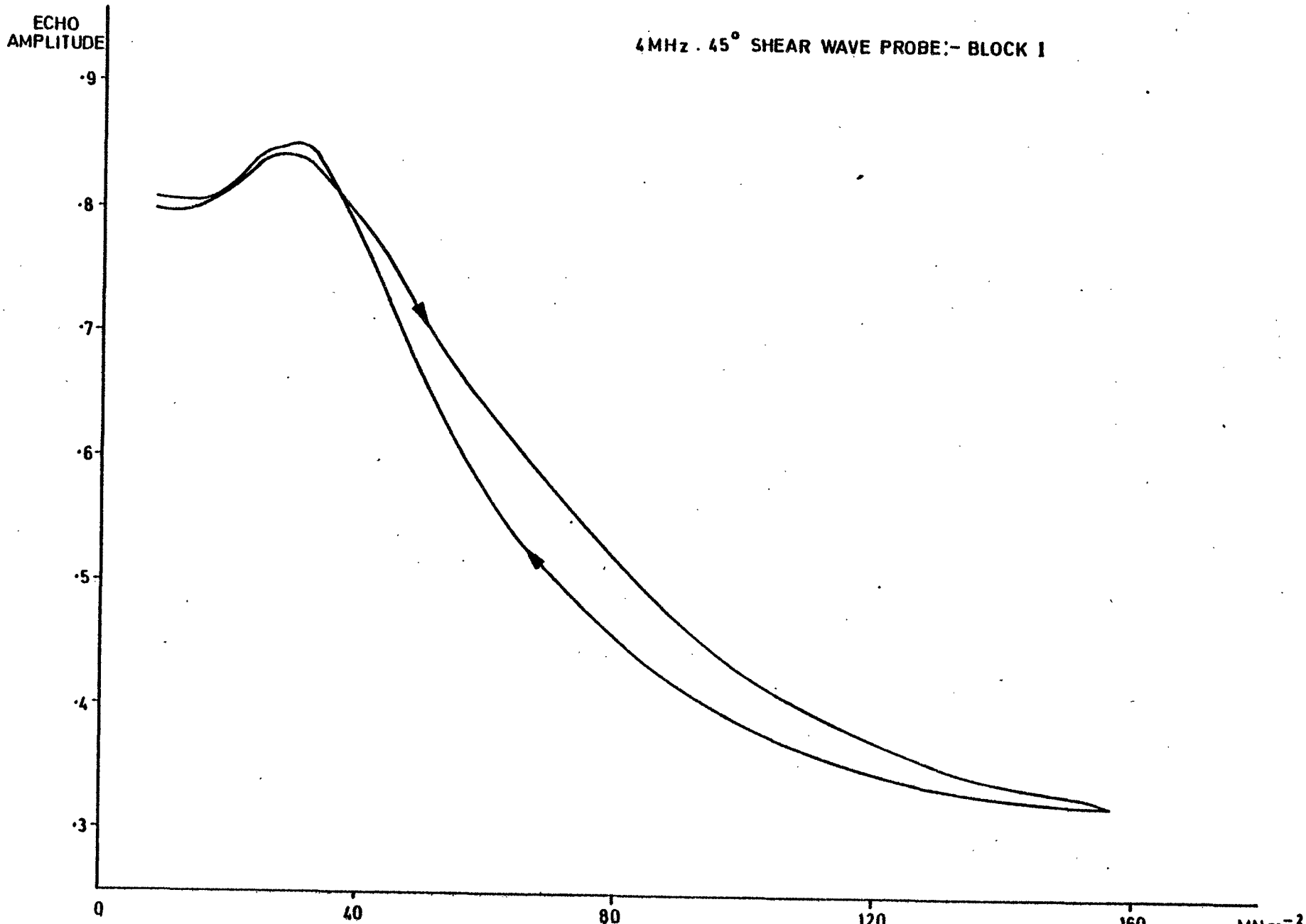

FIG. 8(b). VARIATION IN CORNER ECHO UNDER COMPRESSION: SECOND LOADING CYCLE.

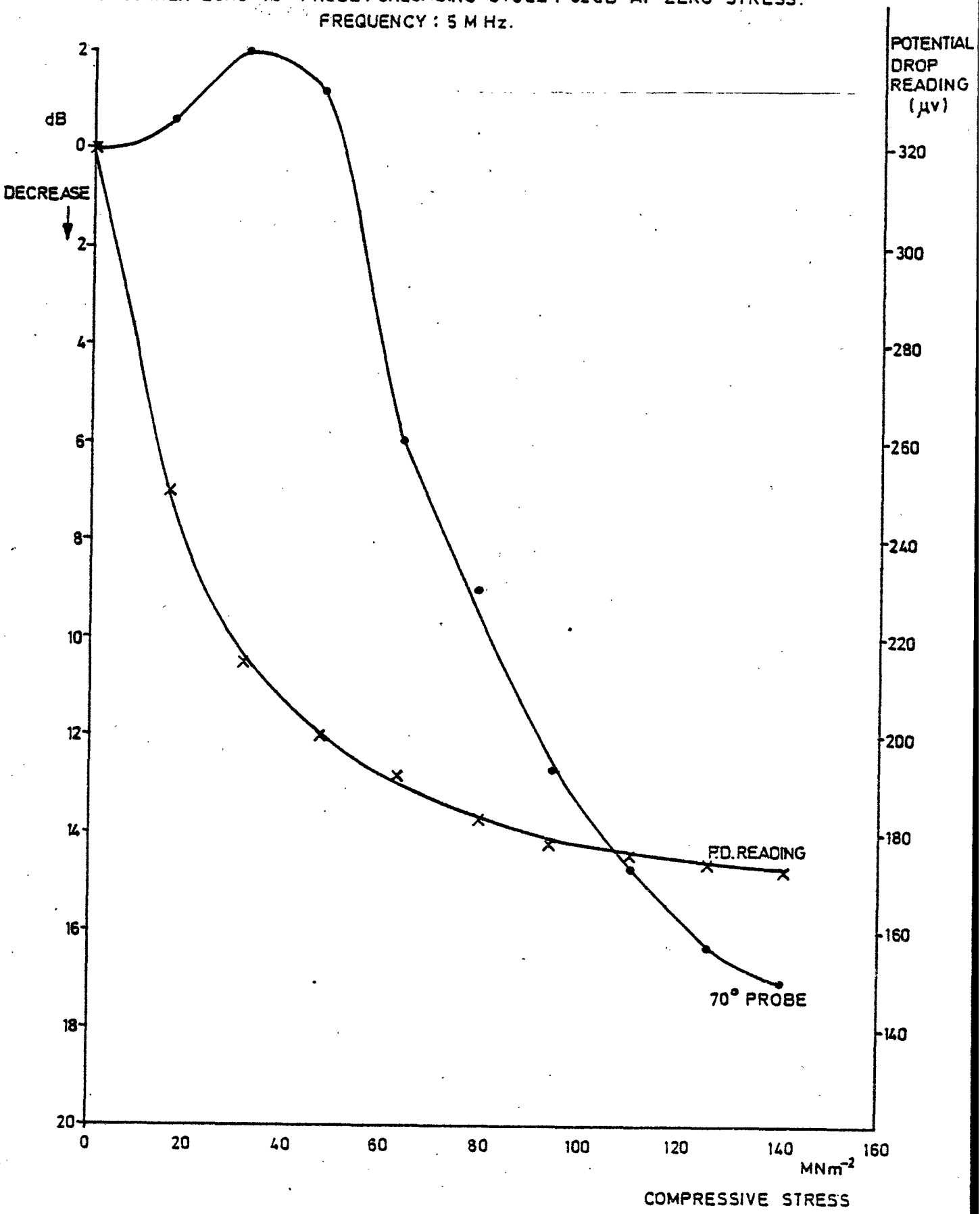

FIG. 9(a). BLOCK F : 70° SHEAR WAVE PROBE ECHO AND POTENTIAL DROP READING.

F2b CORNER ECHO 45° PROBE : UNLOADING CYCLE: 44dB AT ZERO STRESS.
F11 SURFACE WAVE PROBE : UNLOADING CYCLE:
FREQUENCY : 4MHz.

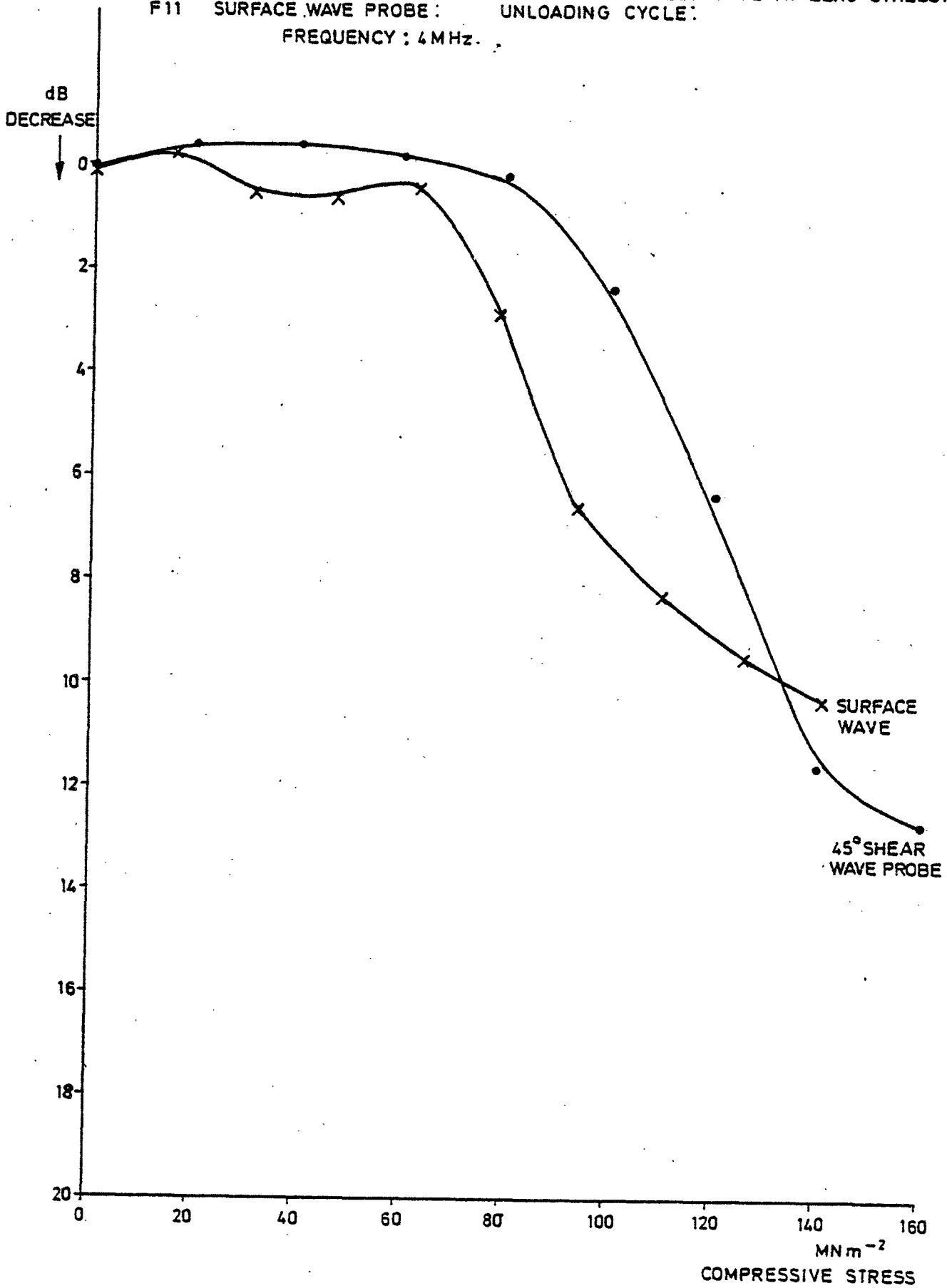

FIG. 9 (b). BLOCK F: 45° SHEAR WAVE AND SURFACE WAVE ECHOES.

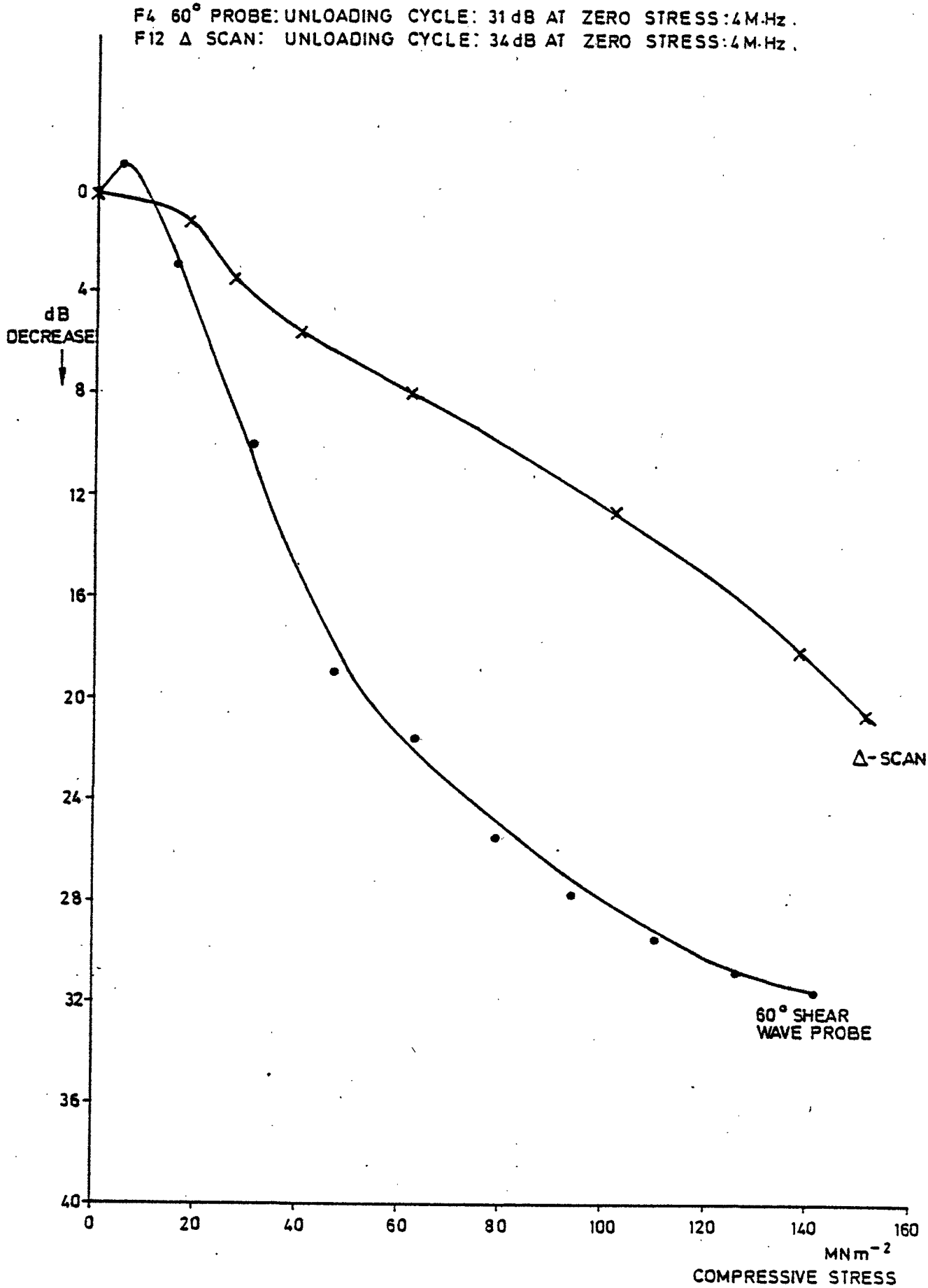

FIG. 9(c). BLOCK F: 60° SHEAR WAVE AND DELTA-SCAN ECHOES.

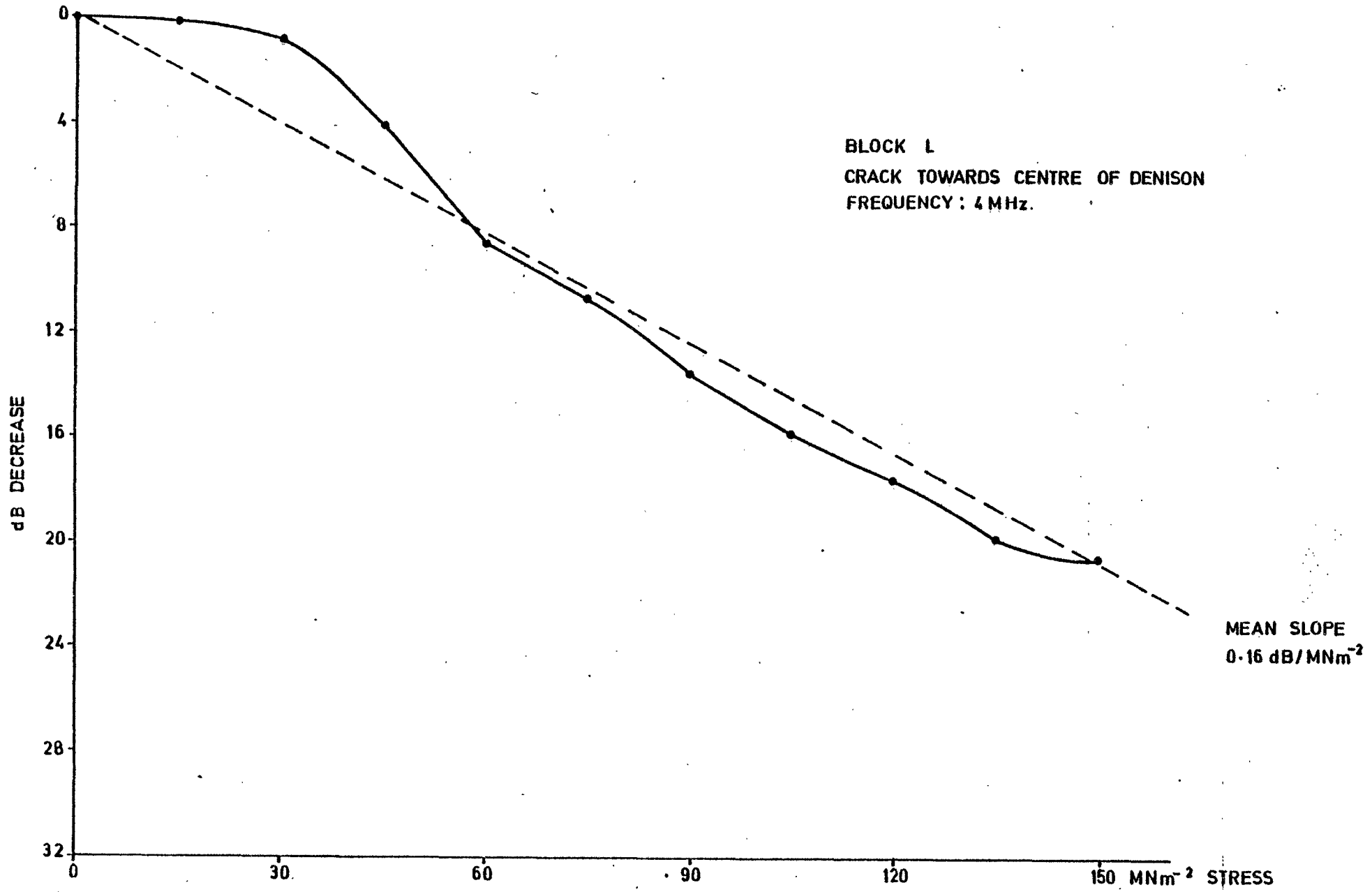

FIG 10(a) VARIATION IN CORNER ECHO UNDER COMPRESSION: 45° SHEAR WAVE PROBE

RC/SSR/A4/1747

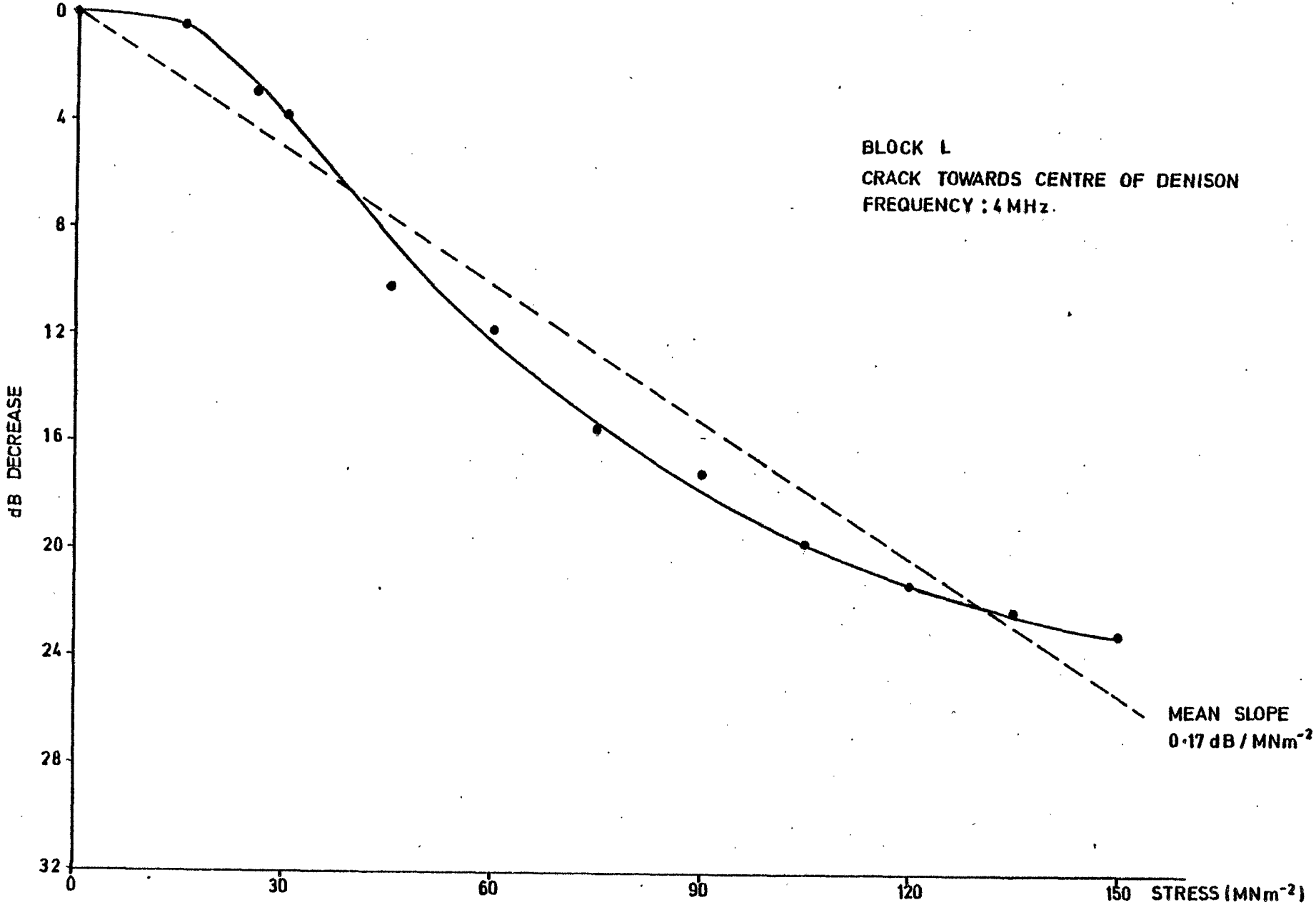

FIG 10(b) VARIATION IN Δ - SCAN SIGNAL UNDER COMPRESSION

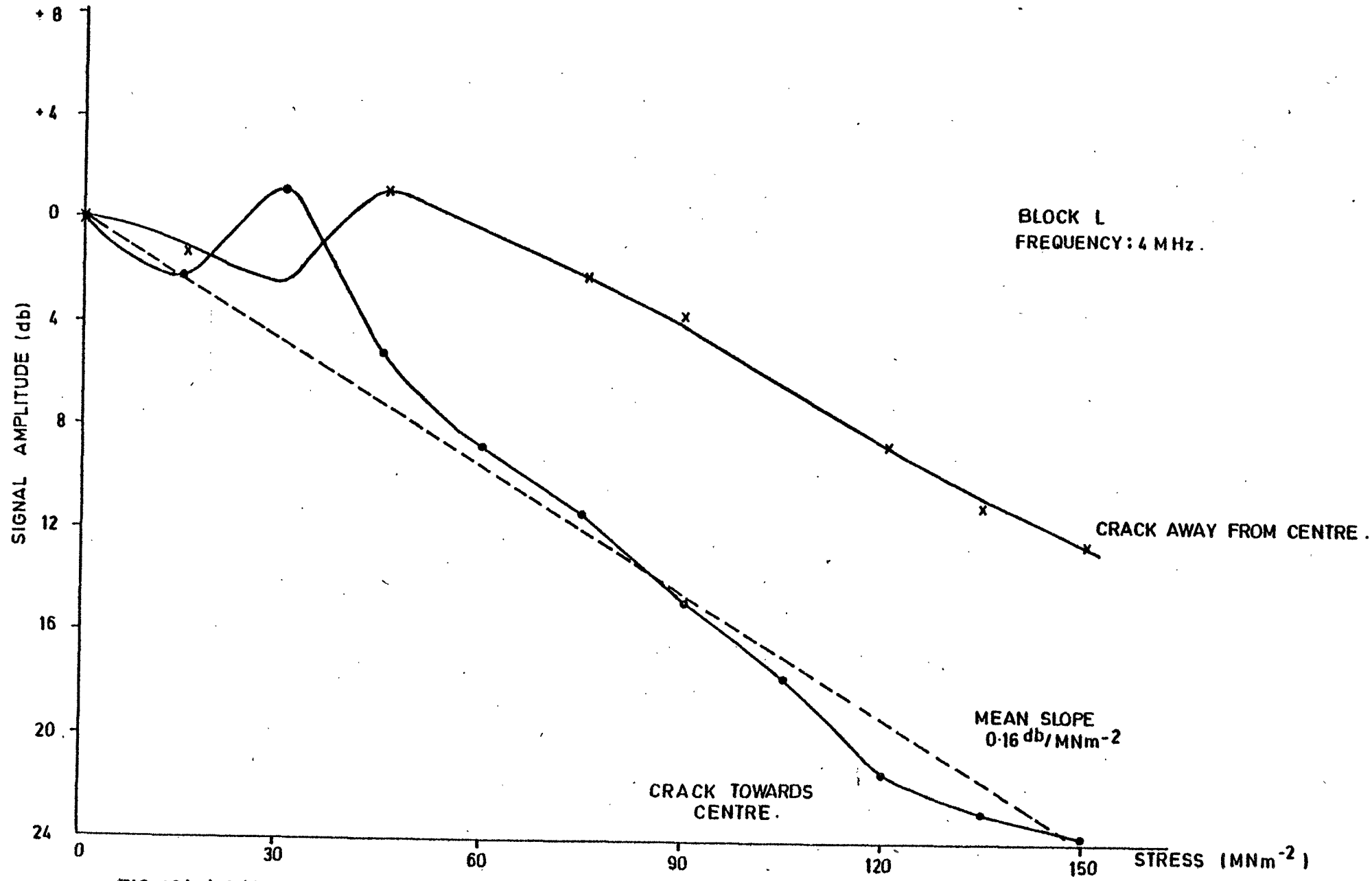

FIG 10(c) VARIATION IN CORNER ECHO UNDER COMPRESSION : 60° SHEAR WAVE PROBE.

RC/SSR/A4/1749

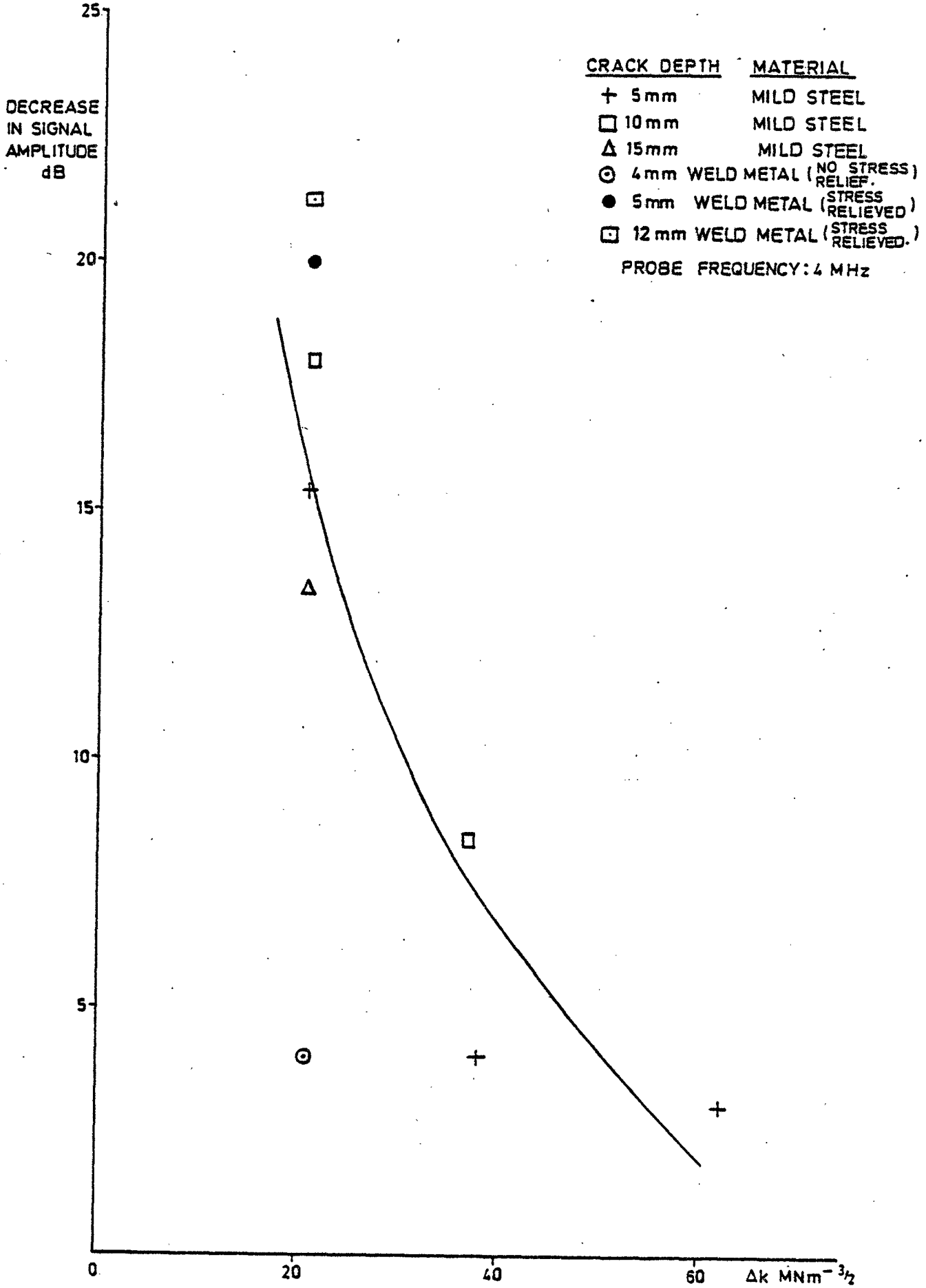

FIG. 11(a). REDUCTIONS IN CORNER ECHO AMPLITUDES FOR A STRESS OF 160 MNm^{-2} : 45° PROBE.

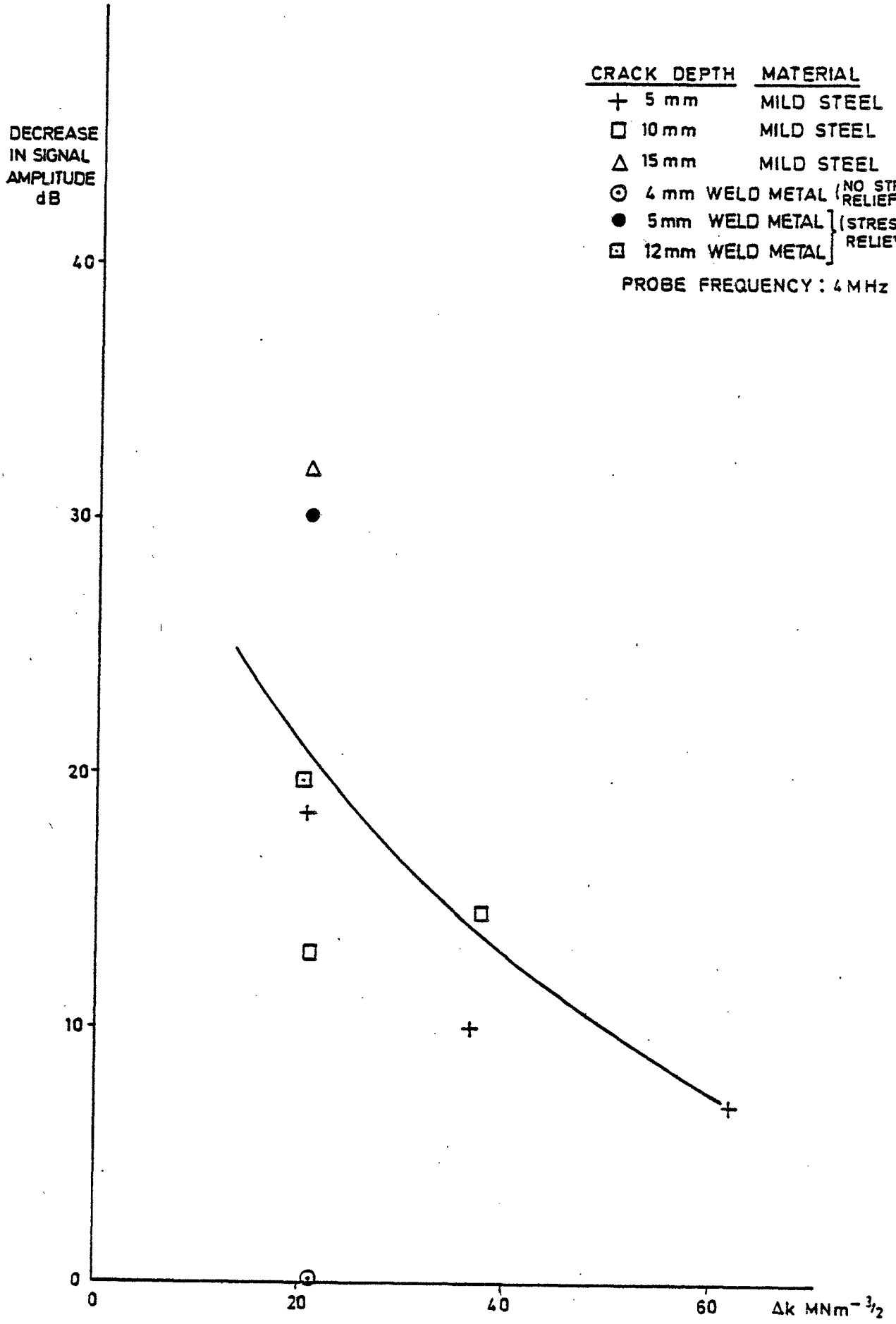

FIG. 11(b). REDUCTIONS IN CORNER ECHO AMPLITUDES FOR A STRESS OF 160 MNm^{-2}: 60° PROBE.

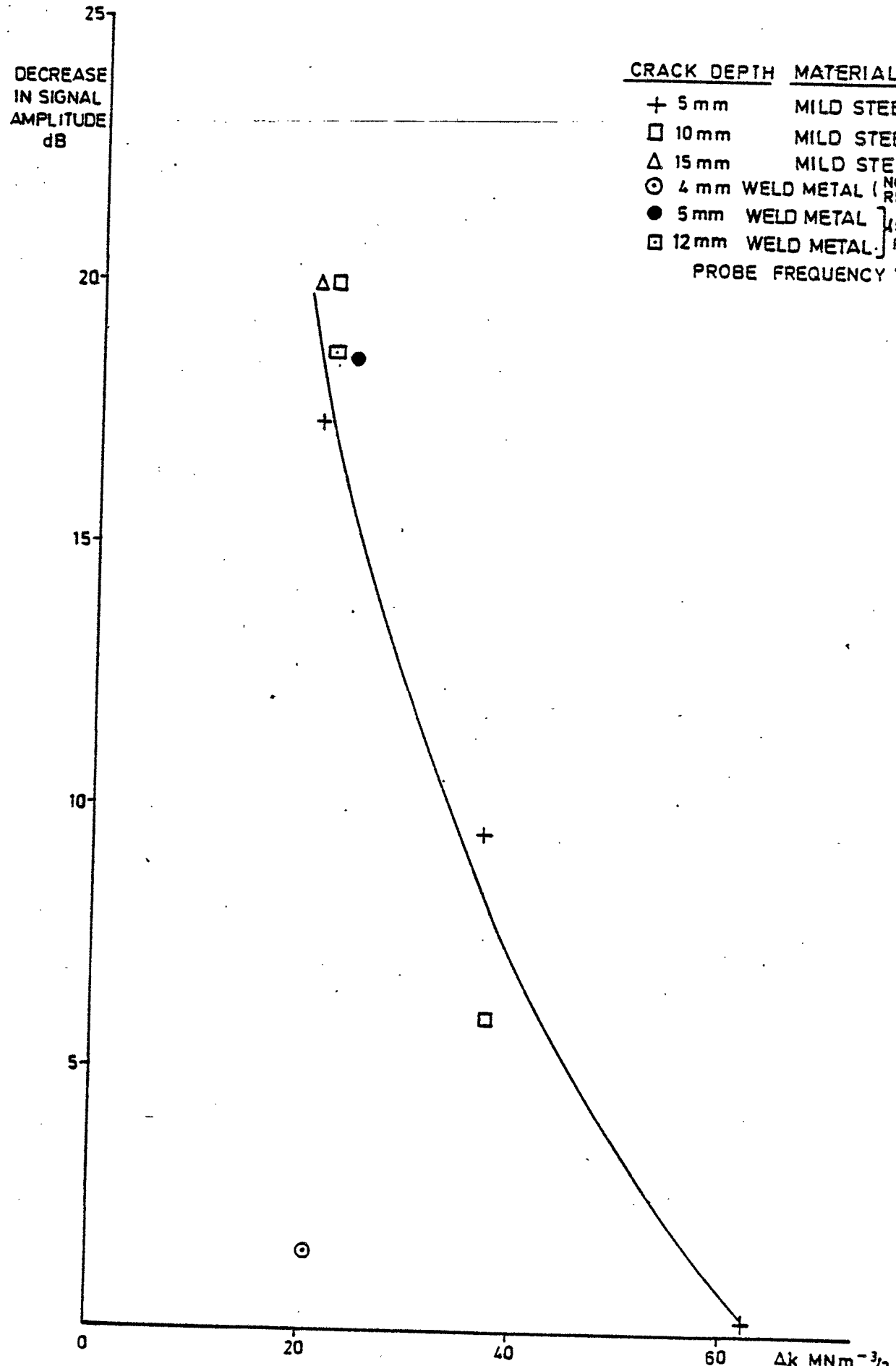

FIG.11(c). REDUCTIONS IN CORNER ECHO AMPLITUDES FOR A STRESS OF 160 MNm^{-2} : 70° PROBE.

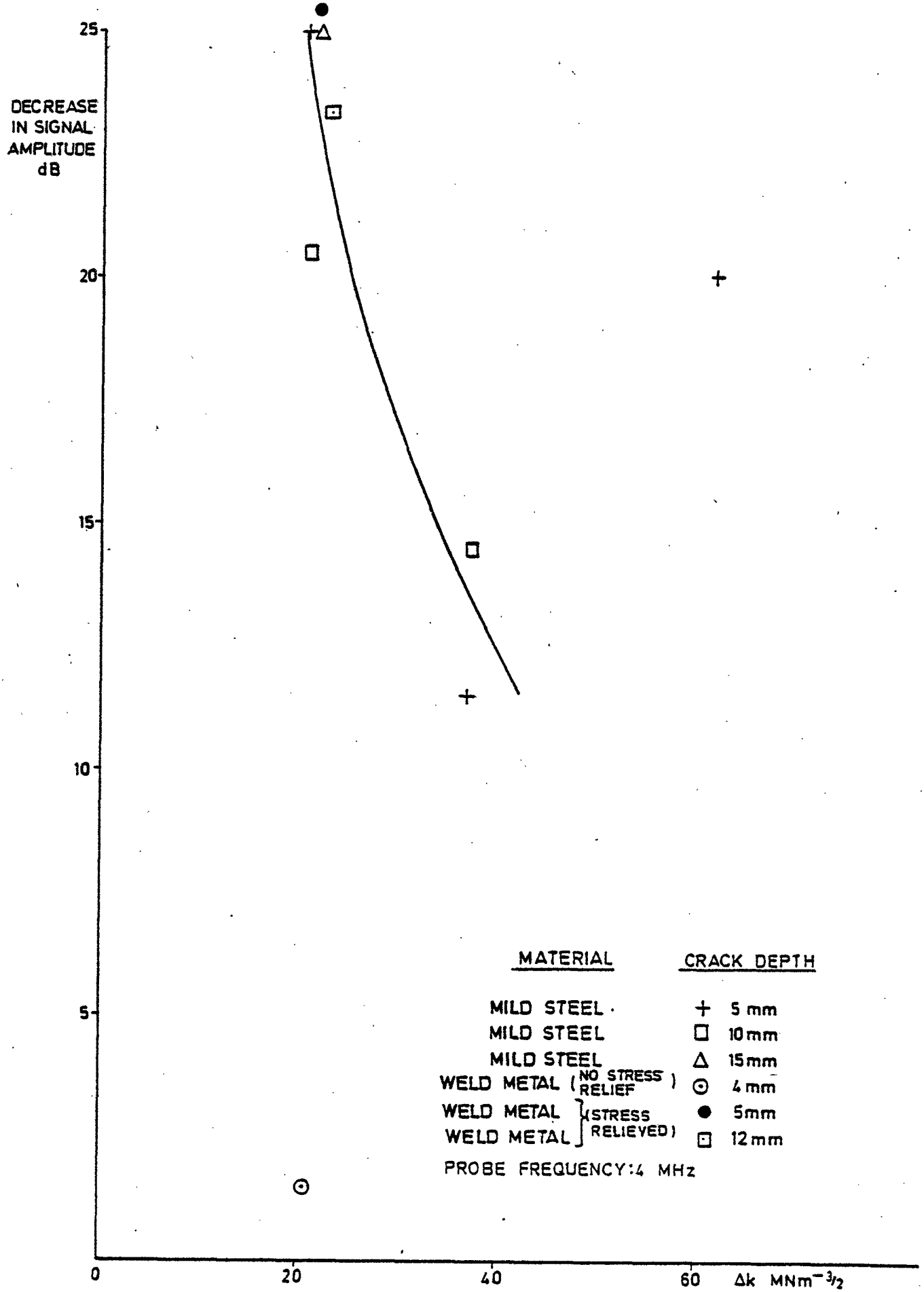

FIG.11(d). REDUCTIONS IN CORNER ECHO AMPLITUDES FOR A STRESS OF 160 MNm^{-2}: DELTA SCAN.

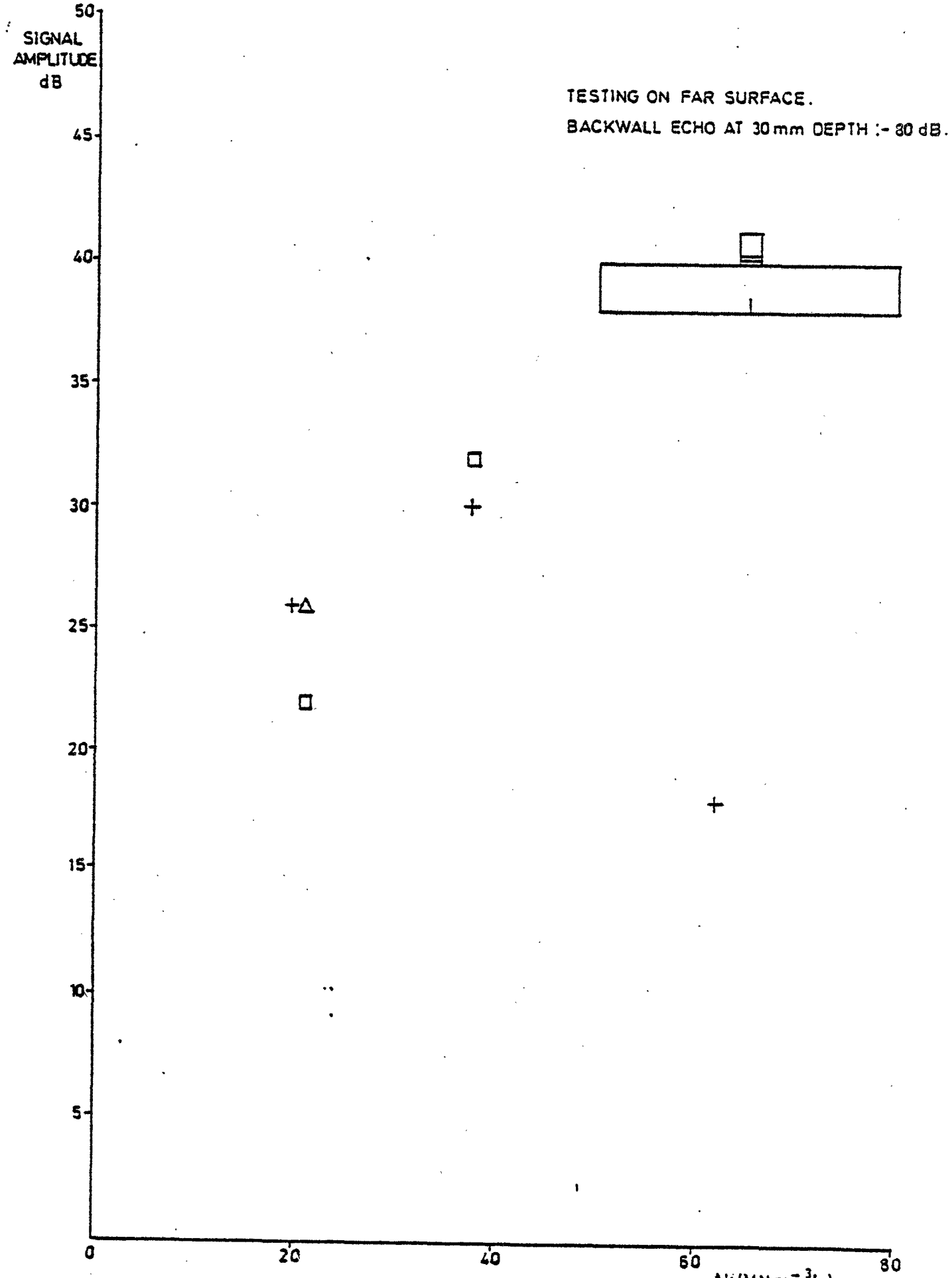

FIG. 12. CRACK TIP ECHO AMPLITUDES VERSUS Δk : 4 MHz MATEVAL COMPRESSION PROBE.

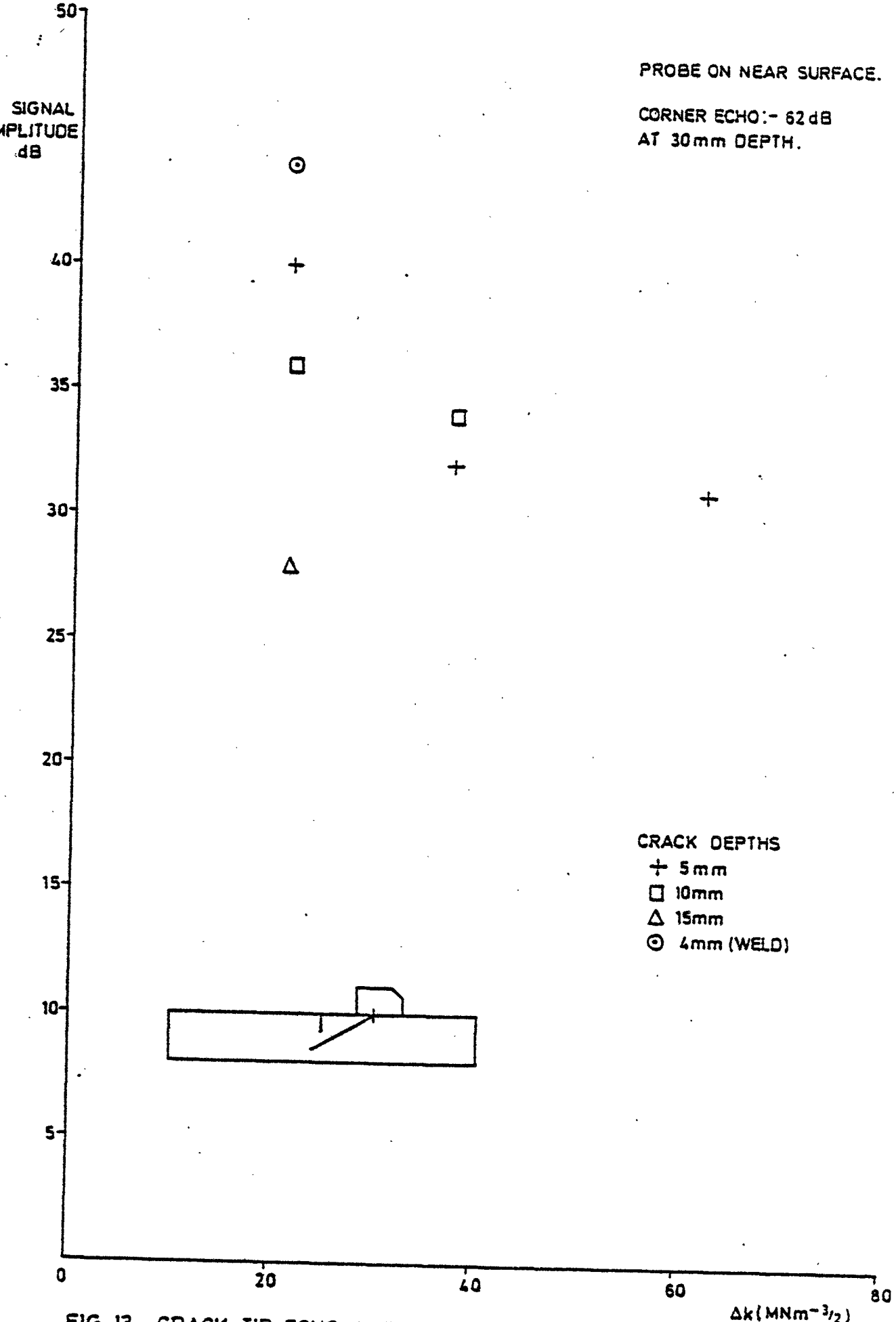

FIG. 13. CRACK TIP ECHO AMPLITUDES VERSUS Δk: 5 MHz 45° PANAMETRICS PROBE.

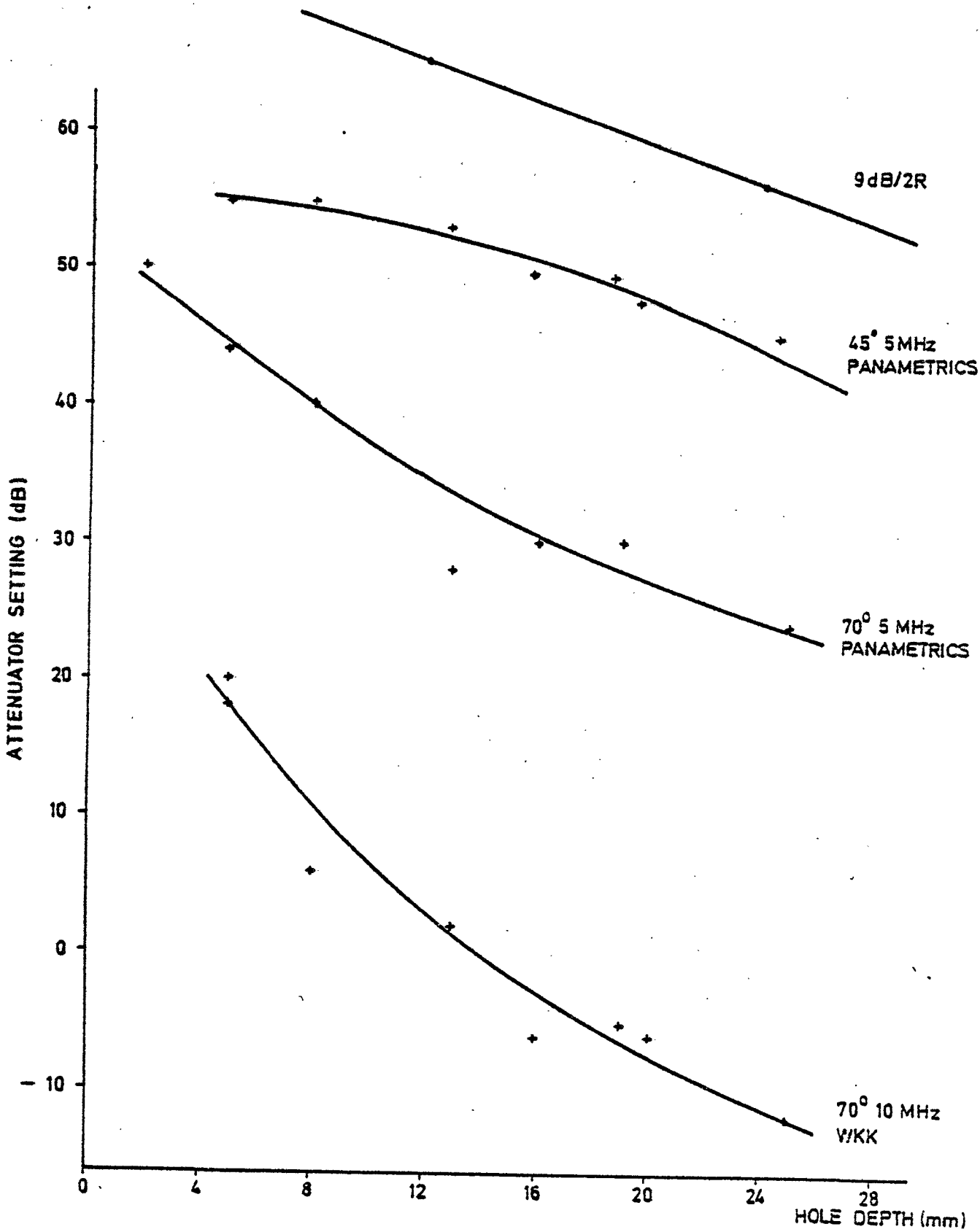

FIG. 14 PROBE SENSITIVITIES MEASURED USING 1·5mm DIA. CROSS-DRILLED HOLES

ALL AMPLITUDES ARE RELATIVE TO A 1·5 mm DIAMETER CYLINDRICAL HOLE AT THE SAME RANGE AS EACH CRACK TIP.

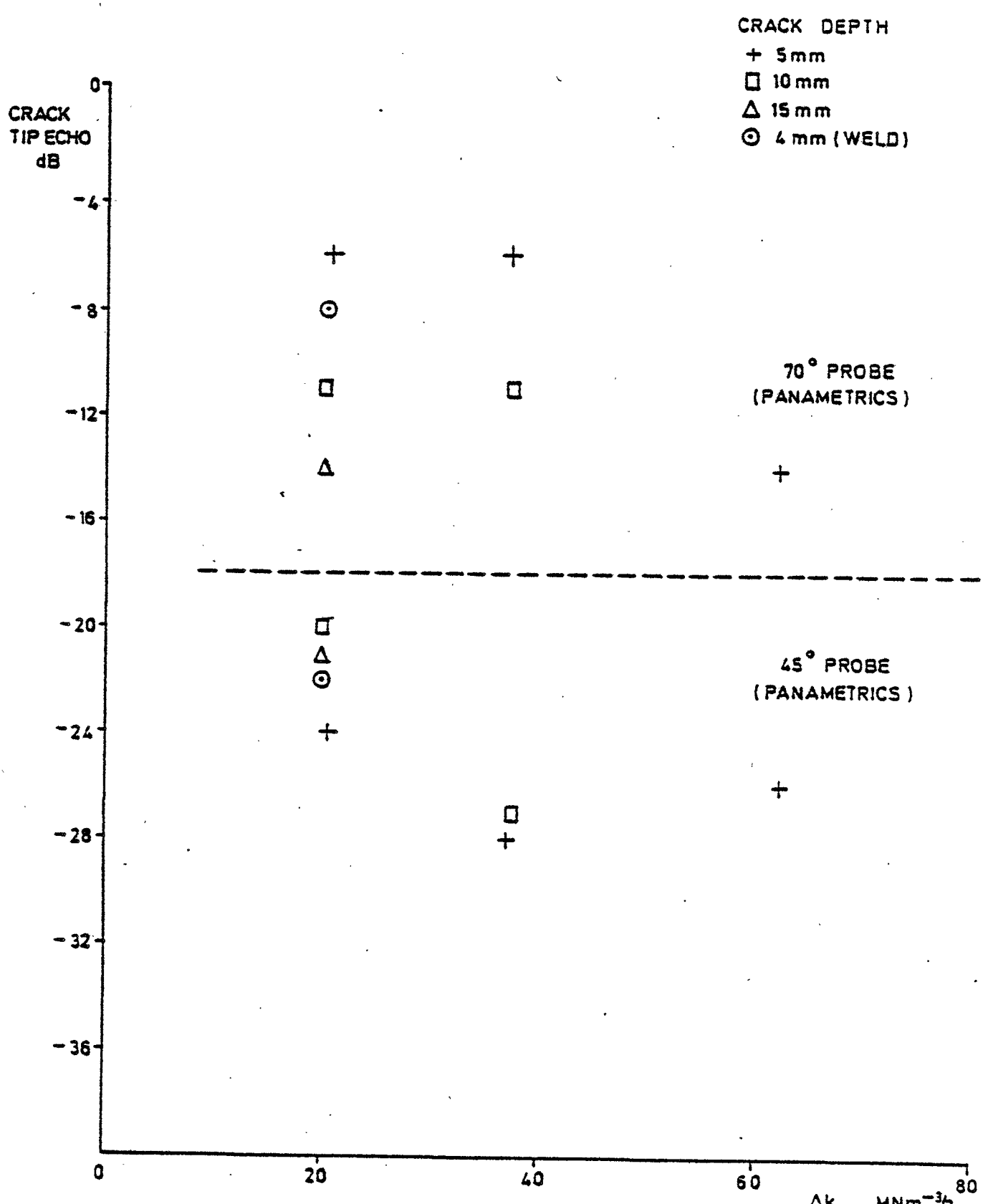

FIG. 15(a). CRACK TIP ECHOES FOR 45° AND 70° 5 MHz PROBES: FAR SURFACE.

ALL AMPLITUDES ARE RELATIVE TO A 1·5 mm DIAMETER CYLINDRICAL HOLE AT THE SAME RANGE AS EACH CRACK TIP.

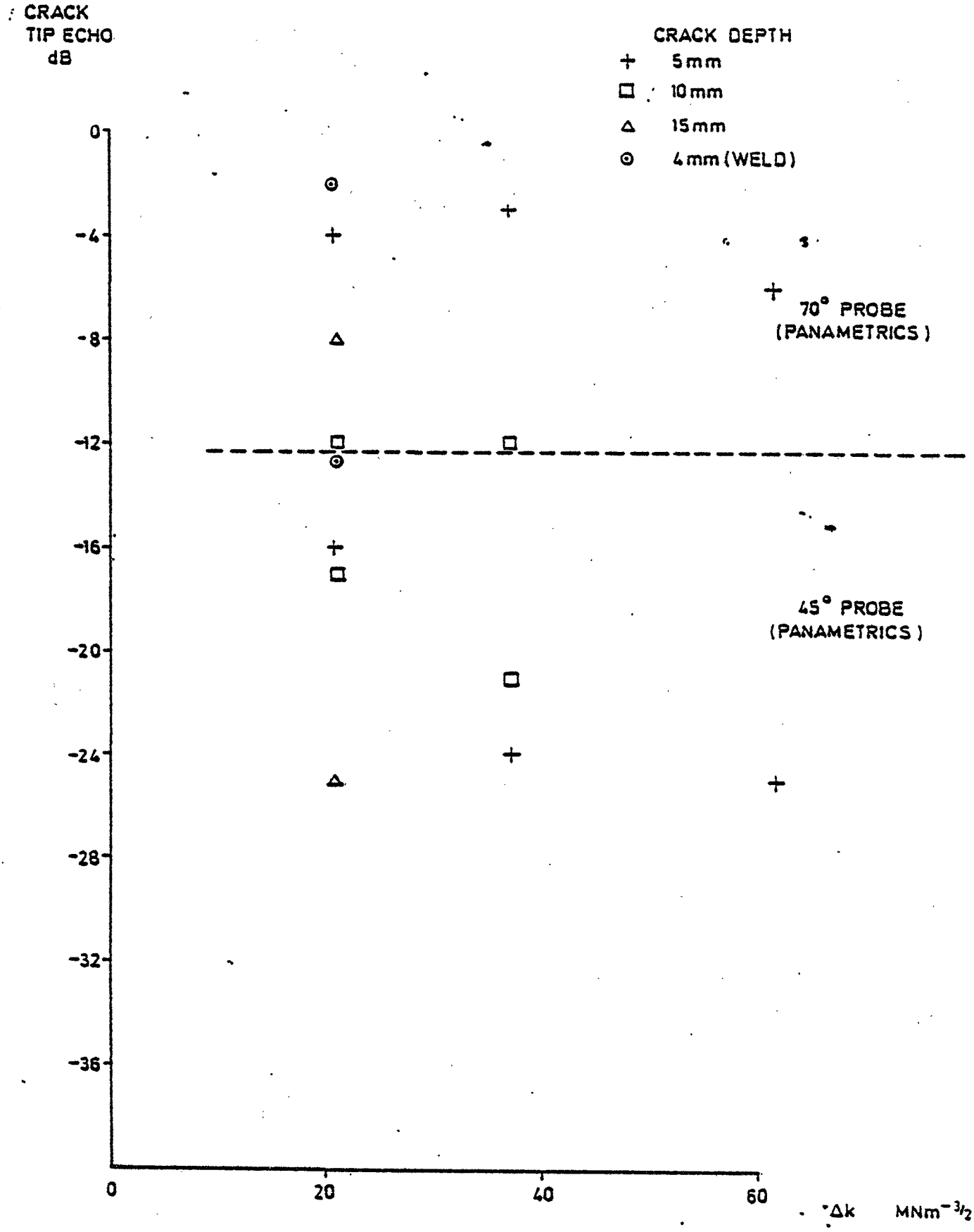

FIG. 15(b). CRACK TIP ECHOES FOR 45° AND 70° 5 MHz PROBES: NEAR SURFACE.

a) PROBES ON FAR SURFACE

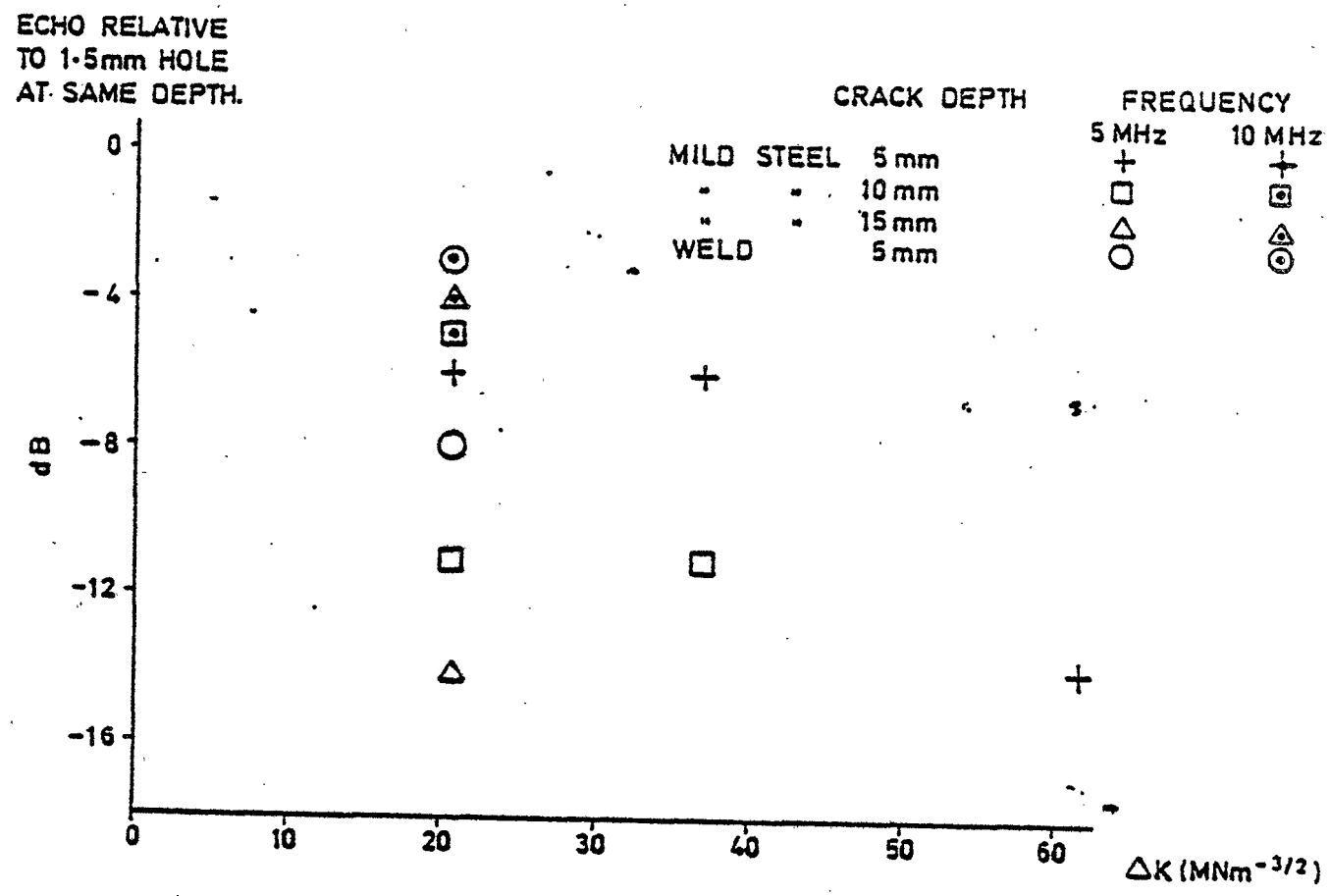

b) PROBES ON NEAR SURFACE

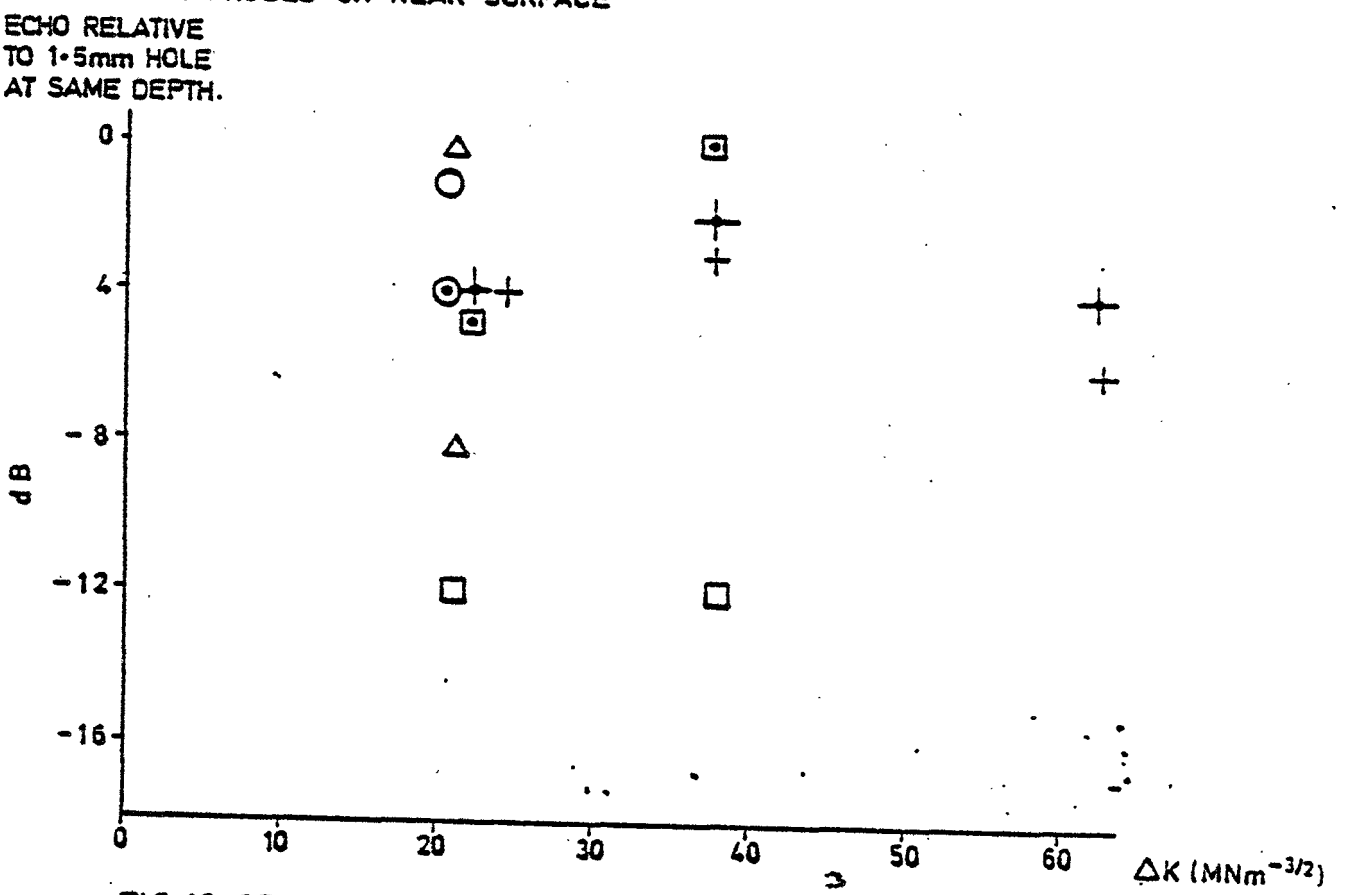

FIG. 16 CRACK TIP ECHOES FOR 5 MHz AND 10 MHz 70° PROBES OF 6·4 mm DIAMETER.

ECHO AMPLITUDES IN dB RELATIVE TO A 1·5mm CYLINDRICAL HOLE AT SAME RANGE.

PROBE	FAR SURFACE		NEAR SURFACE	
	CALCULATED	EXPERIMENTAL	CALCULATED	EXPERIMENTAL
PANAMETRICS 5 MHz 45°	− 29 · 1	− 24 · 0 ± 3 · 1	− 10 · 4	− 20 ± 5 · 1
PANAMETRICS 5 MHz 70°	− 17 · 0	− 10 · 1 ± 3 · 6	− 2 · 8	− 6 · 6 ± 4 · 3
W. K. K. 10 MHz 70°	− 20 · 0	− 4 · 0 ± 1 · 0	− 5 · 7	− 2 · 6 ± 1 · 9

EXPERIMENTAL VALUES ARE THE MEAN VALUES FOR ALL CRACKS MEASURED

FIG. 17. A COMPARISON OF EXPERIMENTAL AND THEORETICAL CRACK TIP ECHOES

		ULTRASONIC					VISUAL	
BLOCK	SURFACE SCANNED	70° 5 MHz PANAMETRIC	70° 10 MHz W. K. K.	45° 5 MHz PANAMETRICS	MEAN	0° 4 MHz MATEVAL	OPTICAL ESTIMATE AT EDGE	DESTRUCTIVE EXAMINATION (CENTRE)
E	NEAR	4 · 1	5 · 1	5 · 0	4 · 7 ± · 6	4 ± · 5	5 ± · 5	
	FAR	8 · 5	*	3 · 5	6 · 0 ± 3 · 5			
D	NEAR	4 · 8	3 · 4	4 · 2	4 · 2 ± · 7	4	5	5 · 3 ± · 1
	FAR	6 · 1	*	3 · 8	5 · 0 ± 1 · 6			
B	NEAR	3 · 1	3 · 1	4 · 2	3 · 5 ± · 7	6	5	
	FAR	4 · 7	*	3 · 2	3 · 9 ± · 1			
I	NEAR	8 · 2	9 · 6	11 · 3	9 · 7 ± · 6	8	10	
	FAR	10 · 8	*	8 · 8	9 · 8 ± · 4			
J	NEAR	9 · 6	9 · 6	11 · 3	10 · 2 ± 1 · 0	9	10	
	FAR	11 · 5	9 · 5	10 · 2	10 · 4 ± 1 · 0			
F	NEAR	9 · 6	13 · 7	17 · 0	13 · 4 ± 3 · 7	12	15	14 · 0
	FAR	13 · 9	15 · 1	13 · 0	14 · 0 ± 1 · 0			
G	NEAR	2 · 1	4 · 1	2 · 8	3 · 0 ± 1 · 0	5	5	3 · 7
	FAR	9 · 5	8 · 1	10 · 2	9 · 3 ± 1 · 1			

* TIP ECHO NOT DISTINGUISHABLE FROM CORNER ECHO. ALL DIMENSIONS IN M.M.

FIG. 18. A COMPARISON OF ULTRASONIC AND VISUAL MEASUREMENTS OF CRACK DEPTH

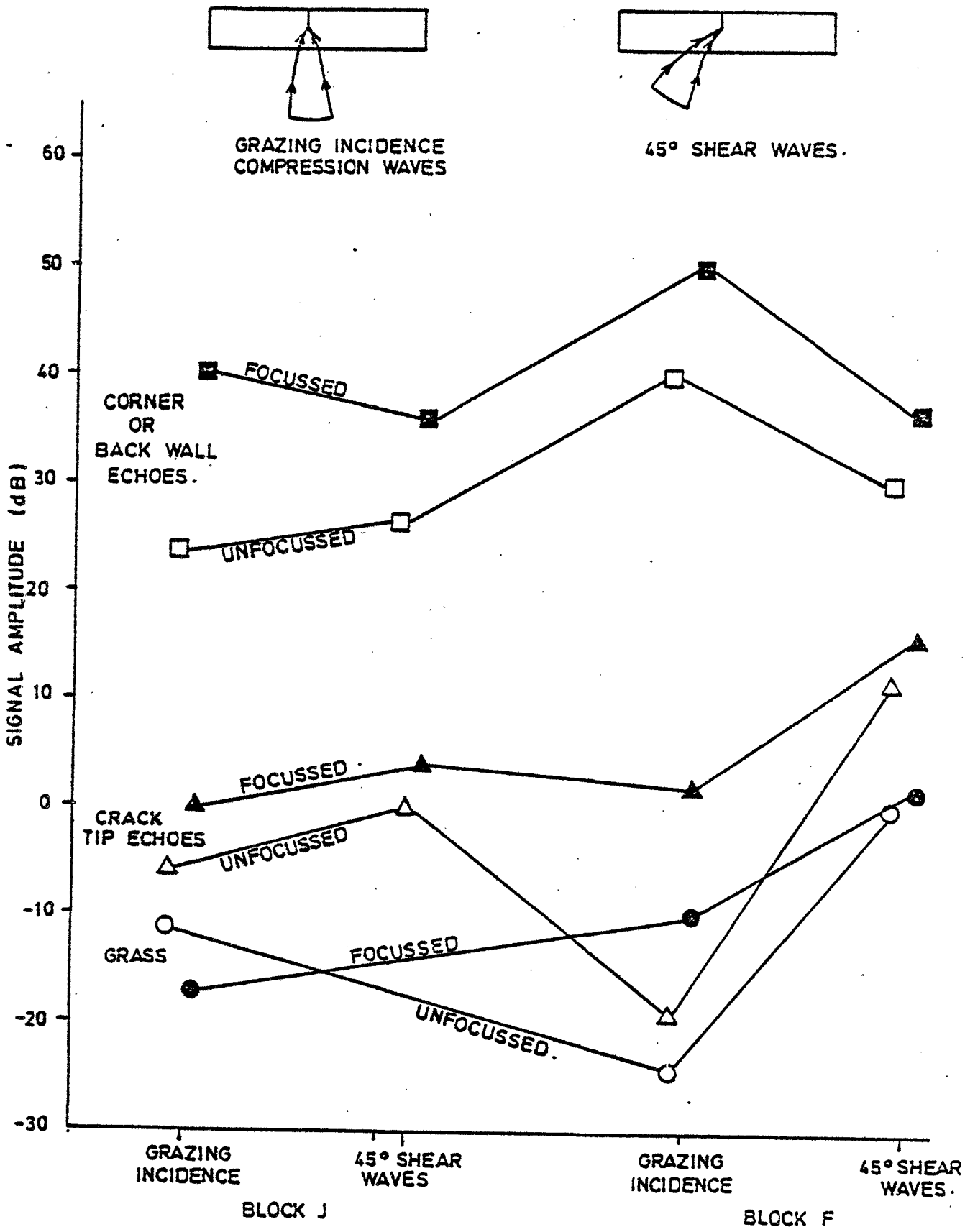

FIG·19. A COMPARISON OF FOCUSSED AND UNFOCUSSED PROBES.

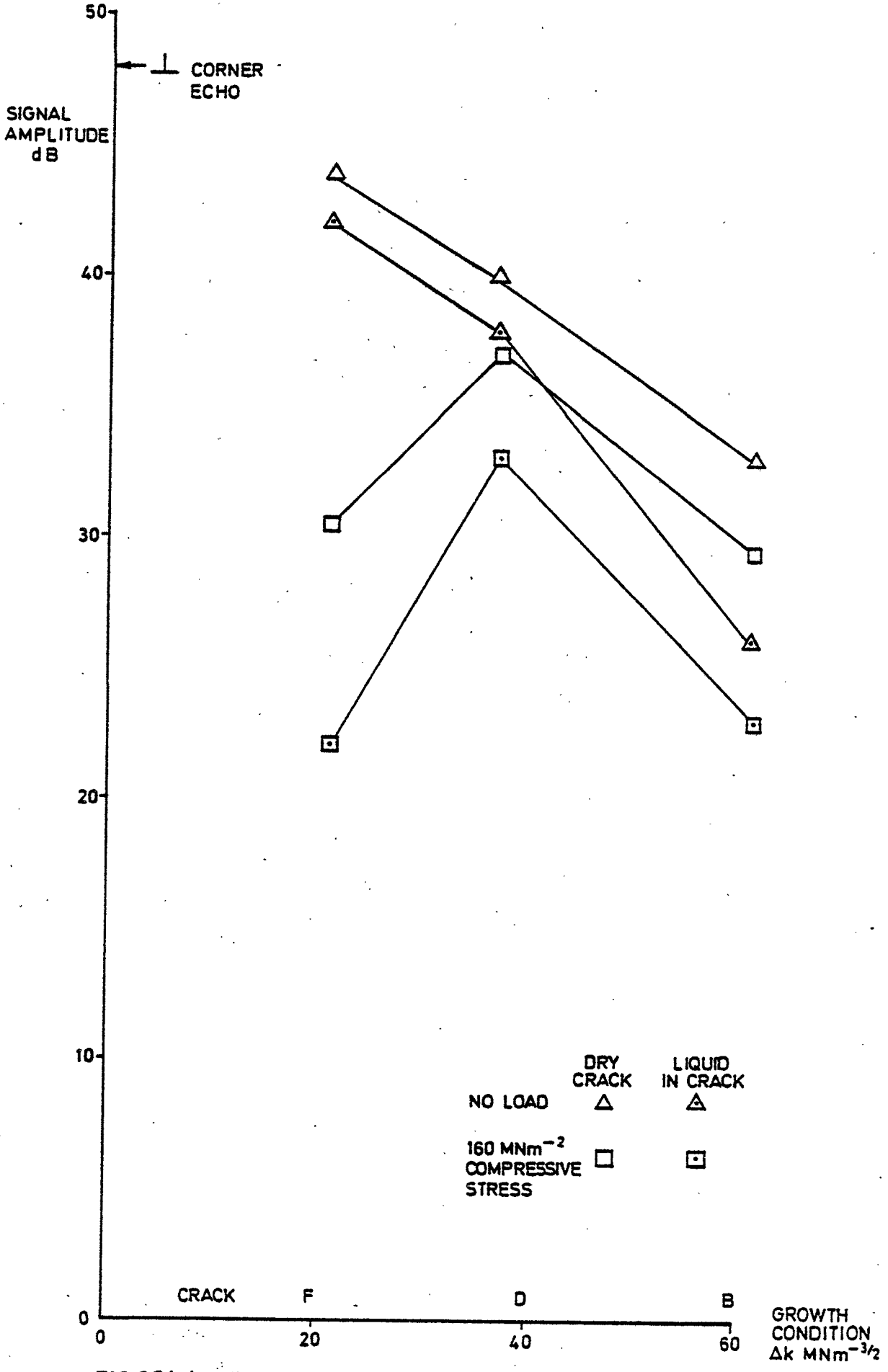

FIG.20(a). THE EFFECT OF LIQUID IN CRACKS WHEN UNLOADED AND UNDER COMPRESSION: 45° 4 MHz PROBE.

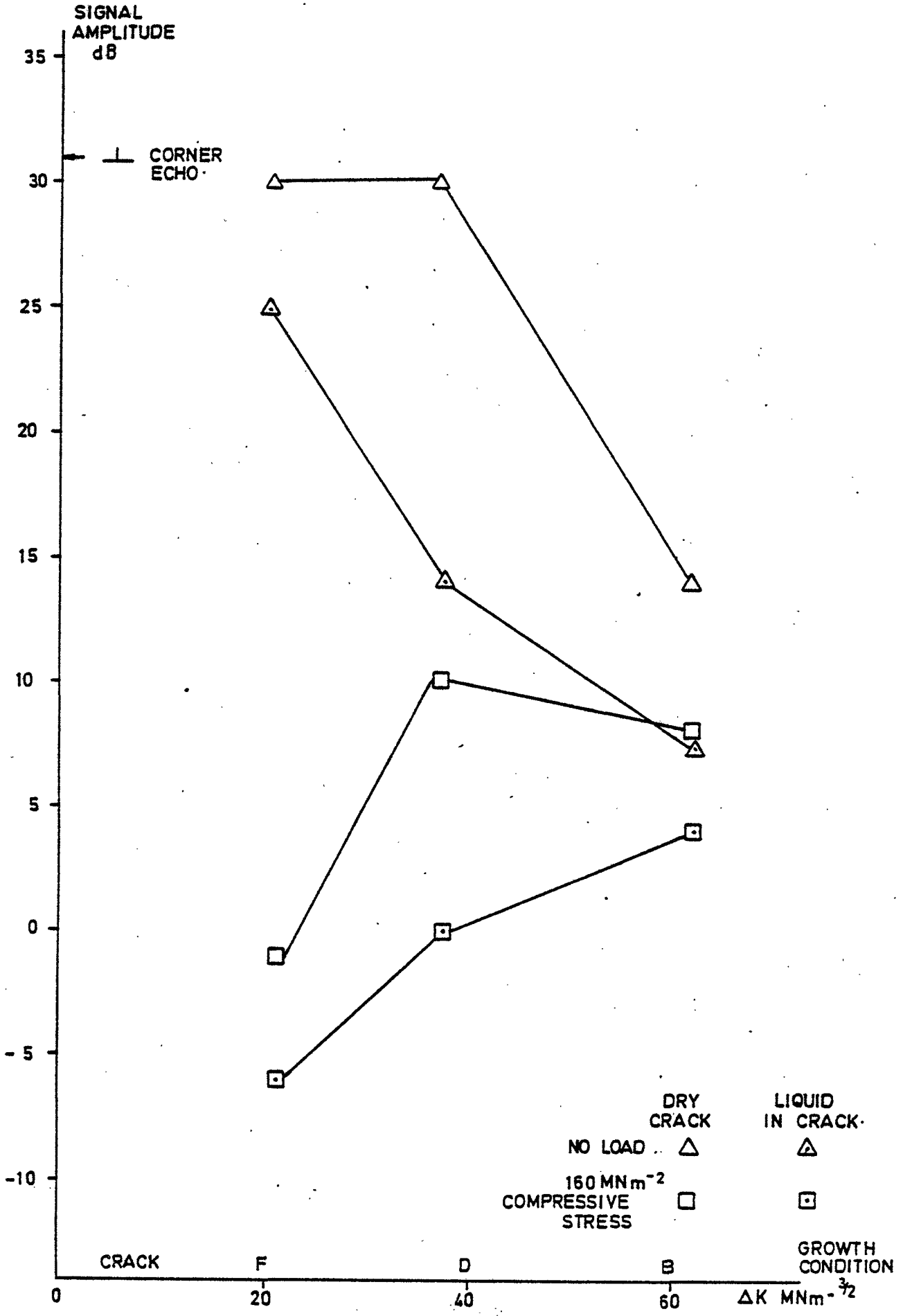

FIG·20(b) THE EFFECT OF LIQUID IN CRACKS WHEN UNLOADED AND UNDER COMPRESSION : 60 ° 4 MHz PROBE.

RC/SSR/A4/1755

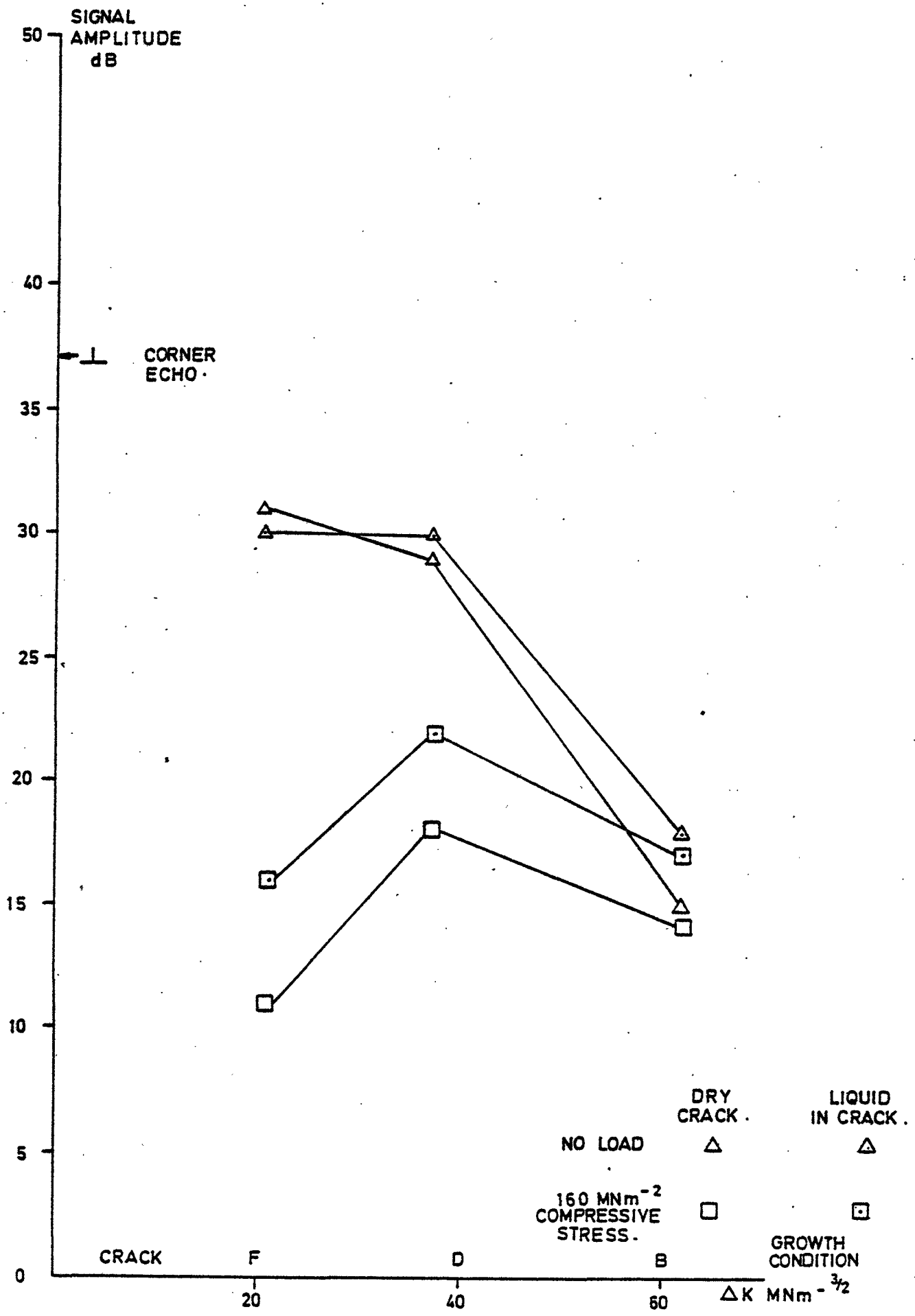

FIG. 20(c) THE EFFECT OF LIQUID IN CRACKS WHEN UNLOADED AND UNDER COMPRESSION : 70° 5MHz PROBE.

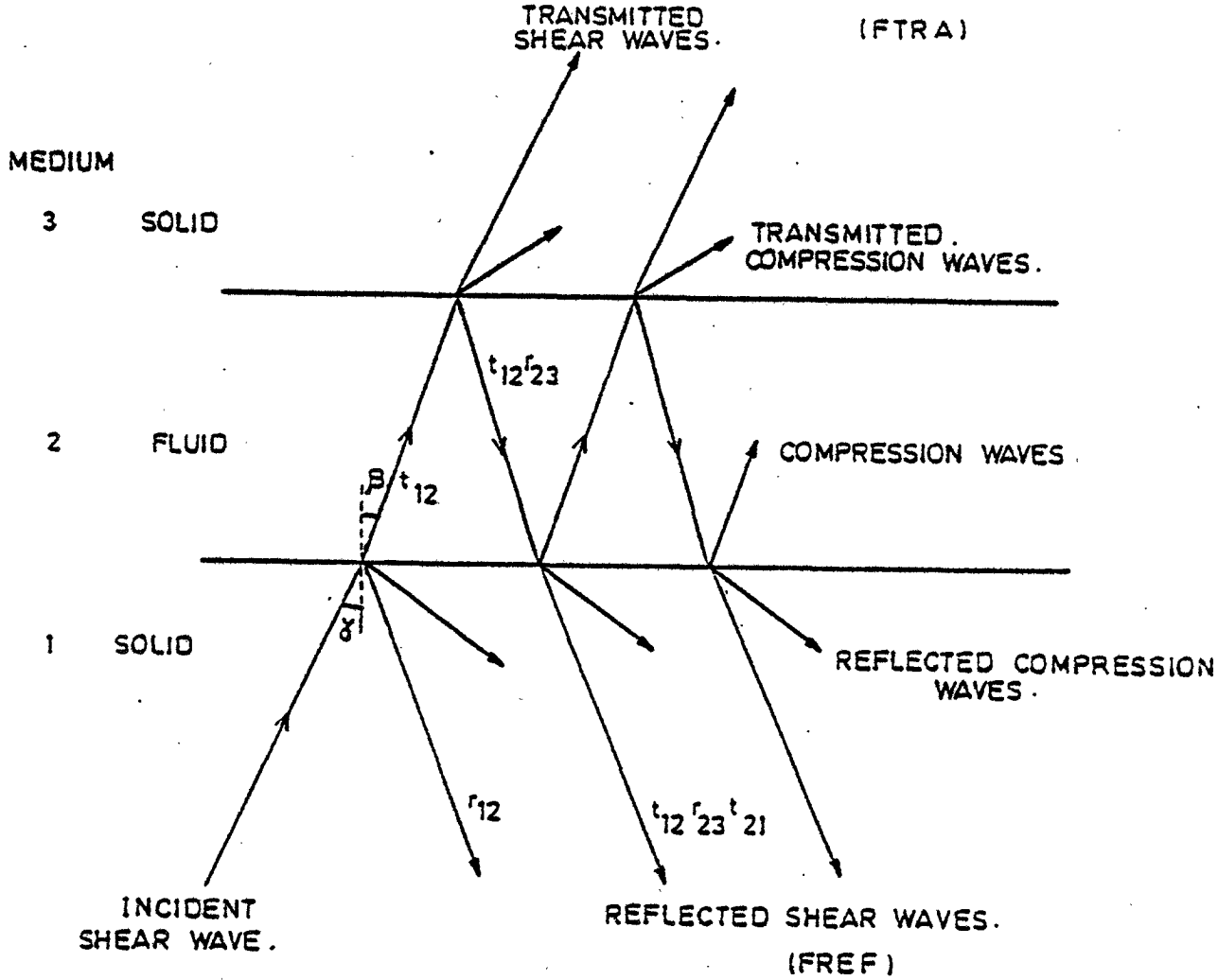

FIG.A1 · MULTIPLE REFLECTIONS AT A PARALLEL-SIDED FLUID GAP.

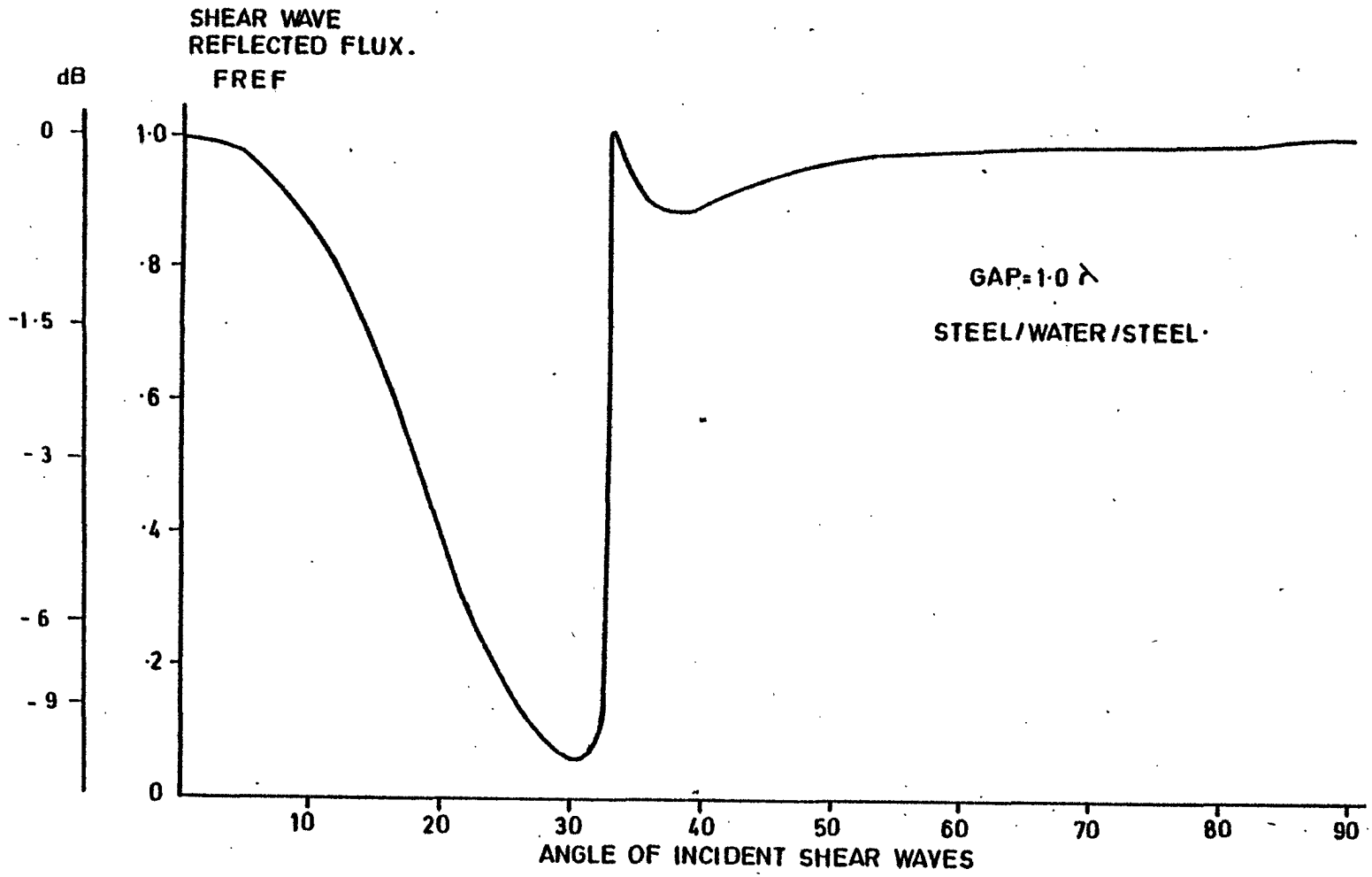

FIG A2. REFLECTION OF SHEAR WAVES AT A WATER GAP (GAP = 1·0)

RC/SSR/A4/1735

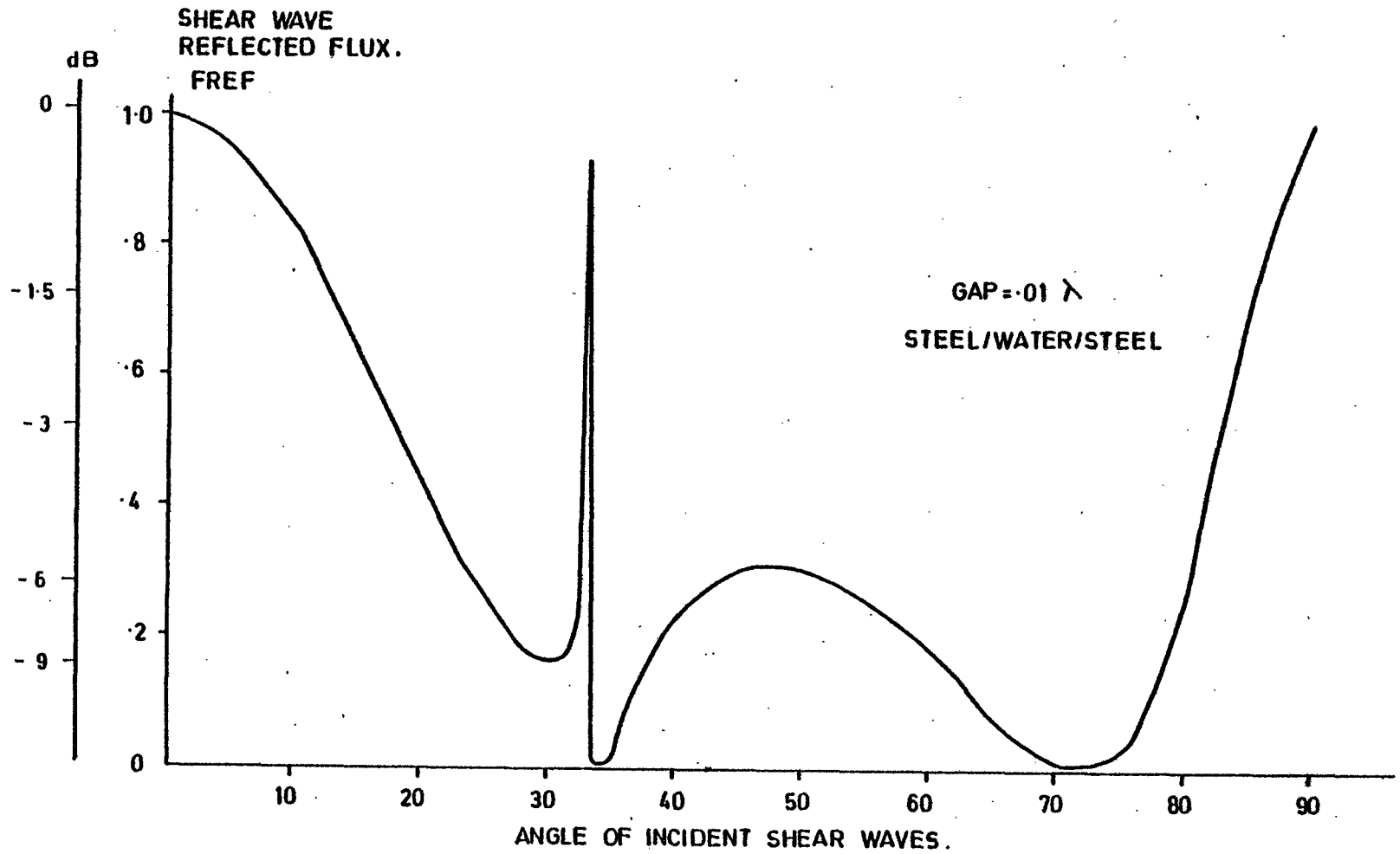

FIG·A3. REFLECTION OF SHEAR WAVES AT A WATER GAP (GAP = ·01)·

RC/SSR/A4/1736

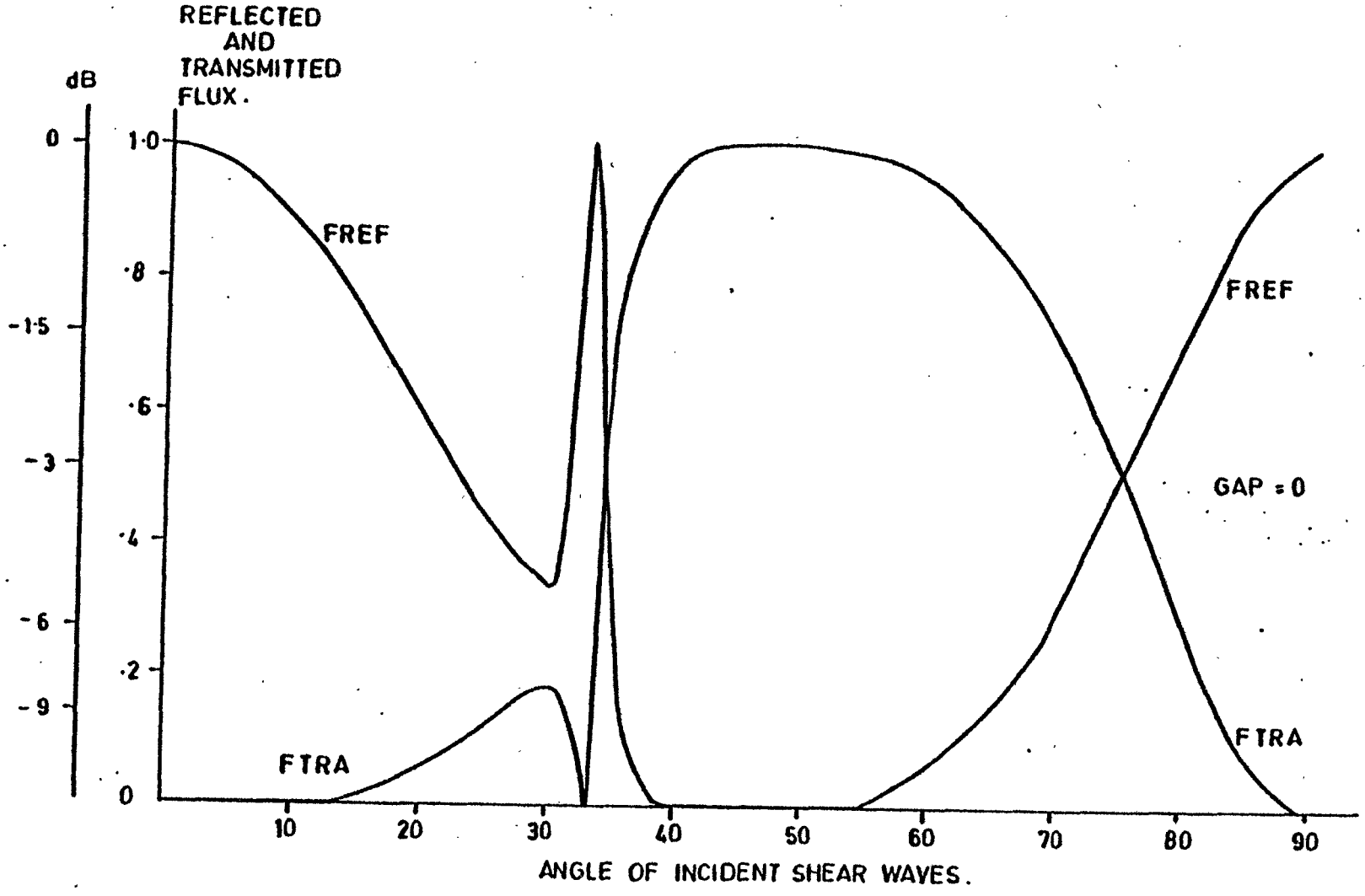

FIG.A4. REFLECTION OF SHEAR WAVES AT A ZERO THICKNESS FLUID GAP IN STEEL.

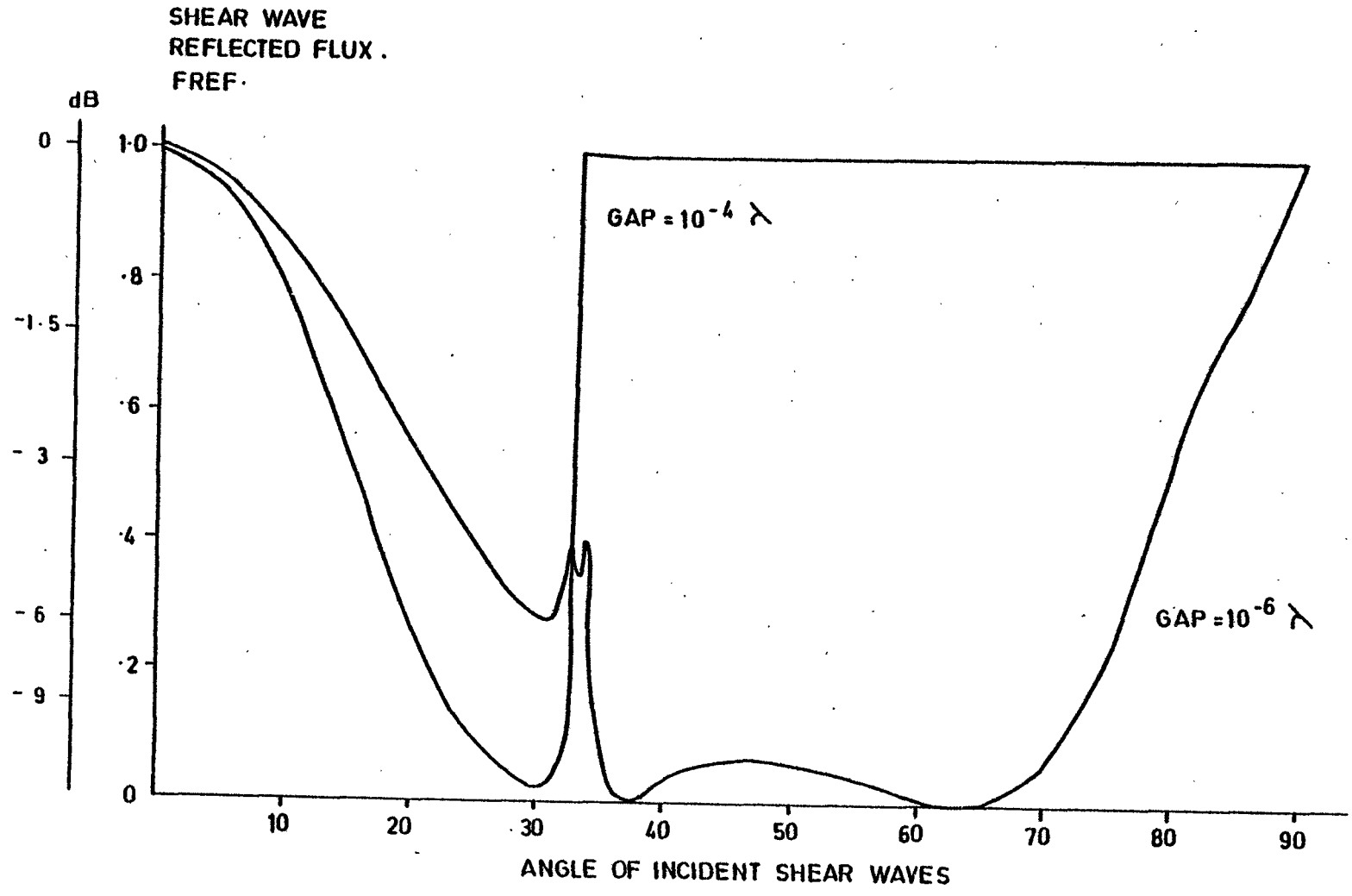

FIG. A5. REFLECTION OF SHEAR WAVES AT AN AIR GAP IN STEEL.

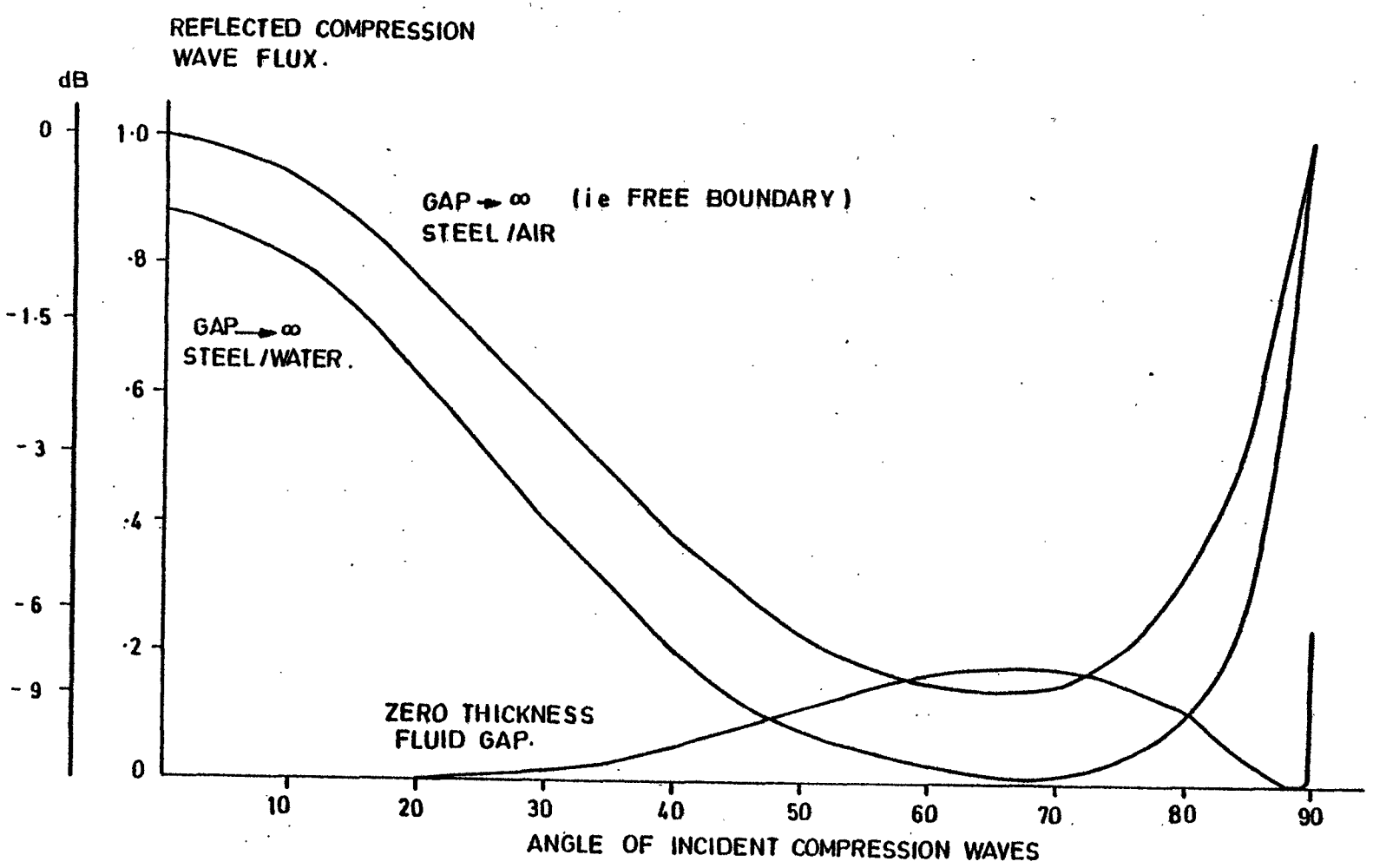

FIG. A6. REFLECTION OF COMPRESSION WAVES IN STEEL AT A FLUID GAP AND AT FREE BOUNDARIES.

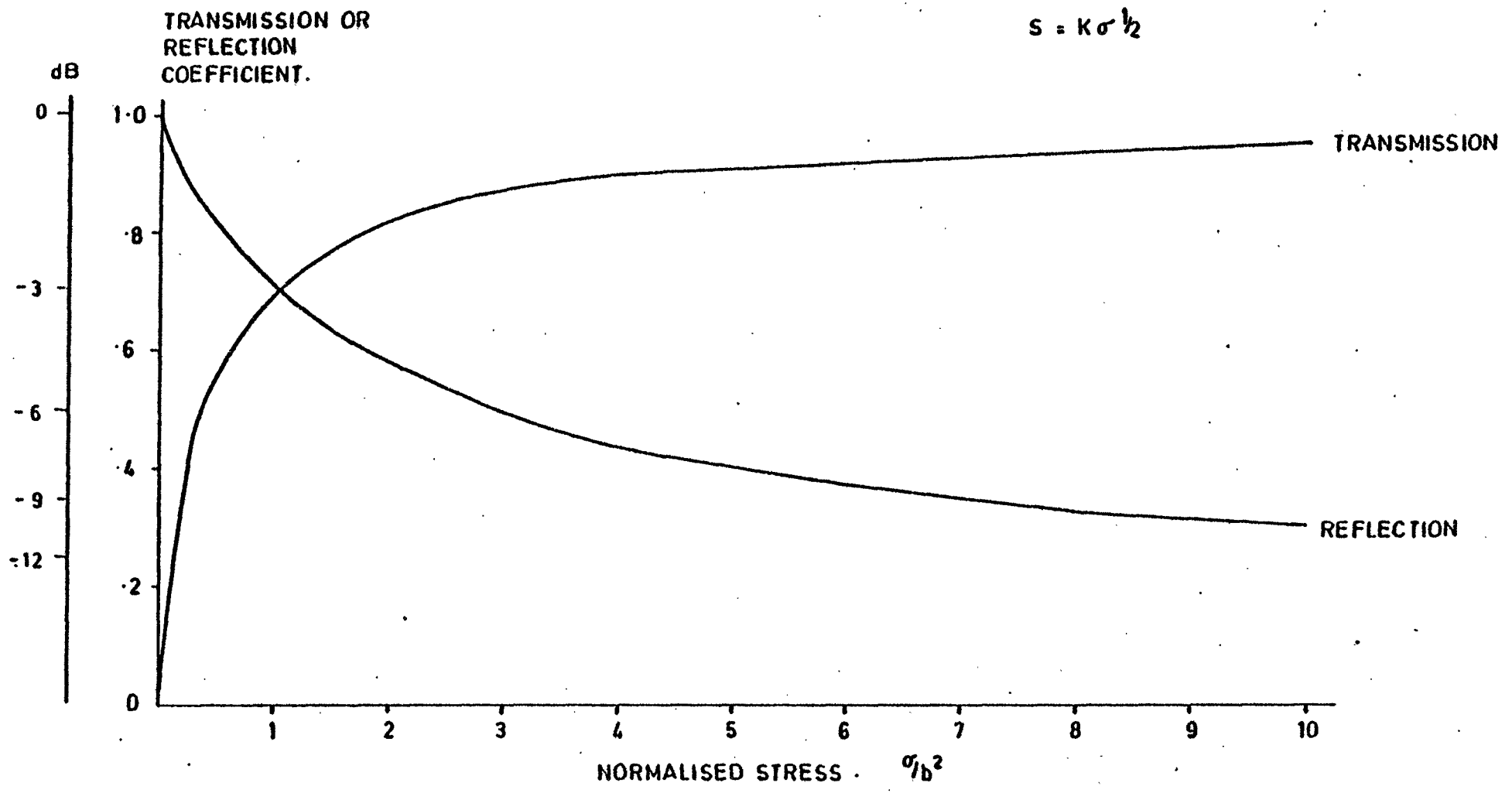

FIG. B1. THEORETICAL REFLECTION AND TRANSMISSION COEFFICIENTS FOR NORMAL COMPRESSION WAVES.

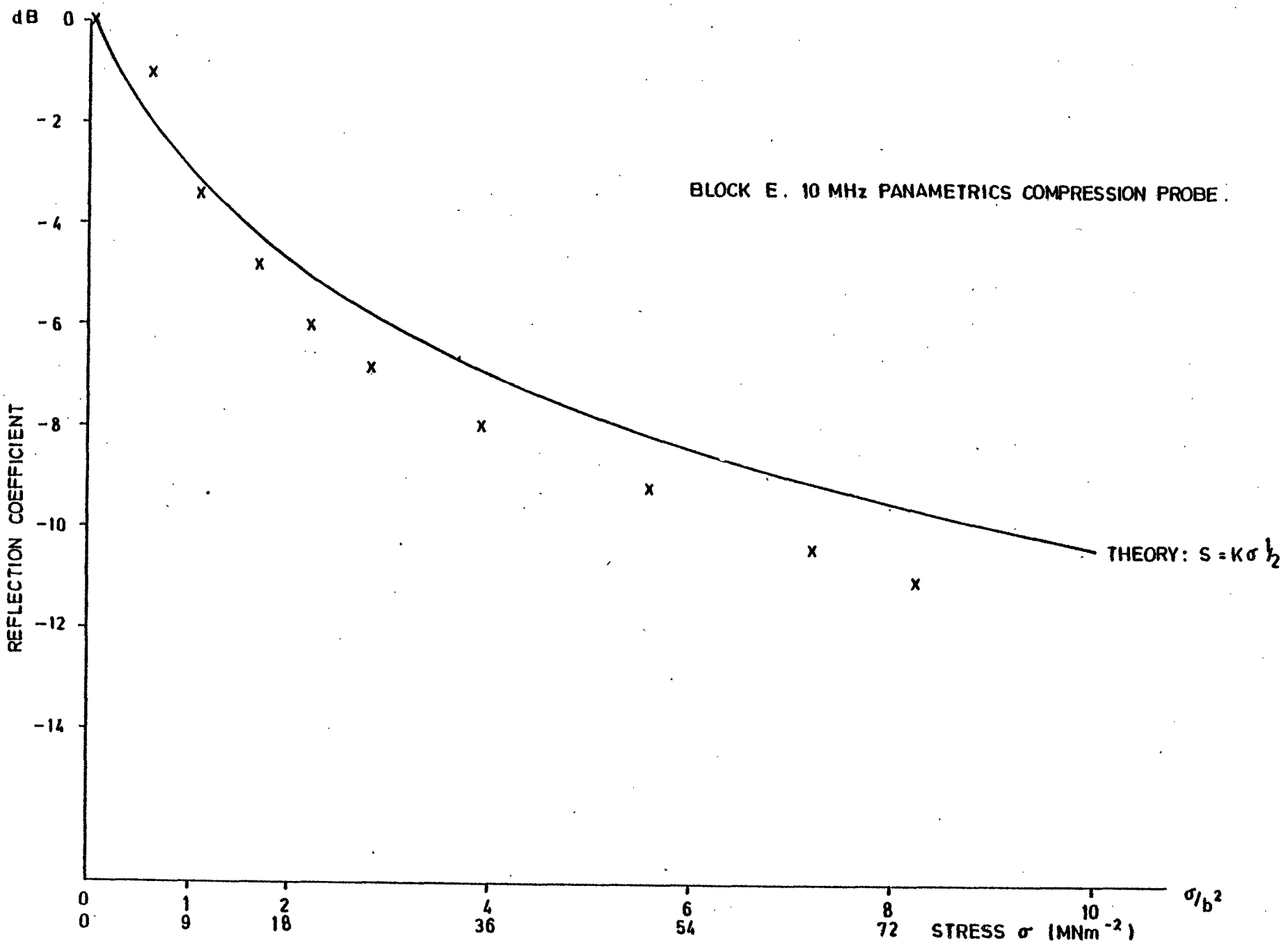

FIG. B2. REFLECTION OF 10 MHz. NORMAL COMPRESSION WAVES.

RC/SSR/A4/1741

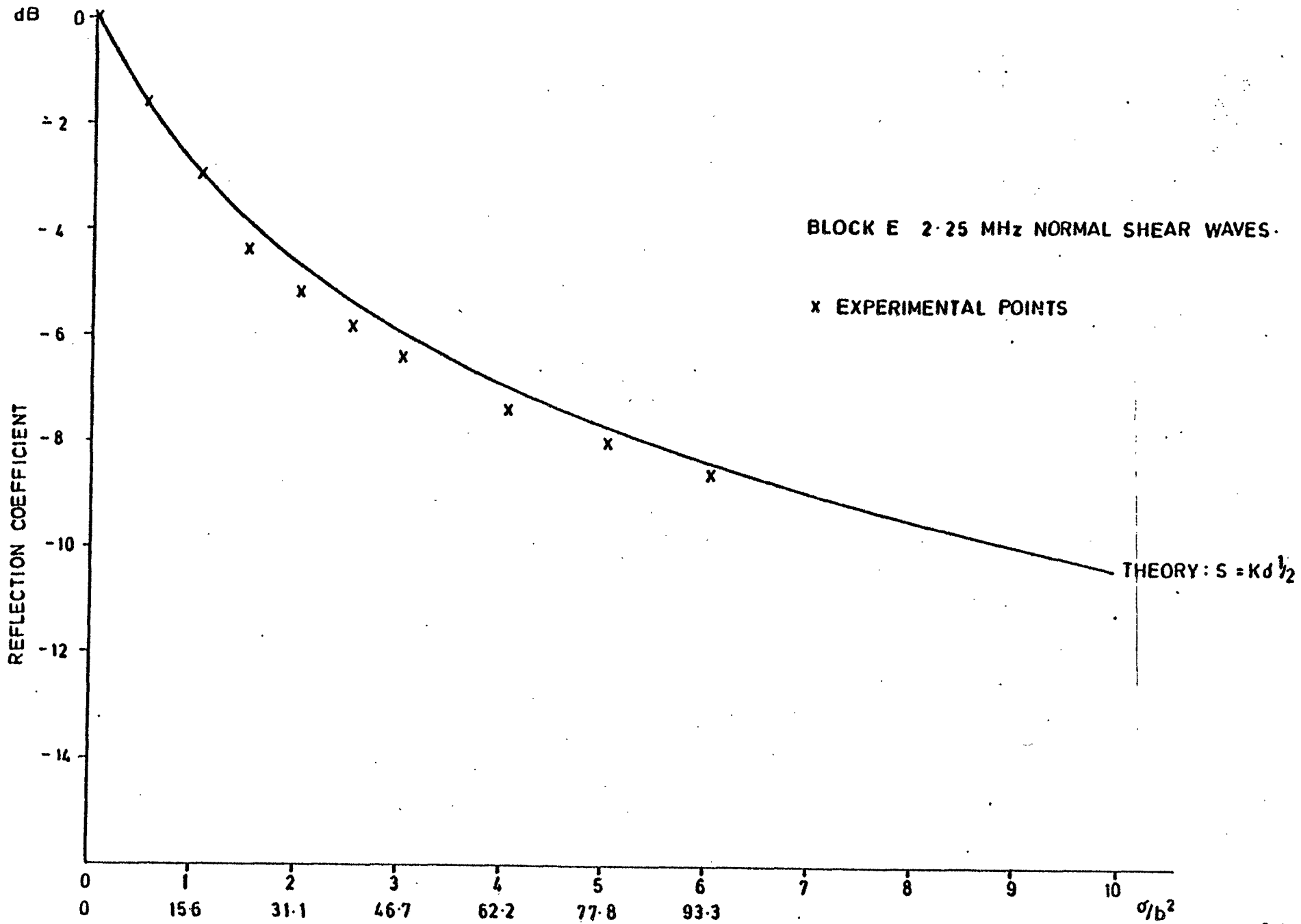

FIG·B3· REFLECTION OF 2·25 MHz SHEAR WAVES·

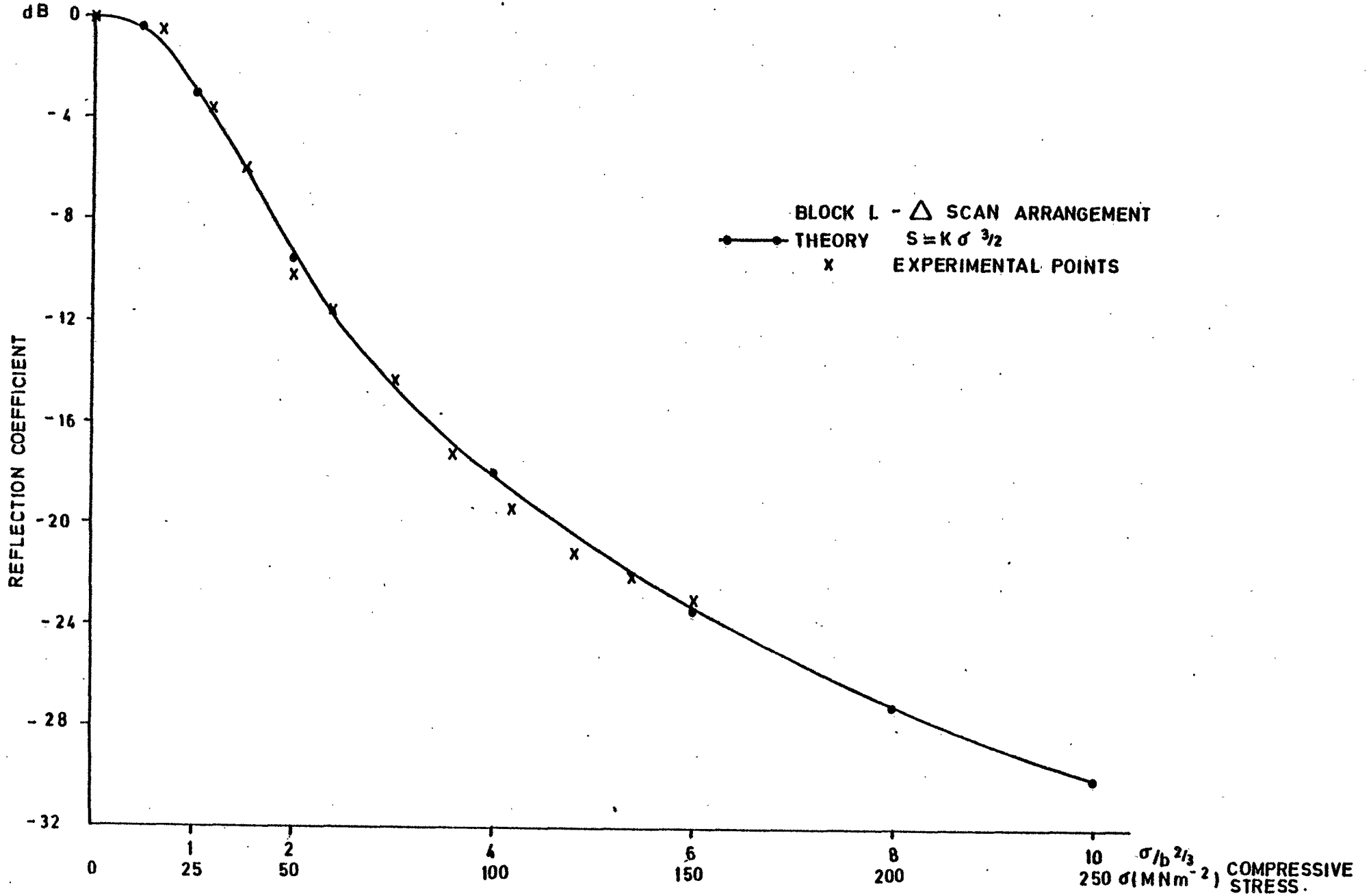

FIG.B4. Δ SCAN USING 4 MHz SHEAR WAVES INCIDENT AT 30°

RC/SSR/A4/1743